UNIVERSITY OF SOUTHAMPTON

FACULTY OF ENGINEERING AND THE PHYSICAL SCIENCES

School of Engineering

Volume 1 of 1

Graphene Oxide based enhancement of electrical, thermal and mechanical properties of CFRP materials for wind turbine applications

by

Evangelos C. Senis

ORCID: 0000-0002-7500-2778

Thesis for the degree of Doctor of Philosophy

November 2019

UNIVERSITY OF SOUTHAMPTON

ABSTRACT

FACULTY OF ENGINEERING AND THE PHYSICAL SCIENCES

School of Engineering

Thesis for the degree of Doctor of Philosophy

Graphene Oxide based enhancement of electrical, thermal and mechanical properties of CFRP materials for wind turbine applications

Evangelos C. Senis

The increasing use of carbon fibre reinforced polymers (CFRP) in weight critical structures have introduced new challenges associated with heat dissipation and electric current flow paths within the composite structure due to their anisotropic behaviour. The low transverse and in particular through-thickness electrical and thermal conductivities have been highlighted as the main parameters affecting the response of the laminates. Enhancing the properties in these directions is essential to enable the use of CFRP in aircraft, wind turbine blade and automotive applications and reduce the risk of damage. To establish a reference point, the anisotropic electrical and thermal behaviour of CFRP was experimentally quantified through self-developed measurement protocols.

To enhance the electrical and thermal response of CFRP, commercially available graphene oxide (GO) nanoflakes were dispersed into the epoxy matrix studied considering two different case studies. In both cases the filler was added to the epoxy matrix prior being vacuum infused into dry carbon fabric to form CFRP laminates. Initially, the characterization of CFRPs containing randomly oriented GO showed that the electrical conductivity in the through-thickness direction increased markedly, reaching values up to 0.18 S/cm, when 6.3 vol% of GO was added into the epoxy, showing a threefold increase compared to the neat CFRP. Similar improvement was also found in the thermal through-thickness conductivity for the same filler content, where the laminate exhibited identical values in both transverse and through-thickness directions. However, the properties transverse to the fibres were not greatly affected by the GO addition. To assess the effect of the GO on the mechanical properties, interlaminar shear strength (ILSS) tests were conducted that showed that the addition of the GO significantly enhanced the through thickness shear strength, especially at low filler contents.

In the second case study, an optimization of the previously developed laminates was realised aiming to lower the required GO filler content. By utilising an external alternating current (AC) field, the orientation of GO flakes was altered to take advantage of the higher electrical and thermal conductivity along the graphene basal planes. To assess the efficiency of the alignment method a comparison between laminates containing randomly oriented GO and aligned GO modified CFRP (A-GO/CFRP) laminates was realised. Measurements of the electrical conductivity revealed markedly increased values for the A-GO/CFRP even with low filler contents, validating the efficacy of the alignment. Further morphological characterization by means of scanning electron microscopy (SEM) revealed the formation of a chain-like conducting network interconnecting adjacent fibres. The thermal conductivity, albeit increased in A-GO/CFRP, only resulted in modest improvements. Mechanical tests of the ILSS showed that the A-GO/CFRP laminates exhibited significantly improved behaviour and retained higher ILSS values (than the randomly oriented GO CFRP laminates) even at high filler contents.

Table of Contents

List of Tables

List of Tables

List of Figures

Academic Thesis: Declaration Of Authorship

I, Evangelos C. Senis declare that this thesis and the work presented in it are my own and has been generated by me as the result of my own original research.

Graphene Oxide based enhancement of electrical, thermal and mechanical properties of CFRP materials for wind turbine applications

I confirm that:

1. This work was done wholly or mainly while in candidature for a research degree at this University;
2. Where any part of this thesis has previously been submitted for a degree or any other qualification at this University or any other institution, this has been clearly stated;
3. Where I have consulted the published work of others, this is always clearly attributed;
4. Where I have quoted from the work of others, the source is always given. With the exception of such quotations, this thesis is entirely my own work;
5. I have acknowledged all main sources of help;
6. Where the thesis is based on work done by myself jointly with others, I have made clear exactly what was done by others and what I have contributed myself;
7. Parts of this work have been published as:

Journal articles

1. E. C. Senis, I. O. Golosnoy, J. Dulieu-Barton and O. T. Thomsen, "Enhancement of the electrical and thermal properties of unidirectional carbon fibre/epoxy laminates through the addition of graphene oxide", Journal of Materials Science, **https://doi.org/10.1007/s10853-019-03522-8**

Journal articles accepted for publication

1. E. C. Senis, I. O. Golosnoy, T. Andritsch, J. Dulieu-Barton and O. T. Thomsen, "The influence of graphene oxide filler on the electrical and thermal properties of unidirectional carbon fibre/epoxy laminates: effect of out-of-plane alignment of the graphene oxide nanoparticles", Polymer Composites, **https://doi.org/10.1002/pc.25637**

Conference papers

1. E. C. Senis, O. Vryonis, S. F. Madsen, I. O. Golosnoy, J. M. Dulieu-Barton and O. T. Thomsen, (June 2017), "Improved current conduction capability of nanomodified CFRP for lightning protection of wind turbine blades". In Joachim Holbøll (chair) in the Lightning protection of wind turbines. Symposium conducted at the Wind Energy Science Conference, Copenhagen, Denmark.
2. E. C. Senis, I. O. Golosnoy, J. Dulieu-Barton, O. T. Thomsen and S. F. Madsen, "Characterization of through thickness thermal conductivity of wind turbine blade CFRP materials using a steady-state technique", International Conference on Composite Materials, 20-25 August 2017, Xi'an, China.
3. E. C. Senis, O. Vryonis, I. O. Golosnoy, J. M. Dulieu-Barton, O. T. Thomsen, L. Carloni and S. F. Madsen, "The Influence of Graphene Oxide on the electrical conduction in unidirectional CFRP laminates for wind turbine blade applications", International Conference on Lightning and Static Electricity,13-15 September 2017, Nagoya, Japan.
4. E. C. Senis, I. O. Golosnoy, J. Dulieu-Barton and O. T. Thomsen, "Assessing the dispersion of nanoinclusions in nanoreinforced CFRP laminates using electrical resistance measurements", European Conference on Composite Materials, 24-28 June 2018, Athens, Greece.

Conference papers (contributing author)

1. A. A. M. Laudani, I. O. Golosnoy, J. Kremer, E. C. Senis, O. T. Thomsen, P. L. Lewin, "Experimental characterization of contact resistivity of CFRP wind turbine spars' equipotential bonding", 65th IEEE Holm Conference, 15-18 September 2019, Milwaukee, USA

Poster presentations

1. E. C. Senis, I. O. Golosnoy, J. Dulieu-Barton and O. T. Thomsen, "Analysis of through-thickness thermal conductivity of wind turbine blade CFRP", Universities High Voltage Network Colloquium,16 January 2018, Winchester, UK

Signed: ……

Date: ……

Acknowledgements

I would like to thank my supervisors Professor Ole T. Thomsen, Dr. Igor O. Golosnoy and Professor Janice Dulieu-Barton for their patience, support and advice throughout the PhD.

I would like to recognize the financial support provided by the European Commission, Horizon 2020 Marie Sklodowska-Curie actions grant agreement No 642771, who provided funding for the SPARCARB project. Thanks are also due to the project partners who provided valuable insight throughout the course of the PhD by hosting me: GLPS A/S (currently part of PolyTech A/S) (DK), Zoltek (USA) and Nordex-Acciona (DE).

Thanks go to Dr. Thomas Andritsch, Dr. Richard Chippendale, Dr. Andrew Robinson and Dr, Wendell Bailey for lavishly providing their knowledge and expertise.

I would like to thank the Tony Davies High Voltage Laboratory for the technical support and providing the necessary equipment, Mr. Brian Rodgers, Mr. Ian Virtanen, Mr. Neil Palmer and Mr. Mike Smith thank you for all of the little things that made a huge difference.

Thanks also go to my fellow PhD students of the SPARCARB project, Orestis, Andrea and Tim for the excellent collaboration throughout the years.

To my friends made during my PhD: Alex, Tobi, Geir, Jack, Giannis, Amy, David, Dimitris, Julian thank you all for the company and the fun we had.

To my dearest friend Orestis, thanks for being a good companion for all of our trips across the globe all of these years.

Finally, special thanks go to Maria for supporting every endeavor of mine however far away they kept me from her.

This work is dedicated to the loving memory of my mother Margaret, the person that always believed in me and motivated me to reach for my goals wholeheartedly.

Definitions and Abbreviations

AC: Alternating Current

BDS: Broadband Dielectric Spectroscopy

CB: Carbon Black

CFRP: Carbon Fibre Reinforced Polymer

CNF: Carbon Nanofibres

CNT: Carbon Nanotubes

CVD: Chemical Vapor Deposition

DC: Direct Current

DWCNTs: Double wall carbon nanotubes

FRP: Fibre Reinforced Polymer

GFRP: Glass Fibre Reinforced Polymer

GHP: Guarded Hot Plate

GNP: Graphene Nano Platelets

GO: Graphene Oxide

ILSS: Interlaminar shear strength

MWCNTs: Multi Wall Caron Nanotubes

SEM: Scanning Electron Microscopy

SnW: Silver nanowires

SWCNTs: Single Wall Carbon Nanotubes

Chapter 1 Introduction

1.1 Introduction to wind energy

Since the earliest times of recorded history, humans have harnessed the energy of the wind to their benefit propelling boats along the Nile River as early as 5000 B.C. By 200 B.C., simple windmills in China were developed in order to pumping water, while vertical-axis windmills with woven reed sails were grinding grain in Persia and the Middle East. By the 11th century, people in the Middle East used windmills extensively for food production (grind cereals). Returning merchants and crusaders carried this idea back to Europe [1]. The Dutch refined the windmill, Fig. 1.1 (left), and adapted it for draining lakes and marshes in the Rhine River Delta. Similar windmills were developed in the Aegean sea, Fig. 1.1 (right), for grinding cereals because of the high wind speeds in islands like Mykonos. When settlers took this technology to the New World in the late 19th century, they began using windmills to pump water for farms and ranches and later to generate electricity for homes and industry [1].

Figure 1. 1: Examples of a Dutch and a Greek windmill [Source www.TodaysPhoto.org].

The first recorded windmill, Fig. 1.2 (left), built specifically for the production of electricity was developed in the July of 1887 in Scotland by Prof. James Blyth in order to charge accumulators for the lighting of his holiday cottage [2]. On the other side of the Atlantic Ocean Charles F. Brush designed and constructed in Cleveland, Ohio in the winter of 1887-1888 a wind turbine, Fig. 1.2(right), with a rotor diameter of 17 m mounted on an 18 m tower generating 12 kW of power [3].

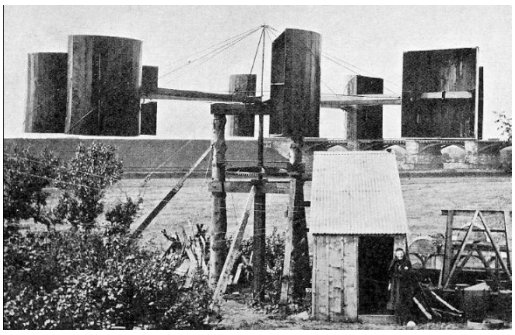

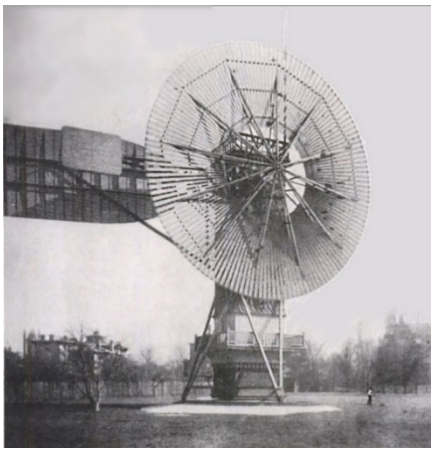

Figure 1. 2: (left) Blyth's windmill at his cottage in Marykirk in 1891 [http://www.strath.ac.uk/archives/iotm/march2012/] and (right) Brush's windmill of 1888 [windpower.org]

Today wind energy is the fastest-growing source of electricity in the world, with a global installed capacity of 539,123 MW (end of 2017) [4]. These numbers are encouraging and show a way to a greener path for the global energy production, and the EU has committed to legally set a target to meet 20% of its energy consumption via renewable energy sources by 2020 targeting to decarbonize the economy by 80-95% by 2050 [5], [6]. Wind turbines are considered the major contributor to the production of renewable electric energy, where offshore wind power is expected to play a key role to achieve the above-mentioned targets.

1.2 CFRP materials used in the wind turbine blades

To reach higher rated power outputs, the size of wind turbines has been drastically increased over the past decades, Fig. 1.3. The reason for this is that the rated power scaled quadratically with the rotor diameter or blade length, but also because the of the wind shear effect, which means that the mean wind speed increases with the height above the ground [7]. However, larger rotor diameters or blade lengths are accompanied by higher rotor/blade mass. Considering the size of wind turbines and by using normal scaling laws the weight (mass) of a wind turbine blade would be expected to increase with length to the power of 3, but because of the improvements of the aerodynamic design as well as improved design, experience shows that the blade mass raises only to the power of 2.3-2.5, depending on the particular design of the manufacturers [7], [8], i.e. the optimization of the manufacturing process and materials used has led to significant weight reductions. Increasing blade length and mass results in significantly higher loads on bearings and drive trains [8], in particular due to the significantly increase of gravity and inertia loads that are

accompanied by the increase of mass. Thus, the extra mass leads directly to an increase at the torque transmitted through the rotor, and as the rotor diameter scales to the torque by a power of three, this has a significant impact on the size of bearings, gears and generators required to handle this extra load, thus adding significantly to the overall cost. Conventionally and until recently wind blades were overwhelming manufactured using glass fibre reinforced composites (Glass Fiber Reinforced Polymer or just GFRP), but for longer blades GFRP will add will add even more weight to the construction creating higher loads to the main components of the turbine system due to the lower specific stiffness and strength (i.e. stiffness and strength relative to mass) when compared with carbon fibre reinforced composites (Carbon Fiber Reinforced Polymer or just GFRP) [7]. Thus, to reduce the blade mass and the costs (derived from added mass) it is vitally important to utilize lighter and more efficient materials for the wind turbine rotor systems, if future wind turbines with even higher rated power outputs and lower "Cost of energy" (CoE) are to be realized. CoE is the primary driver behind the introduction and increased utilization of CFRP materials into wind turbine blades [8].

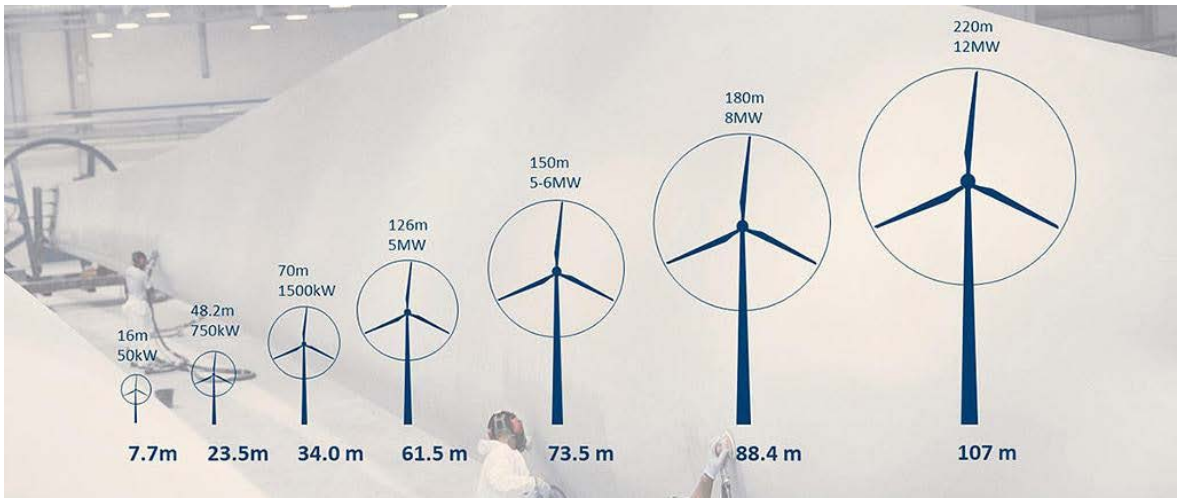

Figure 1. 3: Evolution of the wind turbine size and power outputs (source: https://www.lmwindpower.com/)

CFRPs are utilized in the manufacturing of the main load carrying structures of wind blades, also known as sparcaps or spars, Fig. 1.4 and Fig. 1.5 [9]. The role of the sparcap during loading is to carry the tensile/compressive loads that together forms the so-called flapwise bending moment generated by the aerodynamic loads acting on the aerodynamic airfoils/shells during operation [7], [8]. To fulfill this function, spars are usually made as unidirectional composite laminates located under the outer blade skin which is manufactured from Biax GFRP (to produce torsional stiffness) [10].

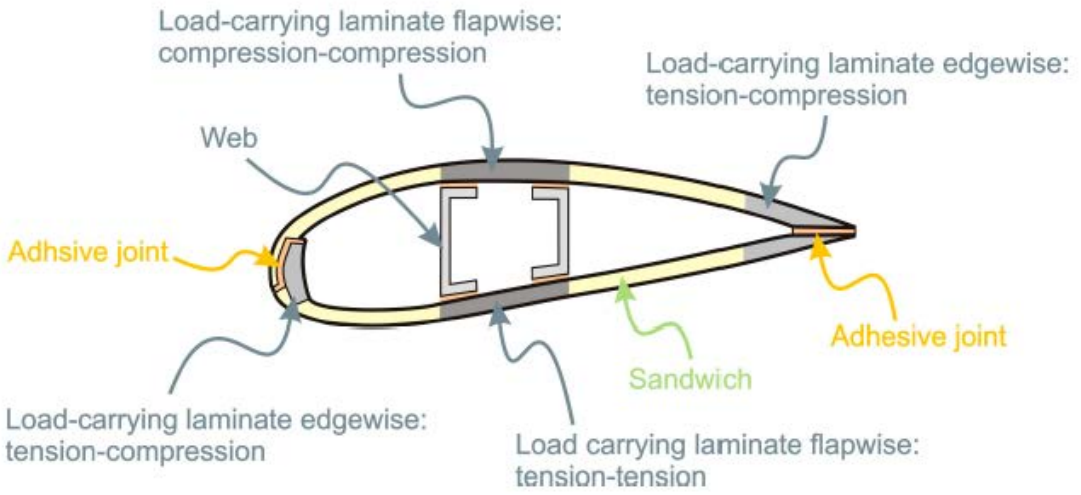

Figure 1. 4: Schematic of a wind turbine blade section [10]

With current wind turbine designs incorporating blades reaching up to 107m, allowing power outputs up to 12 MW (GE Haliade-X 12MW), and with even longer blades being planned for future wind turbines with rated power output of up to 20MW, the use of CFRP has become an essential part in the development of the next generation of MW wind turbines for both on and offshore wind farms.

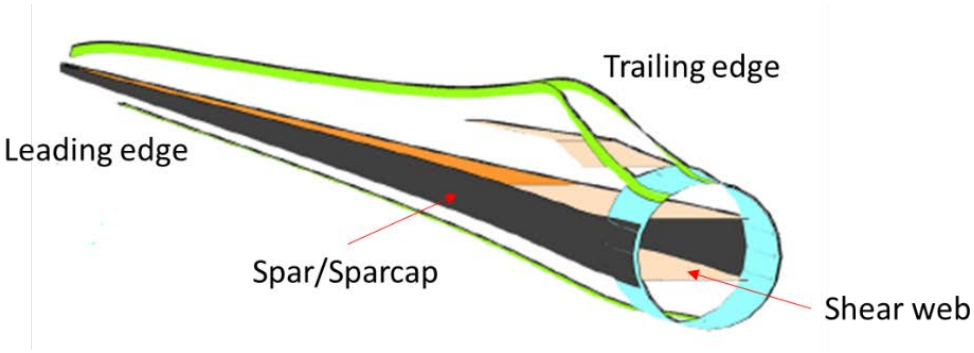

Figure 1. 5: Typical blade design with continuous sparcaps [9].

1.3 Anisotropy of CFRP and lightning exposure

Long before their incorporation in wind turbine blades, CFRPs were introduced in the aerospace sector, initially on aircraft non-key structural components [11]. Since then, their usage have experienced a continuous growing over several decades, making them a favourable choice of material for the manufacturing of parts such as the aircraft's fuselage, wings, tail, doors and interior. However, with the use of CFRP in aerospace and WT blade applications, driven by mechanical and aerodynamic performance requirements and design drivers, new challenges are introduced when electric current and/or heat is introduced into the composite structure [12], [13]. CFRPs are highly

anisotropic as their properties depend on the direction in which the carbon fibres are oriented. This is true for the mechanical properties, but even more so for the thermal and electrical properties, thus making the design process of structures ever so complicated in managing electric current paths and heat dissipation while at the same time achieving structural integrity [14], [15]. In unidirectional CFRP the electrical conductivity in the longitudinal direction can be up to 1000 times larger than in the transverse direction, perpendicular to the fibres. In addition, the out-of-plane conductivity is at least an order of magnitude lower than in the perpendicular direction, depending on the laminate type, composition and constituents [16], [17]. This behaviour has created particular issues with regard to the lightning performance of CFRP since the low out-of-plane electrical and thermal conductivity impedes the electrical current distribution and heat dissipation within the composite laminate making them vulnerable to lightning strikes [18], [19]. When exposed to lighting impulses CFRPs exhibit a wide range of damage types, from resin deterioration and fibre breakage, on their, up to delaminations in their internal structure [16], [17], [20]. To overcome these effects, the aircraft sector has introduced expanded metal foils on the composite laminate surfaces (typically the wings) to avoid that lightning strike induced current penetrates the composite aircraft skin [21]. However, the addition of metals in the structure create a number of issues like galvanic corrosion as well as adding weight. An alternative and potentially more well suited approach would be to alter the material properties of the composite material, specifically increasing the electrical and thermal conductivities to mitigate the induced damage [13]. Besides the use for aerostructures, this approach could also be applicable to the wind turbine blades. Briefly, as wind turbines are reaching heights up to 260 m, they become more susceptible to lightning [22]. The combination of a tall structure permanently grounded to earth, sometimes on high mountain ridges, and the geometry of the wind turbine's blade tip, sharp conical shape, able to disrupt the electric field around it, have been identified as the main parameters causing lightning to be intercepted from the wind turbine during thunderstorms [23], [24]. Due to aforementioned factors wind turbines exhibit higher probabilities of intercepting lightning strikes, with 5 times higher energy levels, compared to aircrafts [25]. The blade is the most exposed part of the wind turbine to lightning, with the area around the blade tip to suffer the majority of the lightning damages [23], [26]. Thus, new methods of lightning protection need to be developed and validated considering their 25 year service life [27], [28].

1.4 SPARCARB project

This PhD project is part of the European project; Marie Skłodowska-Curie Action, H2020-MSCA-ITN-2014, 'Lightning protection of wind turbine blades with carbon fibre composite materials' (SPARCARB) that aims to address the lightning related issues in modern wind turbine blades that

incorporate CFRP materials into their structure. The research challenges embraced by SPARCARB can be divided into four major research tasks, each corresponding to an individual PhD project carried out by an ESP (Early Stage Researcher):

- Electrical, Thermal and Mechanical Properties of wind turbine CFRP materials (ESR 1- ***this PhD project***)
- Modelling the electrical and thermal response of wind turbine blade CFRP materials in response to a direct lightning strike (ESR 2)
- Development of resin systems for CFRP that are optimized to enhance electrical and thermal properties, without compromising mechanical properties (ESR 3)
- Characterization of lightning strike induced damage in CFRP laminates and components for blades (ESR 4)

As part of SPARCARB the ESRs are trained to be familiar with both Industry and Academia. Thus, out of the 36 months of the project, half of its duration (18 months) has been spent in an academic institution (University of Southampton) and the rest (18 months) in non-academic organizations in the form of industrial secondments. Out The 18 months of industrial secondments, 15 months was spent at GLPS A/S (currently Polytech A/S, Denmark) and 3 months in two partner organizations.

For the case of ESR 1 (this PhD project) the two 1.5 month secondments were spent at Zoltek, USA (carbon fibre and composite manufacturer) and Nordex-Acciona, Germany (wind turbine manufacturer).

1.5 Aims and Objectives

The aim of this research is to develop CFRP laminates that exhibit enhanced electrical and thermal properties through the addition of a secondary reinforcing phase, without compromising their structural integrity, with potential applications to the manufacturing of large structures (like wind turbine blades) using commercially available materials.

To achieve the aim, the following objectives must be addressed:

- To understand how the electrical and thermal conduction mechanisms in each direction are affected by the addition of conducting nanoinclusions, reliable experimental procedures need to be developed and validated.
- Nanomodified CFRP laminates needs to be able to manufactured, using low cost commercially available materials, using a route that is relevant and applicable on an industrial scale.

- Obtain a multiscale composite material with enhanced out-of-plane electrical and thermal conductivity and explore the possibility of achieving isotropic properties, i.e. obtaining electrical and thermal conductivity similar to the along the fibre direction. As it is critical for structural applications, the laminate should be able to retain its structural integrity.
- Investigate whether an optimization of the manufacturing process or method of incorporating the nanofiller into the CFRP laminate can lead to reduction of the amount of filler required to improve the electrical and thermal properties.

1.6 Research question and Novelty

The presence of CFRP materials in aircraft and wind turbine blades introduces new challenges to be dealt during the design process of their lightning protection systems. Improved electrical current distribution and heat dissipation within the bulk of composite laminates are essential to avoid structural damage [16], [18], [29]. Aircraft composite CFRP structures are currently designed such that direct effects of lightning exposure to CFRP are mitigated by the addition of metallic foils and meshes that add considerably to the weight of the overall structure, and new methods need to be devised for aircraft as well as other applications including wind turbines. By substituting such metallic foils by adding functionality to the composite through the incorporation of a conducting filler to the bulk and/or surface of composite laminates, both performance and weight of the structure can be enhanced. However, if nanomodified composites are to be utillised in the manufacturing of large structures, special considerations need to be taken into account regarding the manufacturing process and potential added cost. Although several methods can be adopted for the manufacturing of such composites, an industrially scalable process should be exploited. Considering the anisotropic properties of CFRP materials, understanding the corresponding conduction mechanisms in all spatial directions, and how these are affected by the addition of conducting inclusions, is essential to the development of multiscale composites with potential application as an integrated part of lightning protection systems. Furthermore, as the role CFRP is predominately structural, it should be verified that the addition of nanoinclusions does not impair their structural integrity.

Based on the above the following research questions needs to be answered:

- How does the addition of secondary reinforcing phase affect the conduction processes?
- Is it possible to achieve isotropic electrical and thermal conductivity?
- Can nanomodified CFRP be developed using low cost materials and scalable manufacturing methods?

- If further improvements are required, can they be addressed in a cost effective way?
- Will the structural integrity of the laminate be retained after the incorporation of a nanofiller?

Besides the development of laminates with enhanced electrical, thermal and mechanical properties this study contributes to the current state of the art regarding composites science and technology as follows:

- A testing protocol for the electrical conductivity of CFRP is proposed and presented to allow repeatable and reproducible measurements.
- A simple methodology for measuring of the transverse direction thermal conductivity is presented.
- Combining the above, the influence of the addition of conducting nanoinclusions on the transverse electrical and thermal conduction mechanisms is investigated to establish the rate of improvement in this direction and to correlate this with the obtained results in the through-thickness direction.
- Control of the spatial arrangement of GO platelets within the laminate was achieved using an electric field, enabling improved electrical and thermal conductivities in the through-thickness direction while reducing the required amount of filler.

1.7 Thesis Outline

Chapter 2 is focused on conducting a comprehensive review of the available literature in this area. The first aspect considers the individual constituents of CFRP, specifically their electrical and thermal properties. The influence of different constituents on the laminate behaviour is then investigated, including the dependency on temperature. Considering that composite structures are subjected to load/deformation during operation, the influence of mechanical deformation on the electrical properties is also assessed. The final part of the literature review is dedicated to multiscale composites and the efforts that have been made to improve the overall performance of CFRP by embedding inclusions as a secondary reinforcing phase. Emphasis is given to the different methods of adding nanoinclusions to the material, as well as what has been achieved with regard to increasing the electrical and thermal conductivity and their potential applications. Finally, an overview of the most common experimental methods for characterizing the electrical and thermal conductivity is presented.

In Chapter 3, a summary of the experimental methods and techniques used for the development and characterization of the CFRP laminates is presented. The raw materials used in the

manufacturing of CFRP and nanoreinforced CFRP laminates are presented. Finally, the experimental methods developed and commissioned to characterize the anisotropic electrical and thermal conductivity of CFRP are presented.

The baseline properties of selected reference CFRP system are investigated in Chapter 4, to establish a basis for comparative assessment and analyses. The anisotropic electrical and thermal conductivities are characterised by adopting the experimental methods and protocols discussed in Chapter 2.

The first case study is presented in Chapter 5. The influence of Graphene Oxide (GO) nanofiller on the electrical and thermal conductivity in the transverse and through-thickness directions of unidirectional CFRPs is investigated, with the filler being introduced into the laminate by means of bulk matrix modification. The morphology of the nanoreinforced CFRP is examined to understand the mechanisms behind the (potential) enhancement in electrical, thermal and mechanical properties, as well as the dependency from the filler content.

In Chapter 6, the second case study is presented in which the orientation of GO within the CFRP laminate is investigated. Initially, a method of altering the orientation of GO, perpendicular to the fibre direction aiming to promote through-thickness thermal and electrical conduction is introduced. Then, a comparison between laminates containing randomly oriented and aligned GO is presented, with regard to the through-thickness electrical and thermal conductivity and interlaminar shear strength.

In the final chapter, discussion points and conclusions from the entire PhD research project are summarised and synthesised. Finally, some potential future steps are presented.

Chapter 2 State of the art

2.1 Introduction

The purpose of this literature review is to present the research conducted concerning the electrical and thermal behaviour of CFRP, and to correlate this with the lightning performance in the context of wind turbine blade applications. While most of the studies available in open literature concern aircraft applications, information about the response of CFRP will be brought over from this sector. The strategy behind this review is based on the hypothesis that understanding the properties and behaviour of constituent materials and composites can provide the required tools to characterize the response of composite structures. CFRP materials are comprising two constituent phases or materials, carbon fibre reinforcement and a polymer matrix, the properties and behaviour of both constituents will be reviewed and to correlated with respect to their influence on the behaviour characteristics of the composite material. Thus, the electrical and thermal properties of carbon fibres and epoxies are presented separately, followed by a presentation of the properties of the CFRP composite. Further to this, the importance of improving their electrical and thermal behaviour will be discussed along with the strategies and methods developed or proposed in literature so far to achieve this. Finally, an overview of the available techniques for characterisation of the electrical and thermal conductivities of composite materials are reviewed.

2.2 Properties of CFRP constituent materials

2.2.1 Carbon fibres and Carbon allotropes

Carbon is one of the chemical elements known from prehistoric times. Its name originated from the Latin word carbo, charcoal, and it is the fourth most abundant chemical element in the universe by mass. Carbon exhibits the most allotropes or allotropic forms from any other chemical element. The word allotropy comes from the Greek, *άλλος* (allos) meaning other and *τρόπος* (tropos) meaning manner or form, and it refers to the existence of two or more different physical forms of a chemical element (taken from Oxford Dictionary). The list of carbon allotropes include: Diamond, amorphous carbon, Graphite, Fullerenes (buckyballs), carbon nanotubes (CNTs) and Graphene to name a few. It is worth noting that carbon allotropes exhibit extreme variations in their properties, see Table 2.1, ranging from diamond, a perfect insulator and the hardest materials at Mohs scale (10), to graphite, an electrical conductor with a Mohs hardness of 1.

Table 2. 1 Properties of Carbon allotropes, table adapted from [30]

Property	Graphite	Diamond	Fullerene	Single-wall carbon nanotubes (SWCNT)	Multi-wall carbon nanotubes (MWCNT)
Specific gravity (g/cm3)	1.9–2.3	3.5	1.7	0.8	1.8
Electrical conductivity (S/cm)	4000^{p}, 3.3^{c}	10^{-2}–10^{-15}	10^{-5}	10^{2}–10^{6}	10^{3}–10^{5}
Electron mobility (cm^2/ V s)	2.0×10^{4}	1800	0.5–6	$\sim 10^{5}$	10^{4}–10^{5}
Thermal conductivity (W/m K)	298^{p}, 2.2^{c}	900–2320	0.4	6000	2000
Coefficient of thermal expansion (K^{-1})	$-1 \times 10^{-6\ p}$ $2.9 \times 10^{-5\ c}$	$(1\sim3)\times10^{-6}$	6.2×10^{-5}	Negligible	Negligible
Thermal stability in air (°C)	450–650	<600	~600	>600	>600
p: in-plane, c: c-axis					

Until recently carbon fibres were defined as fibres that contain at least 92% carbon, and further that they should be made from a polymeric precursor [31]–[33]. Recent methods allow the development of fibres consisting of nearly 100% carbon by incorporating allotropic forms such as carbon nanotubes (CNTs) and Graphene as well as carbon nano-fibres (CNFs) [32], [34], [35].

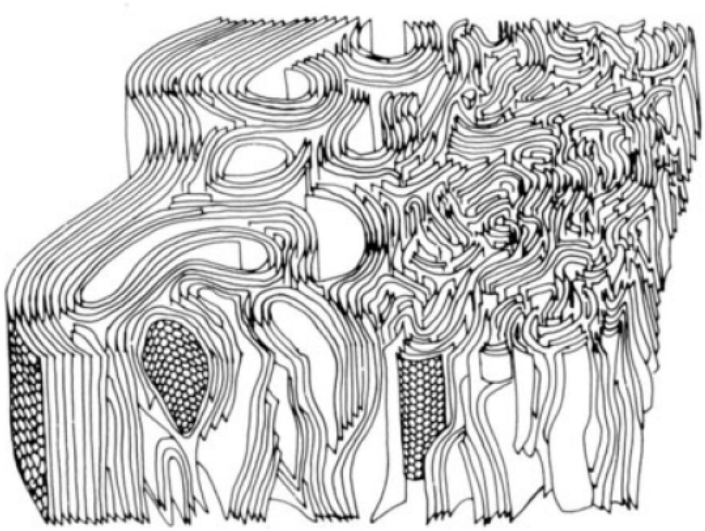

Figure 2. 1: Three dimensional representation of the structure of a PAN-based high Modulus carbon fibre, parallel planes on the left side and disordered core on the right [36].

The most commonly used precursors are PAN (Poly Acrylonitrile), pitch and cellulose-based [32], [37]. The structure of carbon fibres is precursor dependent since different manufacturing routes are followed for each of the precursors and these influence the formation of parallel planes,

crystallites [31], [38], [39]. The existence of these parallel planes or basal planes, Fig. 2.1, is responsible for the variation of the mechanical properties of carbon fibres since a highly ordered structure leads to higher Young's modulus and strength [38]. Pitch-based fibres exhibit higher Young's modulus compared to PAN-based fibres, Table 2.2 because of the way these planes are oriented. This can be observed in the SEM images from Sarafova [40], Fig. 2.2. For a pitch-based fibre (Dialed K63712) a radially orthotropic structure, see Fig. 2.2 (right), can be observed while for a PAN based fibre (Panex 35), Fig. 2.2 (left) the structure is anisotropic with graphite planes formed in the right side and a disordered area in the left side [40]. Besides the influence on the mechanical properties the precursor material affects the electrical and thermal response [41].

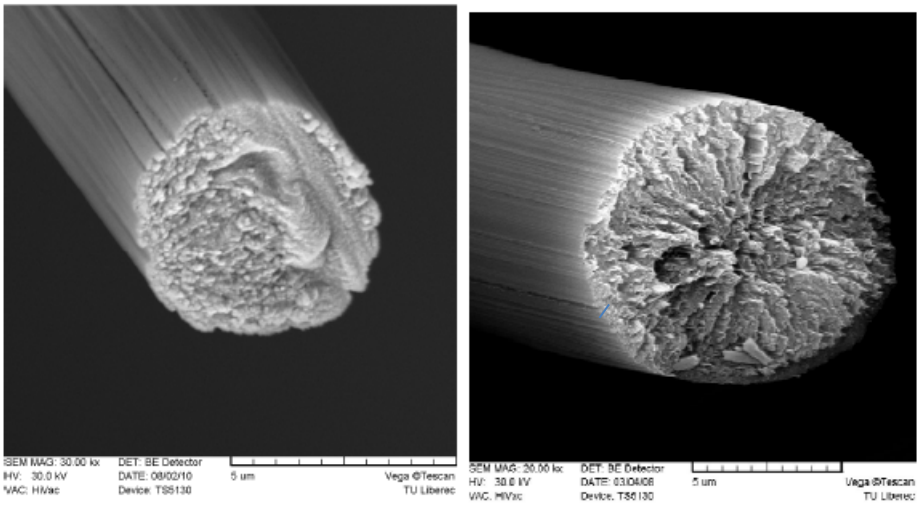

Figure 2. 2: Zoltek Panex 35 (PAN) (left) and Dialed K63712 (Pitch) Mitsubishi (right)

2.2.1.1 Electrical properties of carbon fibres

The crystalline planes of carbon fibres, i.e. the basal planes, are similar to graphite (Fig. 2.3) in which each of the carbon atoms forms 3 covalent bonds at a 120^{o} angle each, overlap of sp^2 hybridized orbitals. The fourth electron is able to form a π–bond with any of the other three surplus electrons so it is considered as delocalized. This freedom in movement can be considered as a kind of metallic behaviour which imparts the high electrical conductivity [31], [41].

As mentioned previously carbon fibres manufactured from different precursors (PAN, pitch and cellulose) exhibit differences in their crystalline structure that affects their electron conduction.

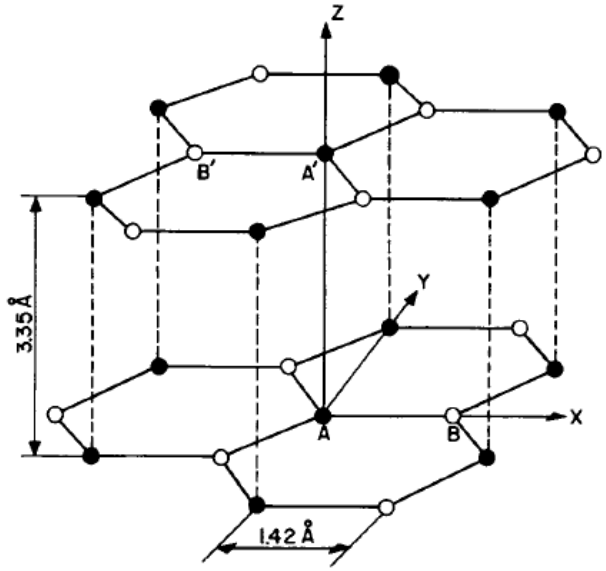

Figure 2. 3: Crystal structure of graphite [31].

Pitch based fibres exhibit both higher electrical and thermal conductivity compared to PAN-based fibres [41], [42], see Table 2.2. By comparing Panex 35 with Granoc CN-80 fibres it is evident, Table 2.2, that pitch-based fibres exhibit significantly lower resistivity, approximately 3 times. This is attributed to their radially orthotropic structure.

Table 2. 2: Physical properties of various PAN and Pitch based carbon tows, table adapted from

Name	Producer	Precursor	Density [g/cm^3]	Tensile Modulus [GPa]	Electrical resistivity [mΩcm]
IMS60E13 24K	Toho Tenax	PAN	1.80	290	1.45
UTS50F13 12K	Toho Tenax	PAN	1.79	240	2.05
Celion 3000	Celion Carbon Fibers	PAN	1.78	230	1.82
Celion 6000	Celion Carbon Fibers	PAN	1.78	230	1.82
Dialed K63712	Mitsubishi	Pitch	2.12	630	0.66
Granoc CN-80	Nippon	Pitch	2.17	780	0.5
Panex 35 50K	Zoltek	PAN	1.81	242	1.55
T700S	Toray	PAN	1.80	135	1.60

2.2.1.2 Thermal properties of carbon fibres

A collection of available literature values for the transverse thermal conductivity can be found in Table 2.3. The thermal conductivity of carbon fibres is directly linked with their structure and intrinsic defects. Depending on the precursor material, PAN, pitch and rayon, the thermal conductivity along the fibre axis can range from 7 W/mK (PAN-based T300) up to 1100 W/mK (pitch based K1100), see Table 2.3. The advantage of thermal conductivity characterization is that unlike

electron microscopy techniques, i.e. a localized view, it provides results for the bulk of the fibre [41], [43]. Because of the structure of carbon planar layers, the conductivity perpendicular to the fibre is significantly lower compared to the parallel axis. This can be verified by comparing two common types of PAN (Toray T300) and pitch-based fibres (Tonen FT700). Rolfes [44] reported that the conductivity in the parallel axis is 7 W/mK and 360 W/mK, and in the transverse direction 2 W/mK and 2.4 W/mK, for PAN and pitch fibres, respectively. Although thermal data for the fibre direction can be found in the literature and for several types of carbon fibres for a wide range of temperatures [45], [46], there is a shortage of available data regarding the thermal conductivity values in the transverse direction, and the data available is typically supplied by the fibre manufacturers without specifying if these values were obtained from physical experiments, or if they are based on estimates obtained from calculations. It has been suggested that the fibre transverse direction has a similar structure as the transverse direction of a single crystal pyrolytic graphite, and thus would have a thermal conductivity value of around 2.39 W/mK [47], [48]. It has also been reported that PAN-based fibres exhibit an isotropic structure, and thus their transverse thermal conductivity is similar, if not identical, to their longitudinal thermal conductivity [49], [50]. As seen in Table 2.3, the reported values of the thermal conductivity of the fibres in the transverse direction exhibit a wide scatter. However, the highest values observed, 7 W/mK, cannot be considered reliable as they cannot be correlated with the out-of-plane thermal conductivity values of CFRP laminates, see section 2.3.4. Knowing the transverse conductivity value is essential for the development of reliable models, as it can greatly affect the model predictions.

Table 2. 3: Carbon fibre thermal conductivity values (transverse direction).

Fibre type	Thermal conductivity (transverse) (W/mK)	Reference
T300	1.178	[51]
T700	1.256	[51]
T300	2	[44]
T300	0.8	[52]
T300	2	[53]
Not specified	0.915	[54]
FT700	2.4	[44]
TR50S	7	[50]

Carbon fibres also exhibit a temperature dependency of the thermal conductivity [41], [46]. After characterizing single carbon fibres from PAN, pitch and rayon, Pradere [55] verified the classification based on the precursor material. From the results depicted in Fig. 2.4 it is observed that rayon-based fibres (TC2 fibres) exhibit the lowest values followed by the PAN based (P33) and

pitch based (P100) material systems. This can be explained based on the larger crystallites and carbon plane structure that pitch based fibres exhibit compared to the other types [38], [46]. The influence of temperature is even more evident at lower temperatures. Measurements conducted by Heremans [46] between 10K -370K on single fibres, Fig. 2.5, showed a similar classification based on the precursor material.

A parameter that has shown to have a great influence on the thermal conductivity of carbon fibres is heat treatment they have undergone, also known as graphitization [31]. By exposing carbon fibres to higher temperatures than during the carbonization stage, up to 3000°C, small turbostratic crystallites are ordered and oriented in the direction of the fibre axis. This process allows for higher thermal conductivities and Young's modulus to be achieved [32], [43].

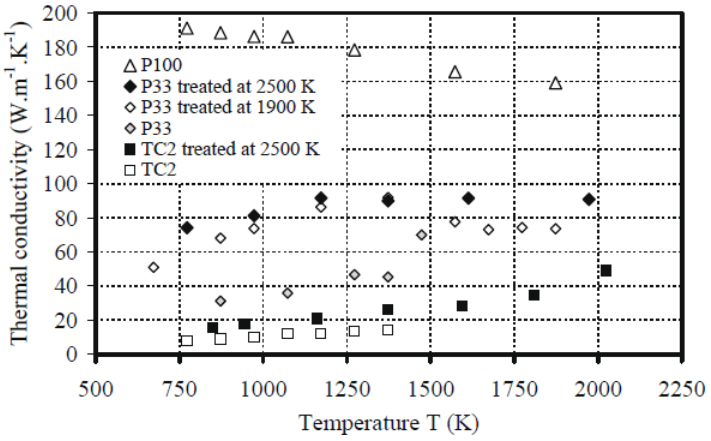

Figure 2. 4: Thermal conductivity versus temperature for several types of carbon fibres [55].

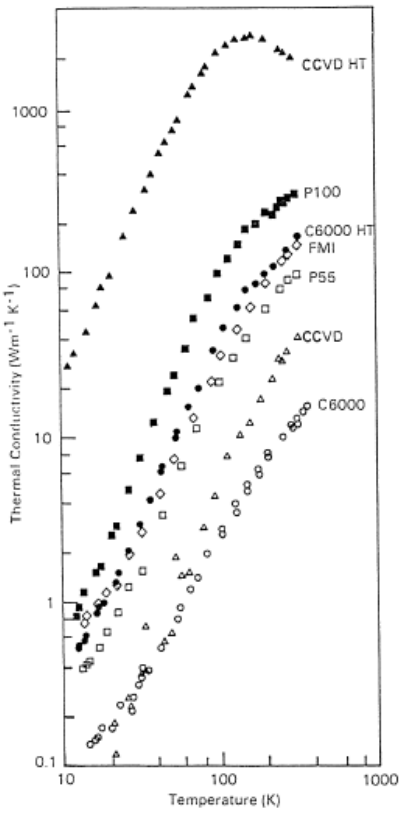

Figure 2. 5: Log-log plot of the temperature dependency of thermal conductivity for various carbon fibres [46]. (Vapor grown: CCVD, CCDC HT, Pitch: P-55, P100 and PAN: FMI, C6000)

2.2.2 Epoxy resins

Epoxy resins are among the most commonly used thermosetting (or just thermoset) polymer systems. Due to their low density, good mechanical properties and excellent adhesive properties, they are used for a wide range of applications from marine, automotive, aerospace and electrical as well as chemical and food packaging [56]. Their use as a matrix material in fibre reinforced laminates has enabled significant improvements in the development of lighter civilian and military aircrafts as well as higher rated power wind turbines allowing the production of lighter and longer blades [10].

2.2.2.1 Electrical properties of Epoxies

The insulating properties of epoxies have made them among the most used thermoset polymers for high voltage applications. The breakdown strength can reach values of 120kV/mm and epoxies are considered as excellent dielectric materials with a relative permittivity between 3 -5 [57]. Their electrical conductivity can range from 10^{-17} S/cm up to 10^{-14} S/cm depending on their chemical structure and the additives added [58].

2.2.2.2 Thermal properties of Epoxies

The most commonly used epoxies are amorphous materials, and because of their disordered structure the heat transfer mechanism differs from other semi-crystalline polymers and metals [59], [60] . In amorphous polymers the molecular chains are not aligned or arranged into a network or a single direction, the randomly positioned chains contribute to high thermal resistance resulting in low heat diffusion rates and low thermal conductivity [59], [60]. The most commonly used epoxy thermosets (DGEBA etc.) exhibit thermal conductivity values in the range from 0.1 W/mK up to 0.3 W/mK [59]–[61]. More advanced thermoset systems containing liquid crystal domains have shown significantly higher thermal conductivity values, up to 1 W/mK [62]. However, they do require complicated synthetic routes as well as high cost thus impeding their commercialization [60], [62].

2.3 Properties of CFRP

2.3.1 Electrical properties of CFRP laminates

When subjected to DC current, the low specific resistivity of carbon fibres and the insulating character of the polymer matrix indicates that the conduction in the longitudinal direction of unidirectional composites, see Fig. 2.6, is governed by the properties of the fibres [63], [64].

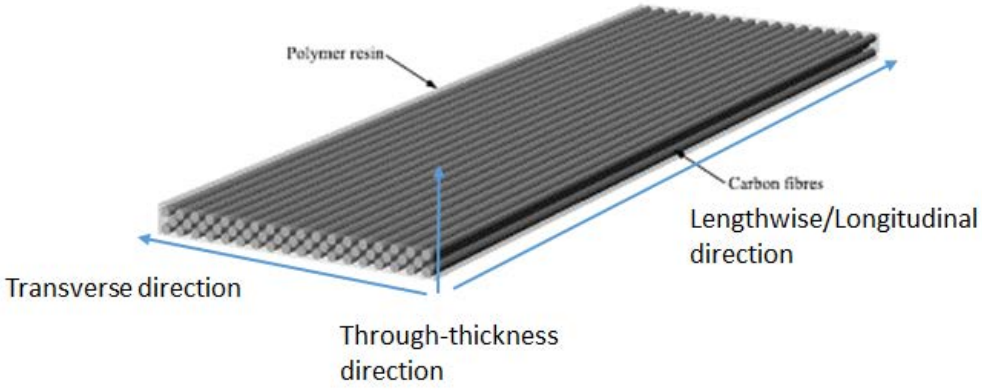

Figure 2. 6: Nomenclature of axis for a unidirectional laminate.

Fibre to fibre contact points is the predominant conduction mechanism in the transverse and through thickness directions, Fig. 2.7, since in these directions the polymer matrix creates charge barriers. The only parameter that has an impact at the properties in these directions is the fibre volume fraction, Fig. 2.8, since it regulates/controls the fibre to fibre contact points, a detailed explanation can be found in the next paragraph and [65]–[67].

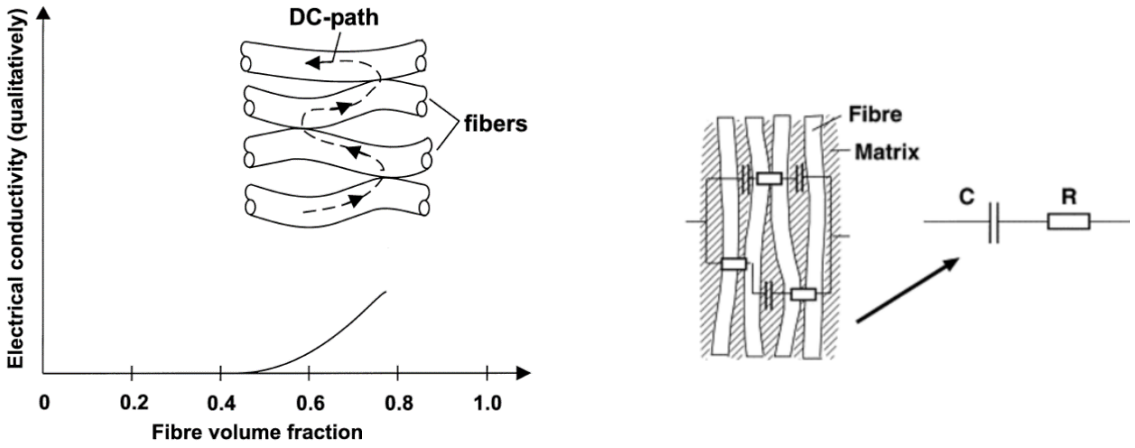

Figure 2. 7: Impact of fibre volume fraction at the transverse conductivity and equivalent circuit [68]

At this point it is considered appropriate to introduce the term *percolation threshold*. The electrical performance of material systems consisting of a polymer matrix, insulator, and a conducting reinforcing phase, such as carbon fibres, is governed by the filler content and the electrical conductivity of the filler [69]–[71]. In general, at low filler/reinforcement concentrations the composite exhibits an insulating behaviour, but as the filler content increases an insulator to conductor transition can be observed. This transition occurs at a critical conductive filler concentration value, also known as the *percolation threshold*, and it is represented by a sharp increase of the conductivity [35], [67], [70]–[72]. As reported by Kupke and Rimska [67], [70], the increase of the fibre volume fraction results in an increase of the number of fibre to fibre contact points. This is attributed to the reduction of the insulation/separation caused by the existence of the polymer in between the fibres in the bulk material.

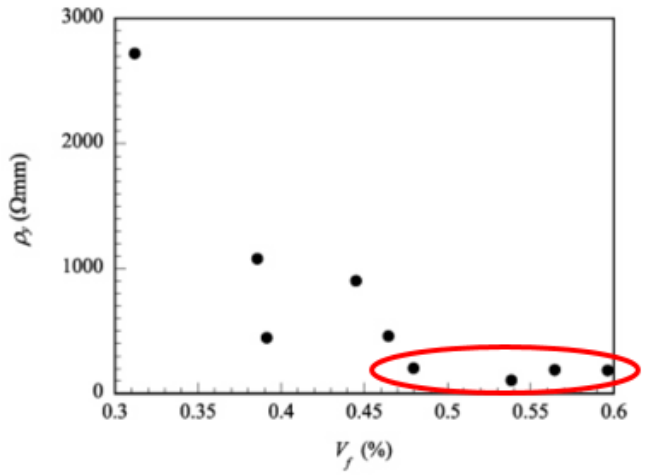

Figure 2. 8: Transverse electrical resistivity versus fibre content for unidirectional CFRP laminate, percolation values marked with circle [73].

To reach percolation in unidirectional CFRP laminates the required filler/fibre content is significantly higher as reported experimentally by Park [73]. As it seen from Fig. 2.8, the transverse electrical resistivity values decrease with the addition of carbon fibres. The resistivity attains a constant value above 48 % fibre volume content, thus reaching percolation. The observed discrepancies at lower fibre contents, around 39 % - 45 %, were quoted to be associated with issues during the manufacturing of the samples [73]. It should be noted that engineering CFRP composites exhibit fibre volume fractions above 50 %, thus they are in percolating state.

Depending on the type of fibres, the fibre volume fraction and the layup of the CFRP laminates, variations can be observed in the electrical conductivity values. As a general rule of thumb, for a unidirectional laminate, the electrical conductivity in the longitudinal direction will be of the same order of magnitude as the electrical conductivity of the reinforcement fibres, i.e. approx. 10^2 S/cm to 10^3 S/cm [74]. In the transverse direction the conductivity will typically be about 3 orders of magnitude lower, approx. 10^{-1} S/cm. For the through-thickness direction the existence of resin rich interlaminar regions between the plies increase the resistance, and the expected conductivity will be in range of about 10^{-2} S/cm [15], so an order of magnitude lower than in the transverse direction. Typical values for an aerospace grade unidirectional CFRP laminates are quoted in Table 2.4 from Hirano [16].

Table 2. 4: Electrical conductivity values of the HTA7/CIBA913 unidirectional CFRP with 58% fibre volume content [16].

Direction	Electrical Conductivity (S/cm)
Longitudinal	340
Transverse	2.08×10^{-1}
Through-thickness	2.5×10^{-2}

Unlike wind turbine blade spars, the majority of the research conducted has been focused on aerospace/aircraft applications [16], [75]–[80] where quasi-isotropic laminates are typically used, with stacking sequences utilizing ply stacks with 0º, 90º, -45º and +45º orientations. In such laminates, the conductivity is generally found to be lower compared to unidirectional laminate configurations in the fibre direction. This is attributed to the increased resistance which originates from the fibres in the 90º, -45º and +45º directions. In addition, it is known that aerospace grade CFRP laminates, usually prepregs, feature toughened interlaminar layers to increase the resistance to delamination [81]. These toughened resin interlayers, which serves to enhance the toughness and damage tolerance of the laminate, leads to increased through-thickness electrical resistance. Due to the wide range of available material systems, i.e. different resin/fibre combinations, stacking sequences and fibre volume fractions, the electrical properties of CFRP laminates can vary significantly, as reflected in the values listed in table 2.5. Although the longitudinal and transverse

electrical conductivities exhibit some consistency in the reported values, the through-thickness values show significant discrepancy, spanning over orders of magnitude even for identical laminate types. This can be attributed to either manufacturing, for instance different curing pressures for prepregs can affect the interlaminar regions, or errors during the measurements.

Table 2. 5: Directional electrical conductivity of CFRP composite laminates at room temperature, table adapted from [82].

Composite material type	**Electrical conductivity (S/cm)**		
	Longitudinal	Transverse	Through-thickness
IM600/133	293	0.787×10^{-2}	7.940×10^{-6}
IM600/133	359.7	1.145×10^{-2}	3.876×10^{-5}
G0986/RTM6-2	146.31	N/A	2.700×10^{-2}
T700/2510	230.9	8.000×10^{-2}	1.1236×10^{-3}
T800/3900	165.8	1.028807×10^{-2}	8.4034×10^{-4}
IM7/977-3	396.8	1.964637×10^{-2}	3.22581×10^{-3}

2.3.2 Temperature dependency of electrical conductivity

It is expected that the electrical conductivities of CFRP materials will also depend on temperature. The polymer matrix in which the fibres are embedded plays a key role since at temperatures above the glass transition (T_g) internal changes in the macromolecular structure occur. When Epoxies pass from the glassy to the viscoelastic (rubbery) state, the internal free volume of the polymer increases and the main chains are able to move with a higher degree of freedom, thus allowing for an easier migration of charge carriers [70]. However, if an epoxy matrix enters the rubbery state it loses its ability to transfer mechanical loading, as it will no longer be able to act as the binding agent that holds the fibres together and allows for the load to be transferred to and between them. Therefore, the investigation of the temperature dependency of the electrical conductivities of CFRP at temperatures near or above the glass transition makes little sense, as the laminate will be damaged and not serving its structural purpose. Previous research confirms that the conductivity of CFRPs exhibit temperature dependency [80], [83], and as can be seen in Fig. 2.9 and Fig. 2.10 that this dependency exists both for DC and AC currents.

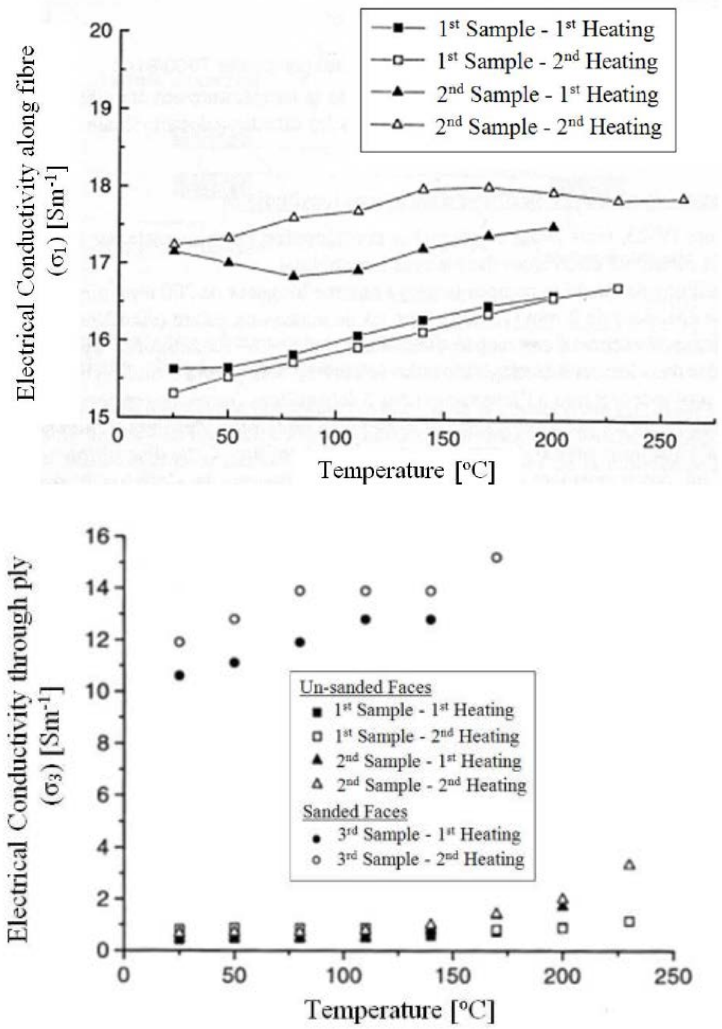

Figure 2. 9: DC Electrical conductivity versus temperature (top) in the longitudinal direction and (bottom) in the through-thickness direction [83].

From Uhlig's results [74], Fig. 2.9, it is seen that the DC conductivity of CFRP exhibits a slight increase with temperature, both along the fibre and the through-thickness directions. By observing the results for the longitudinal direction, Fig. 2.9 (top), where two runs were carried out for each of the two samples, a slight increase can be observed. Since the conductivity in the fibre direction is governed by the conductivity of the fibres, this increase can be attributed to higher electron mobility in the fibres which can be associated to the semiconducting behaviour of the carbon fibres. For the through thickness direction, Fig. 2.9 (bottom), significant differences were observed when the sample surfaces were sanded to remove the epoxy from the surface. The excess polymer layer in the surface of the sample acts as insulation, and as a result it has to be removed to establish direct electrical contact with the fibres to obtain accurate results. Therefore this insulating layer have to be removed and it cannot be considered as part of the sample during the measurements.

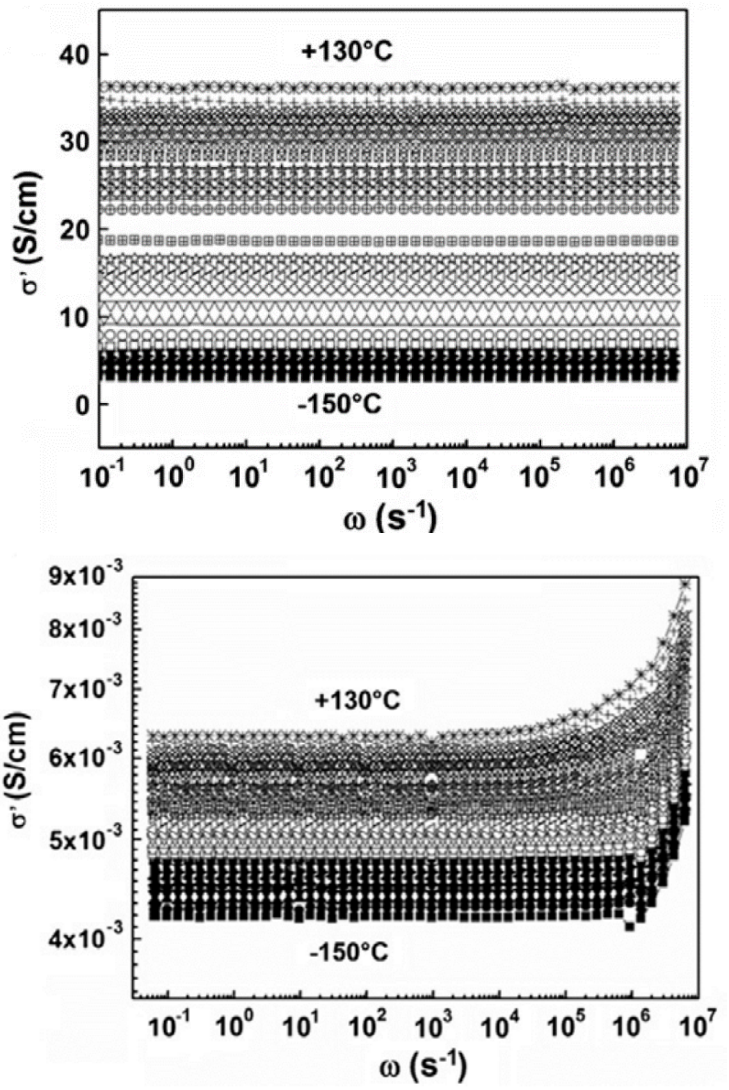

Figure 2. 10: AC electrical conductivity versus frequency at temperatures between -150°C -130°C (top) in the longitudinal direction and (bottom) in the transverse direction [80].

The AC conductivity of CFRP laminates was investigated by El-Sawi [80] by means of a frequency response analyser. By conducting isothermal frequency scans in the temperature range of -150°C to 130°C with a step of 10°C, see Fig 2.10, the temperature dependency/characteristics of the AC conductivities was extracted. The applied voltage was kept at 1V to avoid heating of the sample. From the results reported along the fibre direction, Fig. 2.10 (top), it is seen that the AC electrical conductivity does not exhibit frequency dependency. For the transverse direction, Fig. 2.10 (bottom), an increase of the conductivity values can be observed in the frequency range of 10^5 – 10^7Hz. However, it is known that frequency response analysers, like the one used in the study [80], exhibit a frequency limit at about 1 MHz (10^6 Hz) caused by parasitic inductance of the cable lines and connectors used [84]. Based on this the observed increase for the transverse direction, Fig. 2.10 (bottom), in the frequency range 10^5 – 10^7Hz, should not be taken into consideration. Based on these findings, CFRPs can be considered as a resistor in the frequency range investigated.

2.3.3 Influence of mechanical load on electrical properties

The electrical resistance of CRFP materials also depend on the (mechanical) strain, and this phenomenon is known as piezoresistivity [85], [86]. This underlying mechanism/principle behind this is that when a unidirectional CFRP laminate is subjected to uniaxial tension, the fibres will tend to try to stretch and align themselves because of the stress that is applied to them, Fig. 2.11. This leads to mitigation of fibre to fibre contact points, which in principle can affect the transverse direction conduction mechanism. Piezoresistivity can be expressed as the relative change of the resistance of the sample, eq. 2.1 [85].

$$\frac{\Delta R}{R_0 \varepsilon} = 1 + 2\nu \qquad \text{eq. 2.1}$$

where ΔR is the increase in resistance caused by the application of a strain ε (this part of the equation is also known as gauge factor), R_0 is the resistance at zero strain, and ν is the Poisson's ratio.

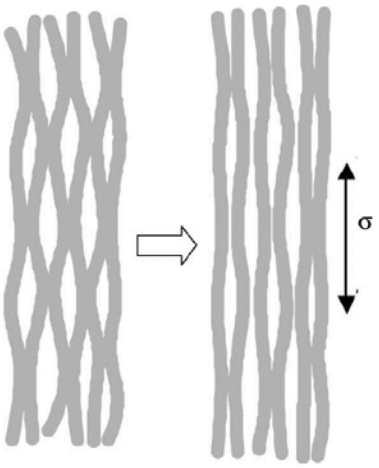

Figure 2. 11: Schematic representation of the effect of mechanical load at the fibre to fibre contact points [87].

By taking advantage of this property Baron and Schulte [88] introduced the Electrical Resistance Change (ERC) method for monitoring the fatigue behaviour of CFRP. Internal changes to the conducting network such as delaminations and fibre breakage can be quantified through changes in the resistance of the sample. Several researchers have adopted this technique [89]–[92] and several variations of have been developed, but the fundamental principles remain common for all reported investigations; conducting electrical resistance measurements while the sample is undergoing mechanical deformation. An increase in the measured resistance during static or dynamic loading is associated with the formation of either fibre breaks or delaminations.

Considering the scope of this part of the literature review, i.e. with a focus on understanding the electrical conduction mechanism in CFRP and how it would be affected by mechanical deformation, it is clear although changes of the electrical resistance when loading is applied occur, the difference/change is marginal compared to the resistance of an unloaded sample. In practical engineering laminates, with fibre volume fraction between 50%-70% [93], the percolation threshold has been surpassed significantly. Thus, the number of fibre-to-fibre contacts create a complex 3D network within the laminate that in reality cannot be disrupted. Since fibres are not perfectly straight and a certain waviness is created due to the manufacturing process, the contact points between the fibres cannot be eliminated [94]. Hence, at high volume fractions, the transverse and out-of-plane conduction mechanisms will not be affected by the applied load, thus the electrical performance of the laminate is not altered.

2.3.4 Thermal conductivity of CFRP laminates

The properties of fibre reinforced composites exhibit significant variation depending on their constituent materials, fibre orientation, stacking sequence and fibre volume fraction [95]–[97]. The same applies for the thermal conductivity of CFRP [39]. Due to the widespread and increasing use of CFRP materials for aerospace applications the thermal response of these materials has been the focus of significant scientific interest. The use of CFRP composites in areas such as leading edges of wings, and the inlet or exhaust areas for gases in jet engines, require effective heat dissipation since localized thermal loads are generated in the vicinity all such locations [98], [99]. The range of the thermal conductivity of a CFRP laminate depends on the longitudinal thermal conductivity of the carbon fibres used, as well as the thermal conductivity of the polymer matrix. As presented in section 2.2.1.2, the fibre thermal conductivity can range from 7 up to ~1000 W/mK. The thermal conductivity of CFRP follows a similar anisotropic behaviour as exhibited by their electrical conductivity but to a lower extent, see Table 2.6. As a general rule of thumb for a CFRP unidirectional laminate the conductivity in the fibre direction can reach values of the same order of magnitude as the reinforcement fibres [42]. In the transverse and through-thickness directions the fibre volume fraction and the properties of the polymer matrix in conjunction with the fibre orientation lead to lower values. Akin to the through-thickness electrical conductivity, the polymer rich interlaminar regions reduce the ability to dissipate heat through the bulk of the laminate.

Table 2. 6: Physical properties of the IM600/133 quasi-isotropic CFRP, transverse thermal conductivity value is not measured [77].

Direction	Thermal Conductivity (W/mK)	Electrical Conductivity (S/m)
Longitudinal	11.8	29.3
Transverse	(0.609)	$7.78*10^{-4}$
Through-thickness	0.609	$7.94*10^{-7}$

As the out-of-plane properties of composite laminates are of key importance during for many applications, in the forthcoming part if the literature review the main emphasis will be placed on the through-thickness direction data that are reported in literature. In Table 2.7 the through-thickness thermal conductivity values are presented for CFRP laminates for a range of fibre volume fractions. As seen, no direct correlation between fibre volume fraction and the thermal conductivity can be observed. This is mainly due to differences in the manufacturing process and properties of the matrix, fibre properties do not contribute significantly in this direction. Laminates manufactured by means of vacuum infusion and prepreg show higher values since better compaction can be achieved [49], [100], [101], while laminates manufactured by a hand layup process can exhibit considerably lower thermal conductivities because of possible air voids and lower compaction rates. Furthermore, the thermal conductivity of the polymer matrix clearly affects the measured values since it can vary from 0.1 to 0.3 W/mK. Altering the processing parameters has also been reported to influence the through-thickness thermal conductivity. Specifically, Han [50] reported that increasing the curing pressure from 0.1 to 2 MPa can increase the thermal conductivity up to 60% in PAN-based prepregs. By increasing the curing pressure, a reduction in the interlaminar distances and lamina thickness can occur, which again alters the out-of-plane heat conduction process.

Table 2. 7: Through-thickness thermal conductivity

Laminate type	V_f (%)	Thermal conductivity (Through-thickness) (W/mK)	Reference
TR30S/Epoxy	48.5	0.742	[49]
T300/Epoxy	58	0.65	[100]
SIGRAFIL CE 1222-255-37	63	1.04	[101]
Unspecified	Unspecified	0.54	[102]
SigmaTex 199/Epoxy	45	0.38	[103]
T300/RTM-6	55.3	0.755	[53]

Regarding the transverse direction thermal conductivity, little measured data has been published, with literature values most often assuming that the transverse thermal conductivity is equal to the through-thickness conductivity, as seen in Table 2.6 [77]. This assuming is reasonable to make for unidirectional laminates, where fibres are perpendicular to the heat flow direction, but the assumption is less meaningful and probably incorrect for cross-ply or quasi-isotropic laminates where reinforcement fibres can be found parallel to the heat flow thus facilitating heat conduction.

Measurements in the out-of-plane direction (through-thickness) for a unidirectional laminate were carried out by Rolfes [44] for two fibre volume fractions, 44.7% and 64.3%, respectively, and at two different temperatures, 30°C and 120°C, respectively, see Table 2.8. It is observed laminate with the higher fibre volume fraction exhibits higher values of thermal conductivity.

Table 2. 8: Transverse thermal conductivity of unidirectional laminates at different temperatures [39].

Fibre volume fraction	k (W/mK) T=30°C	k (W/mK) T=120°C
44.7%	0.484	0.528
64.3%	0.708	0.808

An increase of the thermal conductivity values with temperature was reported both by Sweeting [104] as well as Rolfes [44] for laminates with fibre volume content ranging from 45 vol% to 65 vol%. From the results in Fig. 2.12 it is seen that the thermal conductivity in the longitudinal direction exhibits higher values compared to the through-thickness direction, as the considerably higher thermal conductivity of the fibres dominate the conduction process. Usually the longitudinal direction values are of a similar order of magnitude as the thermal conductivity of the fibres. The increase with temperature is greater for the in-plane direction since phonon conduction is facilitated along the carbon basal planes through the crystalline structure of the fibres [105]. In both directions the dependency from temperature is linear and the increase is not substantial.

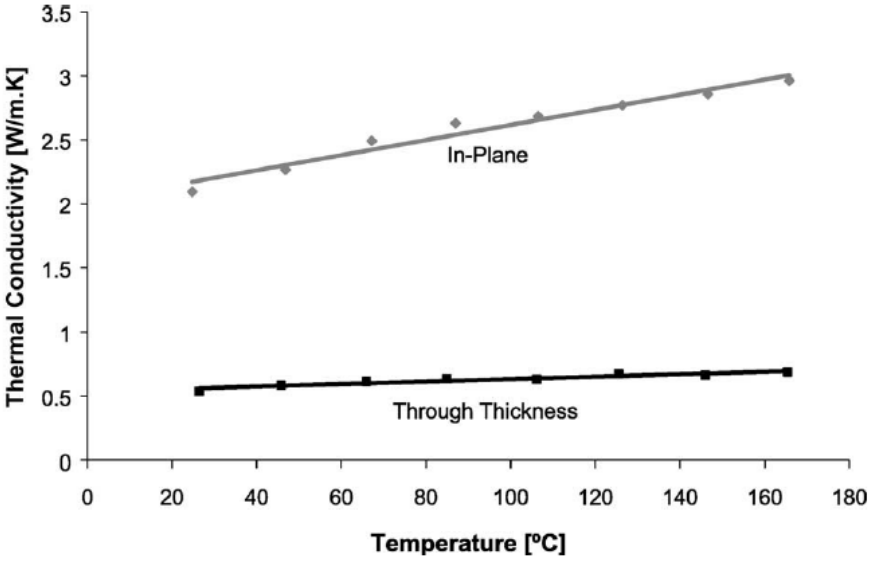

Figure 2. 12: Thermal conductivity versus temperature for the longitudinal and the through-thickness directions [104].

2.4 Nanoreinforced laminates-Multiscale composites

In recent years, several approaches have been proposed to improve the mechanical properties of CFRP materials and to add functionality to composites using various conductive fillers [106]–[109]. These include enhancing the electrical and thermal properties, as well as the stress transfer between the matrix and carbon fibre and the fracture toughness of the material. The key objective behind the addition of conducting fillers/inclusions into the bulk matrix of composite laminates is to interconnect the adjacent laminae with the addition of a secondary conducting phase, aiming to facilitate heat and electrical current conduction from one lamina to another, and simultaneously provide resistance to delamination.

Parameters such as the interlaminar polymer region and the sizing system have been identified as factors that affect the conduction process either between the laminae (plies) or adjacent fibres [101], [110], [111]. Hence, efforts have been focused on improving either the surrounding polymer matrix or the interface between the fibre and the matrix. Different methods for improving the conductive performance have been proposed, which show promising results including the incorporation of nano-fillers in the bulk matrix [80], [109], [112], grafting on the surface of carbon fibres by adding nano-inclusions into the sizing [107], [108], [110], growing nano-inclusions directly on the carbon fibre surface through chemical vapor deposition (CVD) process [63], electrophoretical deposition of the filler on fabrics [113], and nanostructuring in the interlaminar region [101], [114]. To showcase these different methods of adding a nanofiller into a fibre reinforced laminate Fig. 2.13 was created. Consequently, a new category of composites have been created in which the

reinforcing phase exists in different shapes and sizes. Such “multiscale” composites in some cases have been shown to exhibit superior performance compared to conventional laminates, as with the addition of this secondary reinforcing phase, better electrical, thermal and mechanical properties can be achieved, which in turns enables the use of polymer composites in new applications [91], [115], [116].

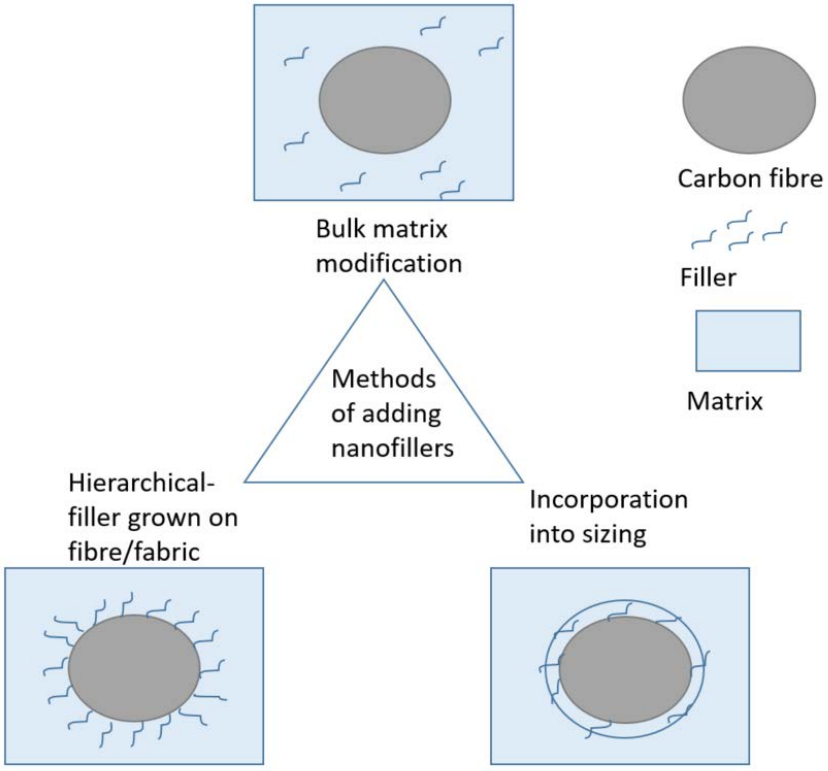

Figure 2. 13: Schematic of most common methods of incorporating a nanofiller into FRP laminates.

2.4.1 Manufacturing related challenges

Several methods can be used to produce multiscale composites as discussed above. However, if multiscale composites are to be utillised in commercial applications, large scale production capability need to be developed. To achieve this, two distinctly different approached can be considered: either by incorporating the filler into the matrix, or the by incorporating the filler into the fibre reinforcement/reinforcement fabric. Composites where the filler has been attached to the fibre surface are often referred to as hierarchical [117]–[119]. Hierarchical composites are mainly manufactured by means of CVD or chemical grafting, but is some instances these methods are not practical, either due to the long processing time and at times potent reactions, or due to the high temperatures required that can increase the complexity and possibly damage to the fibre surfaces

[120]. The other route, also known as bulk matrix modification, appears to be a simpler process, but can introduce several new issues/challenges into the manufacturing of composites. The filler should be finely dispersed within the matrix, and although aggregates are a known problem for nanocomposite polymers, identifying a suitable dispersion method is often challenging as different methods can provide different results and are not always well suited for all filler types [56].

The incorporation of the filler onto the fibre/fabric surface is mainly achieved by modifying the sizing of the fibres, see Fig. 2.14, or by growing the filler to the fibre/s' or fabric surfaces via a deposition method, see Fig. 2.15. Qin [110] grafted graphene nanoplatelets (GNPs) on the fibre surfaces by adding the nanoparticles to the sizing agent of the fibre. Unlike methods in which the filler is grown on the fibre surface [121], usually with a CVD method , the modification of the fibre sizing is a relatively simple process and easily transferable to an industrial scale. By adding conducting fillers to the sizing, percolating effects can be achieved among adjacent fibres that can increase the bulk properties of the laminate. Using this approach, fibre tows with nanomodified sizing can be produced. However, if fabrics are to be weaved from this tow, it should be pointed out that this type of modified sizing might be partially removed from the fibre surface during the fabric weaving process, since one the roles of the sizing is to protect the fibre by acting as a lubricant between the fibre and the weaving machine [122], [123].

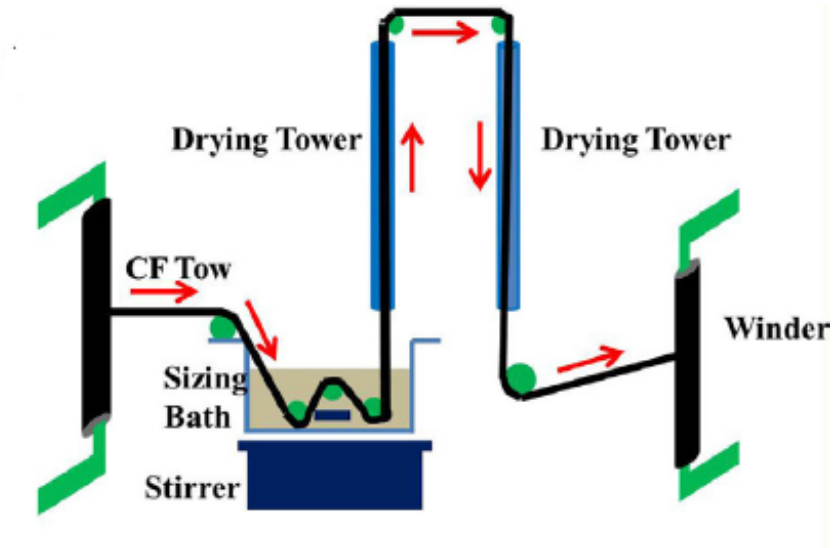

Figure 2. 14: Sizing process for carbon fibres [110].

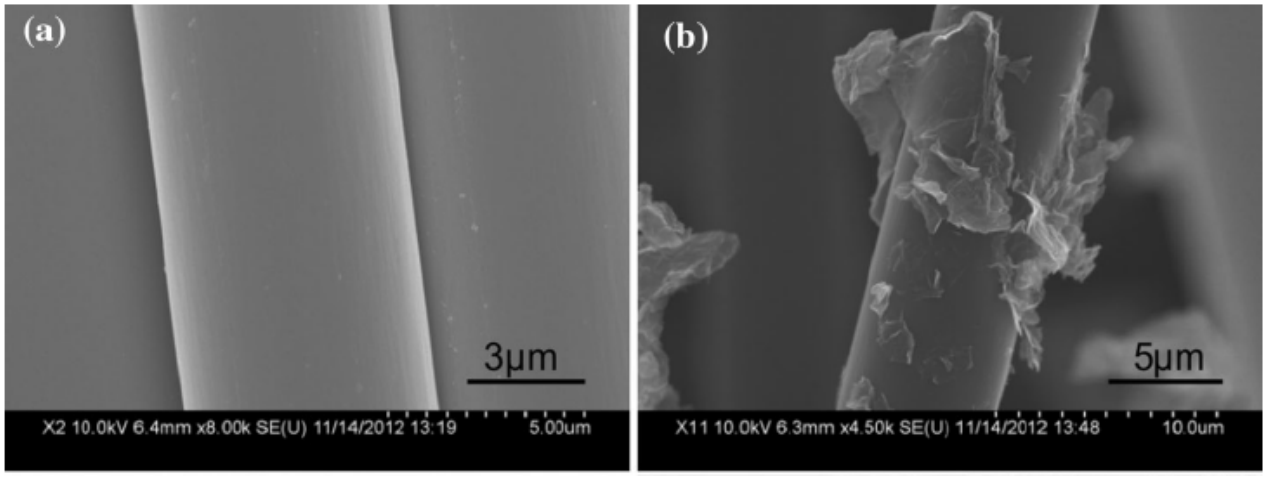

Figure 2. 15: (a) Single carbon fibre and (b) carbon fibre deposited with Graphene sheets [118].

A method that resembles the sizing modification is the electrophoretic deposition of the filler onto a fibre surface [124]. Here, a piece of fabric is submerged into a solution containing the filler, and subsequently the filler is being deposited to the surface of the fabric by applying a DC potential difference between the fabric and the solution. This method has provided promising results with CNTs [124], [125] and GO [126], although it requires a suitable filler that exhibits either ionic or cationic charging to be able to be migrate from the solution to the fibre surface. This can be achieved by functionalizing the filler prior to the deposition, albeit thus adding to the processing time. Growing the filler to the fibre, using a CVD process, almost exclusively used for CNTs, has been demonstrated by several investigations, and this has been applied to a variety of different fibres, from carbon [111] to alumina [127]. The main advantage of this method is that, since the filler is attached to the fibre, there is no need for the filler to be dispersed within the polymer matrix of the laminate, and consequently there is no need for functionalization to achieve a better distribution of the filler. Moreover, the viscosity of the matrix is reported not to be affected, which is crucial for the manufacturing process. However, it has been reported that utilising such (so-called) “fuzzy fibres” [127], [128], can lead to laminates with lower fibre volume fractions than conventional CFRP laminates (although exhibiting improved electrical and thermal properties), and also display detriments in the mechanical response of the laminate as well as damaged fibres [111], [129].

The bulk matrix modification represents a wide variety of lamination processes that are similar in the sense that they a polymer matrix is used in which a nanofiller is dispersed. Laminates can then be manufactured using in several ways, including but not limited to the hand layup process [109], vacuum infusion [130], [131] or prepregs [54], [132], [133]. Even though these processes may appear to be straightforward, the following aspects needs to be considered. The addition of a filler into the matrix can alter the curing characteristics of the polymer by reducing the processing time

and also alter its viscosity, thus hindering the lamination or infusion process [134]. This is heavily influenced by the filler content and the dispersion of the filler within the polymer matrix. Different method of dispersing the filler can create nanocomposites with different properties as the formation of aggregates can alter their properties. The most commonly used dispersion methods consist of solvent mixing, high speed mechanical stirring, three roll milling and ball milling, or a combination of them to name a few [56], [135], [136]. However, most of these methods exhibit limitations with regards to their applicability on an industrial level. Solvent mixing, which can provide composites with good dispersion, Fig.2.16, requires removal of the solvent prior to the curing process [137], [138]. In addition, the use of organic solvents such as acetone is often discouraged due to potential health risks as well as associated costs [139]. Furthermore, sonication (bath or tip/horn sonication) is employed to break the aggregates leading to increased temperature of the mixture, which in turns can decrease the viscosity of the mixture causing the precipitation of the nanofiller. Mechanical stirrers are being used in large scale production but can provide significant variation in the dispersion depending on the mixing speed and temperature of the mixture. Recently, planetary mixing has shown great potential in achieving fine distribution of the filler within the polymer while allowing industry level capabilities, Fig.2.16 [138], [140], [141]. This method introduces high shear forces into the mixture by means of a dual asymmetric centrifuge configuration. Due to the weak Van der Waals forces between the graphene sheets, this method is particularly effective in carbonaceous fillers.

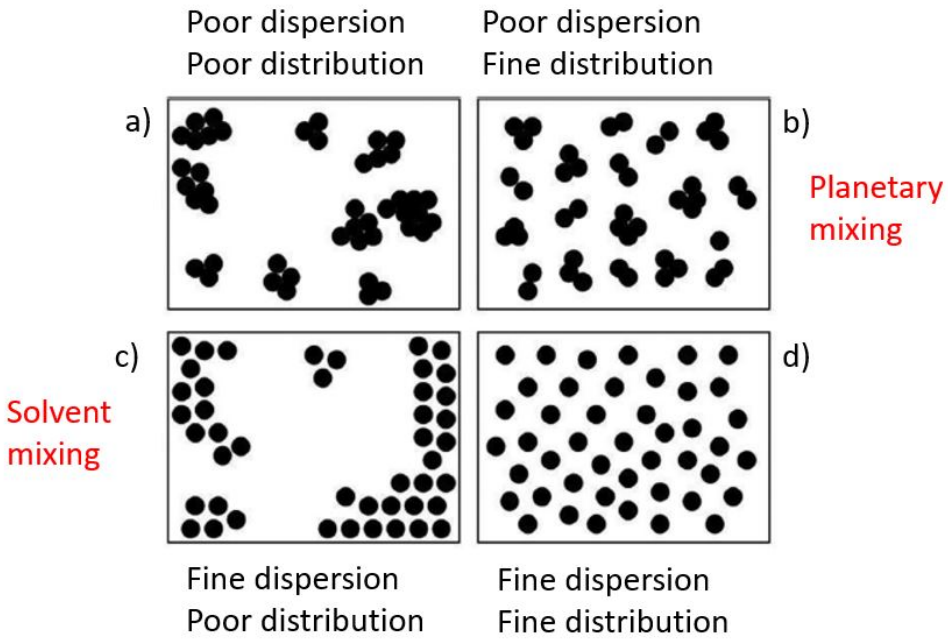

Figure 2. 16: Schematic representation of distribution and dispersion of a filler within a polymer matrix and the outcome (red letters) based on different manufacturing methods [136], [142].

Furthermore, a key differentiation with regards to the manufacturing of nanomodified FRPs is that aggregates can be formed during the consolidation of the nanocomposite matrix by the fibre tows. To overcome these issues, the filler is often functionalized to achieve a better dispersion within the matrix and to assure reduced aggregation [56], [130]. Moreover, graphene-based fillers are used (as is increasingly the case) in the form of platelets and their aspect ratio needs to be taken into account. Most commercially available graphene platelets exhibit lateral dimensions between 5 µm and 25 µm (as supplied by XG Sciences) making them suitable for uses in polymer nanocomposites and efficient in achieving low percolation thresholds, due to their high aspect ratios. However, these dimensions are making them prohibited in multiscale composites manufactured with bulk matrix modification, especially when the nanocomposite epoxy is infused into the fibres, as their diameter is similar to the average fibre diameter, 7 µm, increasing the possibility of inhomogeneous filler distribution in the bulk of the laminate [134]. Thus, a different class of platelets, with smaller lateral dimension, needs to be utilised in the manufacturing of multiscale composites.

2.4.2 Improving electrical and thermal properties

As mentioned in the previous chapter, the anisotropic electrical and thermal properties of CFRP materials introduce challenges in applications where these materials are subjected to electrical current flow or thermal loads [101]. While their mechanical properties can be tailored to meet mechanical performance requirements for a specific application to a certain extent, their poor electrical and thermal conductivities in the transverse and through-thickness directions impede their incorporation to designs/applications thermal and electrical loading phenomena are unavoidable [143]. The use of fibres with higher conductivity, like e.g. pitch-based CFRP, can provide improved electrical and particularly thermal performance along the direction of the fibres, but this does not address the inherent anisotropy of the CFRP laminate, since the insulating character of the polymer matrix governs this behaviour [39], [42]. Also, pitch-based CFRPs are significantly more expensive than PAN based CFRP, which for most applications renders pitch based CFRP of little interest. To overcome this issue, inclusions usually on the nanoscale, have been incorporated into CFRP laminates. While the addition of a nanofiller with high electrical or thermal conductivity compared to the polymer can provide some improvement, it does not ensure the same level of improvement of the electrical and thermal properties [61]. To enhance the thermal conductivity significantly requires very large amounts of filler to be added to the composite, and this in turn may have a negative effect of the mechanical properties, noticeably strength and fracture toughness. Thus, special consideration needs to be made to balance the electrical, thermal and mechanical response elements of the resulting CFRP composite material.

The majority of the research conducted regarding the electrical properties of nanoreinforced composite laminates concerns the out-of-plane properties. This is because the addition of a filler is not expected to alter or improve the conduction mechanism along the fibre direction. This line of investigation was pursued by among others Lin [144], were CNTs were grown via CVD on the fibre surface. The improvement of the longitudinal electrical conductivity of unidirectional and cross-ply laminates is reported to be 11% and 8%, respectively [144]. Similar behaviour was observed by El Sawi [80], when DWCNTs were used to impregnate carbon fibres, with nanoreinforced samples exhibiting electrical conductivity of 63 S/cm compared to 62 S/cm for unmodified CFRP. A similar response was also reported from Bekyarova [125].

The synergistic effects of a carbon based inclusions in conjunction with a metallic nanostructure have been investigated by Kandare [109]. An increase of up to 40% of the thermal conductivity in the through-thickness direction was observed when 0.95% of GNPs and 0.05% of silver nanowires (SnWs) were embedded in the epoxy. The addition of a metallic inclusion in conjunction with the formation of physical conducting paths can promote electron transport and contribute to the existing phonon based conduction mechanism. Similar behaviour was reported also for the through-thickness electrical conductivity for which an increase of approximately 75% was observed. An increase in the through-thickness electrical conductivity of approximately 3 times was reported by Qin [110] after adding 3wt% GnPs in the sizing solution, compared to the un-sized and the epoxy sized fibres.

The influence of MWCNTs and GNPs on the through-thickness thermal conductivity when added to the epoxy matrix was studied by Kostagiannakopoulou [54]. An increase of 48% was observed when 15 wt% of GNPs were added into the epoxy, while the addition of 3 wt% of MWCNTs resulted in a 5% reduction, showcasing that 2D fillers are more efficient in improving the properties, but also are more appealing from a processing standpoint. CNTs with their rod shape, exhibit the tendency to be entangled and form aggregates, and thus hindering both manufacturing and heat conduction processes. Another approach followed by Han [101] was to improve the properties of the interlaminar region with the addition of carbon black (CB) nanoparticles dispersed in an epoxy prepreg. An increase of the through-thickness thermal conductivity up to 210% was reported with the use of 0.8 wt% CB. However, it has to be pointed out that the measurements in this study were conducted in the temperature range of 73-95^{o}C. In addition, it was shown that by adding the filler directly to the interlaminar regions, a decrease in the interlaminar distances was observed, thus making it difficult to distinguish between the influence of the filler and the decrease of interlaminar region on the thermal conductivity. Further increase of the filler content were reported to decrease the conductivity values. The observed reduction is unexpected, since the addition of particles in higher contents should be expected to contribute positively to the phonon conduction mechanism,

especially for the case of fillers such as CB where interface resistance effects are negligible. Therefore, the reason for the observed lower conductivity values most probably can be attributed to poor dispersion of the nanoinclusions, leading to the formation of large agglomerates in the resin that can decrease the thermal conduction due to the increased interfacial resistance. The addition of GNPs at the interlaminar regions, by spray coating the carbon fabric with an epoxy/GNP mixture, was investigated by Wang [102]. The addition of 0.5 wt% of GNPs into the interlaminar regions of the laminate provided a 55.6% increase in the thermal conductivity as well as a 24.5% increase in the ILSS.

It becomes apparent that conductive fillers although provide improvements in the overall performance of the laminates, by increasing the though-thickness properties, they have not been able to provide laminates with isotropic electrical and thermal properties, i.e. increasing the out-of-plane and transverse properties to values similar to the ones exhibited along the fibres, approx. 200 S/cm for electrical conductivity and 3 W/mK for thermal conductivity. Albeit similar values to these have been achieved with polymer nanocomposites [56], this increase in properties have not been able to be transferred to multiscale composites. While in nanocomposites a continuous network is formed within the polymer, in multiscale composites the fibres disrupt its formation and allow only a partially developed network to be formed, usually between plies. Furthermore, the influence of conducting inclusions on the transverse direction conduction has not been extensively investigated, thus it is not clear how improvements in through-thickness direction affect the conduction process parallel to the fibre axis.

2.4.3 Mechanical response of multiscale composites

A key aspect that has to be included in the consideration when adding additives in the form of nanoinclusions to FRPs is not to compromise the mechanical properties of the composite material. In unidirectional laminates the interfacial adhesion between fibre and matrix is very sensitive to the addition of a filler to the matrix, and this plays a very important role in defining the strength of a composite laminate, as it determines the load transfer between reinforcement fibres and polymer matric. A simple method of estimating the interfacial adhesion between fibre and matrix is the measure the interlaminar shear strength (ILSS) [110]. In conjunction with measurements of the ILSS, the 90^{o} flexural strength have also been identified as an additional measure for assessing the interfacial adhesion [99], albeit it should be noted that the flexural strength provides a less obvious or direct assessment method, In fact the concept of flexural strength is somewhat controversial, as it does not really provide a rigorously defined and clearly defined material property, but is rather to be seen as a superficial measure that can be used for comparative purposes only.

Due to the very large number of studies that have been conducted to investigate the mechanical response of composite laminates that have been reinforced by the use of various types of nanoinclusions, it is infeasible to present a complete summary. Instead, in the following section a collection of studies that are more relevant to the research presented in this thesis will be presented.

Qin [110] reported, Fig. 2.17, a significant increase in the flexural strength of the composite laminates with reinforcement carbon fibres containing GnPs in their sizing compared to conventionally sized an un-sized fibres. A similar contribution from the nanofiller was reported for the flexural modulus.

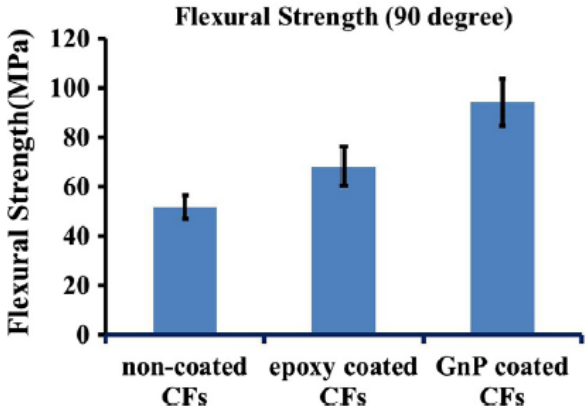

Figure 2. 17: Transverse (90°) flexural (left) strength of un-sized (non-coated), sized (epoxy coated) and GnP sized UD composites [110].

A similar trend was observed in a study by Chen [145], Fig. 2.18, where the ILSS was measured for CFRPs containing graphene nanosheets/platelets. An improvement up to 28% with 1wt% filler content was recorded compared to the baseline composite. Further increase of the filler content, up to 1.5wt% and 2wt%, resulted in the formation of agglomerates leading to a decrease of the shear strength. It should be noted that while the strength decreases compared to the sample containing 1wt%, it still remains higher compared to baseline composite.

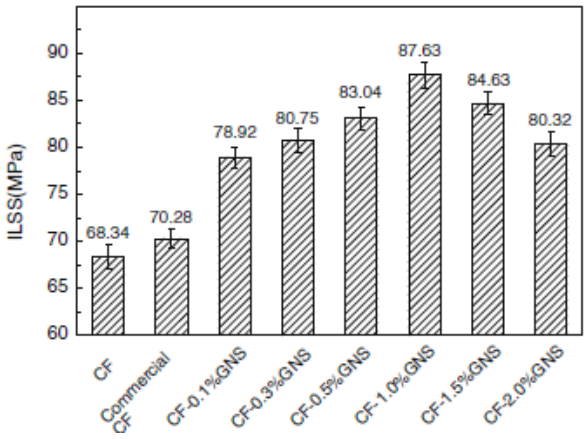

Figure 2. 18: ILSS of unidirectional laminates versus content of GNS (Graphene Nano Sheets) [145].

Considering that not many composite structure for engineering applications can be design safely based on the assumption of static loading conditions, the fatigue response is also a key indicator for whether nanoinclusions can provide improvements in the overall performance of FRPs. The influence of graphene platelets on the fatigue performance of GFRP subjected to bending loading was investigated by Yavari [119], where the filler was added to the composite through bulk matrix modification. An increase of more than three orders of magnitude of the fatigue life of GFRP laminates loaded in flexural bending was observed when adding 0.2wt% of graphene to the epoxy matrix. This is attributed to the toughening of the fibreglass/epoxy interfaces because of the addition of graphene, thus preventing the delamination and delamination driven buckling of glass fibres under compression.

Overall, the literature survey provides a clear indication that the addition of graphene-type nanoinclusions appears not only not compromise the mechanical properties and in particular the strength, but also to enhance the fibre/matrix adhesion, and thus improving the overall mechanical response characteristic of composite laminates. However, a clear dependency on the filler content is reported, with low filler contents observed to be more efficient in improving the strength. This can be seen to encourage the use of nanoinclusions in applications where enhanced electrical and thermal properties are required, by also taking into account the potential advantage with respect to improved mechanical properties.

2.4.4 Graphene Oxide as a filler

Carbonaceous inclusions, like e.g. Carbon NanoTubes (CNTs) [80], [121], [131], [146], Carbon Black (CB) [101], Graphene NanoPlatelets (GNPs) [109], [114], [147] and Carbon NanoFibres (CNFs) [148], have been investigated as potential fillers in nanoreinforced laminates. It has been observed that

fillers with high aspect ratios, rod/wire like shapes or platelets/ellipsoids are the most well-suited, since they can interconnect adjacent fibres and adjacent laminae in the composite system, thus facilitating both current flow and heat dissipation into the laminate bulk [61]. However, most of the studies conducted thus far suffer from manufacturing related issues, specifically regarding the successful dispersion of the filler into the polymer matrix. Several manufacturing approaches have been suggested to overcome this issue, usually by chemically modifying the filler to achieved better dispersion [149].

Graphene Oxide (GO) is a 2D material with a similar structure to graphene. It is produced by the oxidation of graphite; hence, the produced sheets are covered with oxygen, see Fig 2.19. Due to its chemical structure, with hydroxyl and epoxide groups on its basal plane and carbonyl and carboxyl groups on the sheet edges, GO is highly compatible with epoxies, unlike graphene, which tends to form agglomerates due to intermolecular Van der Waals forces [56], [150], [151]. These functional groups are also responsible for excellent dispersion in water polar solvent and polymers which in turns allows the preparation of nanocomposites as well as the production of GO in high volumes [152]. The presence of oxygen groups also affects the mechanical and electrochemical properties of GO, unlike graphene, thus opening up the possibility for achieving tuneable or tailored properties. Furthermore, for the specific case of epoxy resins, the most commonly used type of thermosetting polymer, Rafiee [153] reported that GO is more efficient in improving the mechanical properties of epoxies compared to CNTs, as a better interfacial adhesion between the matrix and the filler can be achieved due to the aforementioned functionalities [154].

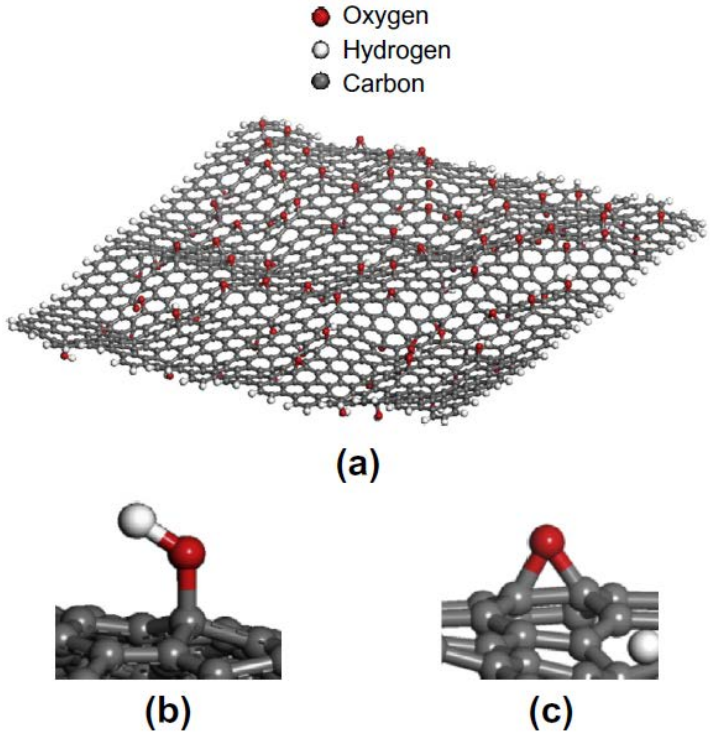

Figure 2. 19: (a) Structure of GO, (b) Hydroxyl group and (c) epoxide group [155].

Although GO appears as a promising nanofiller candidate sytem, the C/O ratio of GO potentially can affect its electrical and thermal properties, and, therefore, a balance must be established if both good dispersion and improved conductive properties are required [156], [157]. For GO filler systems, the oxygen content represents impurities in the crystalline structure of the filler, and these can greatly affect the thermal conductivity of the filler itself [156], [157]. Molecular dynamics simulations have shown that the thermal conductivity of GO can be reduced down to 8.8 W/mK when the oxygen coverage is close to 20% [157]. Similar results were reported after characterizing the thermal conductivity of free-standing GO films. However, annealing of GO at temperatures up to 1000^{o}C has shown a substantial increase in the thermal conductivity from 3 W/mK to 61 W/mK [156].

2.5 Emerging applications of nanoreinforced CFRP composite materials

2.5.1 Lightning strike protection

As CFRPs are being increasingly used for structural applications in the aerospace, transportation and energy (mainly wind turbine blades) sectors, new challenges have emerged regarding their performance in applications were electrical current is introduced into the composite structure.

Modern aircraft comprise larger amounts of composite materials than in previous decades, with CFRPs being incorporated for fuselage, wings, tail, and door structures, as well for interior panelling, braces and supports [11]. The latest generation of wide body civil passenger aircraft, like the Boeing 787 (Dreamliner) and the Airbus A350, CFRP composites represent around 50% of the airframe mass [11]. Unlike traditional engineering metal alloys, the anisotropic properties and also relatively poor conductivities of composite materials lead to significant challenges regarding lightning strike protection [16], [18], [21], [158]. Lightning protection of composite structures have become a major research area over the past years [17], [159]–[161]. It has been concluded that the low through-thickness electrical conductivity is the main factor behind the lightning damage in CFRPs [143]. To mitigate the induced damage in composite aero structures, expanded metal foils have been added to the surface of CFRP laminates to protect them. However, even these cannot provide total protection. Furthermore, they add a number of additional problems such as galvanic corrosion, complicated integration processes and added weight to the overall structure, all counteracting the key advantages of using CFRPs as lightweight and more efficient alternatives to lightweight alloys [13].

A possible alternative solution to the use of expanded metal foils is to increase the out-of-plane electrical conductivity of CFRP by the addition of conducting fillers, as described in section 2.4, to achieve a composite with enhanced properties that allows current distribution through the laminate bulk. The importance of increasing the through-thickness conductivity in suppressing the effects of lightning strike induced damage was highlighted experimentally by Kumar [13]. In this work, laminates exhibiting 1.1 S/cm through-thickness electrical conductivity showed significantly improved lightning protection capabilities, being able to retain 92% of their residual flexural strength after being exposed to a 40 kA lightning impulse according to aircraft lightning testing specifications. In this study, conducting particles or epoxy matrix were not utilised, instead polyaniline (PANI) was employed as matrix. Although PANI exhibits considerably lower mechanical properties than of epoxy thus making it unsuitable candidate for structural applications, this study showcases the efficiency of laminates with high through-thickness electrical conductivity in mitigating the lightning effects.

Besides altering the properties of the polymer matrix of the CFRP laminates, carbonaceous nanomaterials exhibit the possibility to replace metallic meshes in aircraft applications. Han [160] developed a conducting coating consisting of CNTs in the form of a bucky-paper (BP), and an insulating layer of boron nitride/epoxy to separate it from the CFRP laminate. This combination of materials resulted in a weight reduction of 30% compared to metal expanded foils, while successfully protecting the CFRP laminate to lightning currents up to 100kA.

With modern multi MW (rated output power) wind turbines reaching heights up to 260 m (GE Haliade 12 MW) and rotor diameters exceeding 200 m, their exposure to lightning strike is considerably increased compared to smaller wind turbines. According to the IEC standard (IEC 64100-24) for the lightning protection of wind turbines [162], the lightning collection area of a wind turbine is defined as a circular surface area with a radius 3 time the height of the wind turbine, Fig. 2.20.

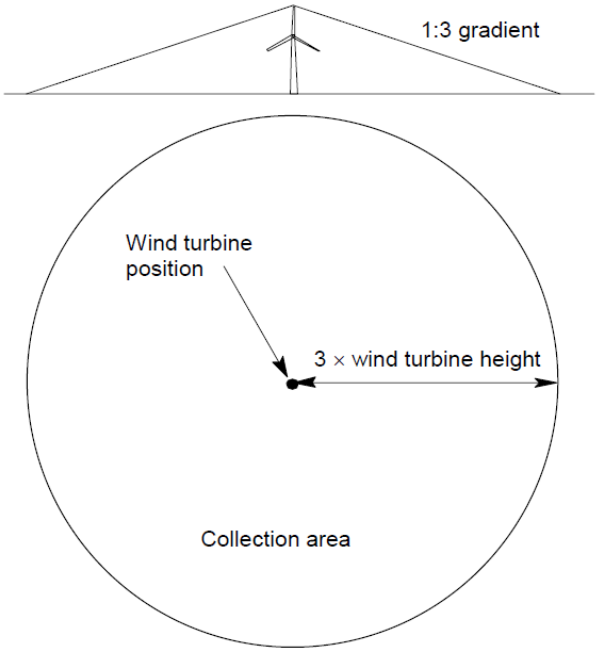

Figure 2. 20: Lightning collection area of a wind turbine [162].

During the lightning incident internal flashovers (i.e. electric sparks) between the down conductor[1] and the CFRP laminate structure may occur at high peak currents and current gradients, causing instant structural damages or extended delamination during continued operation [4]. To avoid these phenomena several equipotential bonding points have to be realized along the length of the blade, to allow sufficient amount of lightning current to flow through the CFRP sparcap to maintain the same electrical potential with the down conductor. The lower electrical conductivity in the transverse and through-thickness directions are responsible for local heat release and associated delaminations in the equipotential bonding areas that can degrade the integrity of the blade spar and potentially lead to major structural damage over time [163]. Efficient ways to evenly distribute current at the CFRP bonding points is a major research area and several approaches have been developed over the years, using conducting paints, copper foils etc.

[1] Down conductor: a high voltage cable that transfers the lightning current from the blade tip to the wind turbine's earthing system.

A key difference between wind turbine and aircraft applications, is that the service intervals for wind turbines blades are significantly longer and repairs in the internal structure of the blade are very difficult to conduct without taking the blades down. Accordingly, alternative routes for design, in particular the lightning strike mitigation/protection system, are sought for. A possible solution for improving the resistance to lightning strike, i.e. to reduce lightning strike induced damage levels, is to alter the material properties by increasing the out-of-plane and transverse electrical and thermal conductivities, as a permanent part of the passive lightning protection system.

2.5.2 Anti/de-icing and heat dissipation

Ice accumulation on aerodynamic surfaces represents a problem for both aircrafts and wind turbine blades. As both are often exposed to temperatures below 0^{o}C, cold water droplets accrete on leading edges, adding weight to the structure and altering the aerodynamic shape of the airfoil leading to increased drag [164]. This is known to affect the control of aircraft, and has been reported to cause fatal accidents. For the case of wind turbine blades, ice accumulations has been reported to result in power losses leading to load imbalances and vibrations [165], [166]. When coupled with strong wind loads, ice accretion has also been found to contribute to structural failure of the entire wind turbine blade [167].

In aircrafts anti/de-icing is often achieved by using hot air produced in the engine compressor and pipping it along the leading edge of the wing. There, the hot air is transferred to the wing outer surface through heat conduction. Due to their low out-of-plane thermal conductivity CFRPs require higher amounts of energy, thus making the process energy consuming and inefficient with the potential for damaging the composite. If the out-of-plane heat conduction could be improved, this would lead to reduced energy requirements, thus increasing the efficiency of the aircraft. The benefits of nanoreinforced CFRPs for this particular case have been highlighted by Yao [164], [168], where CNT webs were embedded in a laminate. The addition of CNTs increased the through-thickness electrical and thermal conductivity of the laminate allowing ice removal from the surface of the laminate (-12^{o}C) within 15s, with negligible increase in the weight of the laminate.

2.6 Experimental methods

As a significant objective of this research is to characterize and the electrical and thermal conductivities of CFRP materials, a short overview of the available experimental techniques is presented. Although there is a plethora of measuring techniques available, special considerations need to be taken into account considering the anisotropy of CFRP in addition to the main selection

criteria such as accuracy, implementation time and cost, either of the apparatus or the consumables required.

2.6.1 Electrical resistance measurements

Resistance measurements in conductors and semiconductors are usually realised utilising a 4-probe method, due to the low resistance of these materials, while in insulators a 2-probe method is preferred, often with the use of guard rings to avoid fringing around the voltage measuring electrode's edges. Although there are standards upon which electrical resistance measurements are carried out there is no specific standard describing resistance measurements for materials exhibiting anisotropy similar to CFRP. The 2-probe method, albeit the simplest in execution, requires characterization of the contact resistance to obtain reliable results [74]. Conventional 4-probe setups are mainly used for characterizing semiconductors in the form of films, but have also been utillised in resistance measurements of CFRP [15], [85], [169].

A key aspect in electrical resistance measurements is that the current distribution should be uniform in the cross section of the sample, which means that the current must penetrate the bulk of the sample homogeneously, something that can be difficult to achieve in anisotropic media such as CFRP, Fig. 2.21. If this is not fulfilled the voltage readings cannot be considered representative of the entire cross sectional area of the sample. This problem originates from the measuring device itself, i.e. that voltage measurements are achieved by measuring the voltage drop across a known resistor. If the surface resistance of the sample is lower than that of the resistor of the multimeter, then the reading depicts the value of the resistance of the multimeter. This is a potential issue for 4-point probe measurements when the voltage measuring electrodes are positioned close to each other. Furthermore, for the particular case of CFRP, an additional consideration needs to be taken into account. The high contact resistance between the CFRP substrate in the electrical contact and the electrode [74] in conjunction with the interface resistance between the voltage measuring electrode, usually a sharp metallic object, and the resin-rich surface of the sample add to the complexity of the measurement . Thus, a 2-probe method can provide more reliable results, once the electrical contact resistance is estimated.

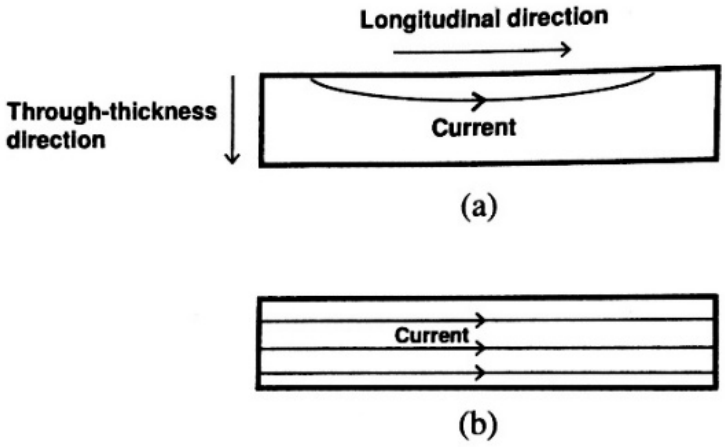

Figure 2. 21: (a) Insufficient penetration of current, (b) homogenous distribution of current in volume resistance measurements [170].

Measurements in the through-thickness directions are more challenging, since the higher conductivity of the fibres along their length, i.e. the path of least resistance, can lead to current flow on the surfaces of the sample rather than through its bulk/thickness as desired. Several concepts have been developed to measure the through-thickness resistance of CFRP featuring conducting paints [171] and alternative positions of current and voltage electrodes [81] to name a few. Similar to any other resistance measurement, minimizing the contact resistance is essential for obtaining reliable results. The influence of surface preparation, removal of surface polymer through sanding has also been highlighted as an area of key importance in achieving low contact resistance [172], since different grades of sand paper can create different surface roughnesses, higher grade sandpapers are more efficient in removing the surface polymer without destroying the fibres.

2.6.2 Thermal conductivity measurements

The measurement techniques for thermal conductivity can be divided into two major groups; transient and steady-state methods. In Table 2.9 an overview of the most commonly used methods can be found. As seen, depending on the examined material, different methods need to be utillised. The principle of steady-state methods lies on the measurement of a heat flux and a temperature gradient over a certain time period in which the temperature across the sample does not exhibit fluctuations apart from small deviations. Under these steady conditions the thermal conductivity is estimated. Opposed to this, transient methods measure the thermal diffusivity by recording temperature data as a function of time following a periodic application of heat to the surface of the sample.

Table 2. 9: Thermal conductivity measurement methods-table adapted from [60].

Method		Temperature range	Conductivity range (W/mK)	Accuracy	Materials	Test standards
Steady-state methods	Guarded hot plate method	80-800 K	<0.8	2%	Glass, polymers and insulation materials	ASTM C177 ISO 8302 EN 12667
	Axial flow method	90-1300 K	0.2-200	2%	Polymers, ceramics, metals	ASTM E1225
	Heat flow meter method	253-523 K	<10	3%	Glass, polymers, insulation materials ceramics	ASTM C518 ASTM E1530 ISO 8301 EN 12667
	Pipe method	293- 2770 K	0.02-200	2%	Metals, high conductivity inorganics polymer composites	ISO 8497
Transient methods	Laser flash method	373- 3273 K	>0.01	3-5%	Glasses, polymers, ceramics, metals	ASTM E1461 ISO 22007-4 ISO 18755
	Transient hot wire method	293-2273 K	<25	1-10%	Glasses, polymers, ceramics, most of liquids, gas, powders	ASTM C 1113 ISO 8894-1 ISO 8894-2
	Transient plane source method	20-1273 K	0.005-1800	5%	Insulation materials, powders, polymers, ceramics, metals, liquids	ISO 22007-2

The advantage of steady-state methods over transient methods is that, besides the thickness of the sample, no other physical property is needed for the estimation of the thermal conductivity [60], [173]. The main concern during steady-state measurements is to ensure unidirectional heat flow through the sample and to minimize the lateral heat losses. However, both conditions can be satisfied by using samples with high aspect ratios and by utilising suitable thermally insulating material, making this method favourable for the characterization of polymer composites.

In addition, although transient methods require shorter measuring times, they do also require prior knowledge of the material's heat capacity and density [60]. Considering the case of polymer composites where the addition of a filler highly affects their density and heat capacity, estimations of the thermal conductivity can be influenced. Thus additional measurements need to be realized, adding to measuring complexity and time of implementation.

Chapter 3 Experimental methodology

3.1 Introduction

In this chapter the experimental methods used in this study are presented. Initially, the constituent materials used in the sample manufacturing are introduced, followed by a description of the experimental techniques which were utilised to characterize the electrical, thermal and mechanical response of the manufactured CFRP laminates.

3.2 Sample manufacturing

3.2.1 Materials

Due to fact that this PhD project was part of a larger project (SPARCARB) investigating CFRP materials for emerging applications in the wind energy sector, with a special focus on lightning strike phenomena in wind turbines, "as-received", low cost, commercially available materials were chosen to be used for the manufacturing of the CFRP laminates. A list of the materials used is shown below:

- BASF Baxxores® ER 5300 epoxy resin
- BASF Baxxodur® EC 5310 curing agent
- Leuna-Harze EPILOX ER 5300 epoxy resin
- Leuna-Harze EPILOX EC 5310 curing agent
- SAERTEX U-C-882g/m²: This type of fabric consists of 852 g/m^2 of ZOLTEK PANEX 35 50K unidirectional carbon fibres, 24 g/m^2 E-glass X and 6 g/m^2 of PES 80, (glass fibres and PES were used for stitching purposes as seen in Fig. 3.1)
- GO nanopowder supplied by Garmor Inc.

The GO (edge-oxidized) used in this study consisted of approximately ten graphene layers and a nominal particle size diameter of 500 nm with 90% of the particles to be below 800 nm. The oxygen content was in the range of 5-10% (stated by the supplier). The oxygen content was verified through X-ray Photoelectron spectroscopy (XPS) and was found to be 8.78% [174].

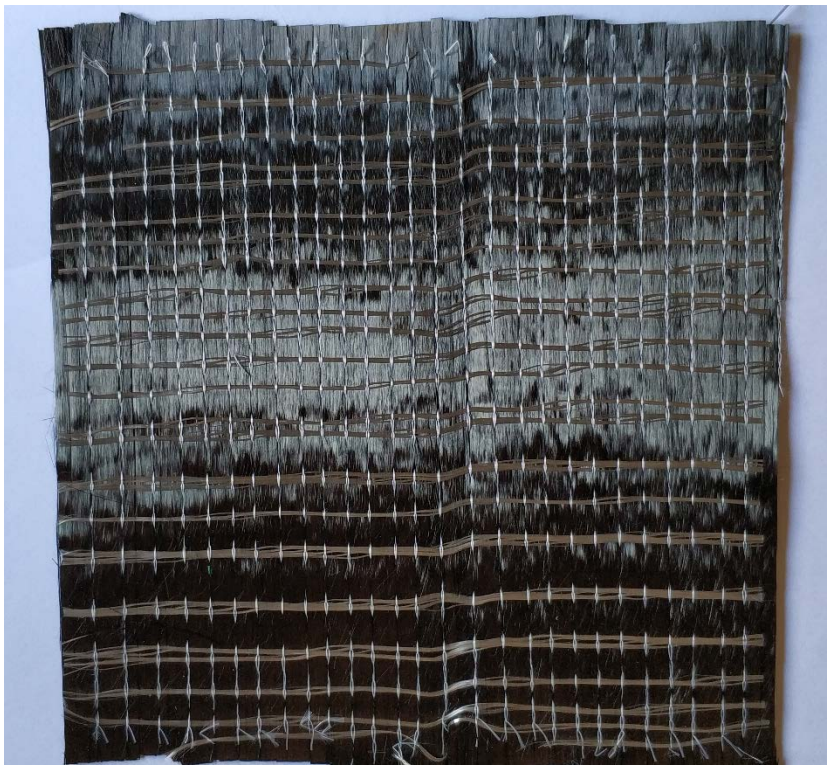

Figure 3. 1: The carbon fabric used in this study.

Technical specifications for the abovementioned materials can be found in the Tables 3.1, 3.2 and 3.3 below. Note that the EPILOX epoxy was used as a replacement matrix, as BASF discontinued the production of epoxy-based products in 2017. Leuna-Harze is a DNV GL (Germanische Lloyd) certified resin manufacturer according to BASF standards.

Table 3. 1: Viscosity and density for the Baxxores® 5300 epoxy resin and Baxxodur® EC 5310 curing agent, same for the EPILOX system (According to datasheet).

Property	ER 5300	EC 5310	ER 5300 + EC 5310
Viscosity (25°C) mPa s	680	8	275
Density (23°C) g/cm³	1.15	0.935	-

Table 3. 2: Mechanical properties for the Baxxores® 5300 epoxy resin- Baxxodur® EC 5310 system after curing at 70oC for 6 hours, same for the EPILOX system (According to datasheet).

Property	Test Method	Units	ER 5300 + EC 5310 (6h, 70°C)
Tensile strength	ISO 527-2	MPa	71
Elongation at tensile strength	ISO 527-2	%	5.2
Elongation at break	ISO 527-2	%	7.5
Tensile modulus	ISO 527-2	MPa	3000

Table 3. 3: ZOLTEK PANEX 35 fibre properties (According to datasheet).

Property	Units	ZOLTEK PANEX 35
Tensile strength	MPa	4137
Tensile Modulus	GPa	242
Density	g/cm^3	1.81
Fibre diameter	μm	7.2
Electrical resistivity	Ωcm	1.55×10^{-3}
Carbon content	%	95

3.2.2 Sample preparation

Several techniques can be used for the manufacturing of large CFRP laminates/structures wind turbine blades. The most commonly used methods are the Vacuum Infusion (VI) process, and its variations, as well as prepregs [175]. Recently the use of pultruded CFRP profiles has been introduced as additional stiffening members to the manufacturing of sparcaps as a mean to achieve higher fibre volume fractions and shorter manufacturing times.

For the purposes of this study the VARTM (Vacuum Assisted Resin Transfer Moulding) process was chosen, see Fig. 3.2, as this is the most commonly used manufacturing method for composite wind blades. The steps followed during the VARTM process can be described as follows:

- Cut the fabric into the desired dimensions
- Apply a release agent to the mould (in this case a flat plate)
- Stack the fabric in the desired order (layup plan)
- Stack vacuum consumables in the mould (peel ply, flow fabric, tacky tape and vacuum bag)
- Insert hoses for the inlet of resin as well as the feed to the vacuum pump
- Seal the vacuum bag
- Set the vacuum pump on and check for leaks
- Infuse the resin through the hose to the sample
- When the sample is fully impregnated form the resin close and clamp both the resin inlet and the feed line to the vacuum pump and then retain the vacuum
- Place the mould inside the oven for curing

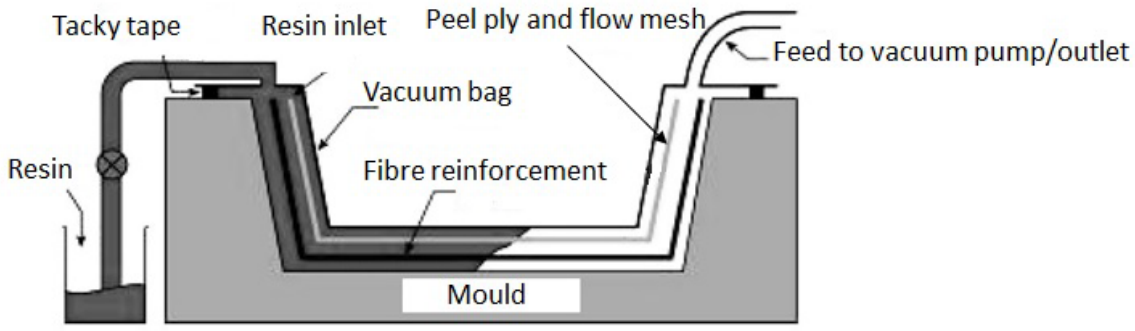

Figure 3. 2: Schematic representation of the VARTM process (http://www.gurit.com/)

Following the instructions of the manufacturer, the resin was mixed with the curing agent at a 100:20 ratio per weight. Then the mixture was stirred gently for 10 min at ambient temperature to avoid the formation of air bubbles. The mixture was then degassed under vacuum in a desiccator at ambient temperature for 20 minutes to remove any air trapped inside. The samples were cured at 70^{o}C for 6 hours, which is the recommended curing profile by the manufacturer. These curing conditions closely resemble the conditions under which large scale wind blades are manufactured. More information regarding the development of GO reinforced laminates will be presented in the following chapters.

3.3 Electrical conductivity measurements

3.3.1 Description of method

To estimate the electrical conductivity of the manufactured laminates, DC resistance measurements were conducted in the three principle material directions, i.e. longitudinal (parallel to fibres), transversely (perpendicular to fibres), and though-thickness (perpendicular to fibres in thickness direction), see Fig. 3.3. Prior to the measurements the electrical contact areas were prepared to achieve optimum current flow from the electrodes to the sample. The sample surfaces that were used as electrodes were initially polished with Silicone Carbide sandpaper (600 and 1200 grit) to remove the excess polymer and expose the fibres to achieve direct electrical contact. To mitigate the influence of surface roughness and to promote ohmic contact across the electrode area, an epoxy based adhesive containing silver particles, supplied by RS Components, with a volume conductivity of 10^3 S/cm was employed. A thin layer of the adhesive was applied to the intended electrode surface followed by curing at ambient temperature for 24 hours. The use of silver paint as a means to achieve lower contact resistance has been reported to be successful in several studies [65], [67], [71], [176]–[178]. The same surface preparation procedure was followed for the all of measurements throughout this study.

For the measurements along the fibre and transverse directions a test cell/fixture featuring a screw actuator was manufactured, Fig. 3.3. PTFE sheets and PEEK rods were utilized as the main components, copper foils of 0.035 mm were employed as electrodes. Resistance measurements were conducted with the use of a TTi BS-407 precision milli/micro-ohmmeter. The applied current was ranging between 0.5mA and 10mA.

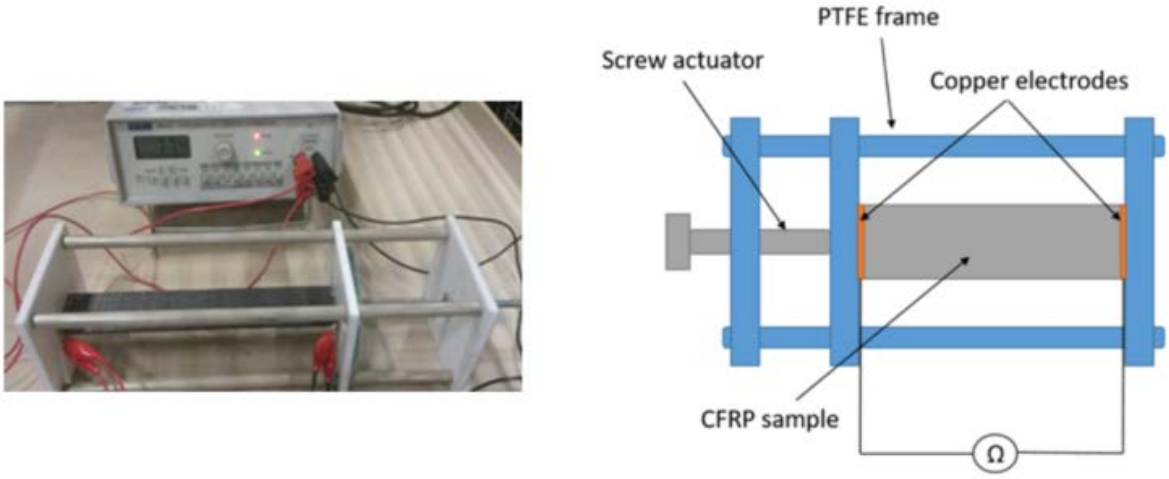

Figure 3. 3: Experimental set-up for measurement of longitudinal and transverse electrical conductivities

Measurements in the through-thickness direction were achieved with the use of two parallel electrodes, featuring a guard ring according to ASTM D 257 test standard [79], Fig. 3.4. To control the applied pressure during the measurements a hydraulic press was utillised, Fig.3.5. Both electrodes were electrically insulated with PTFE sheets to avoid current leakage to the press. The applied pressure was 10 MPa.

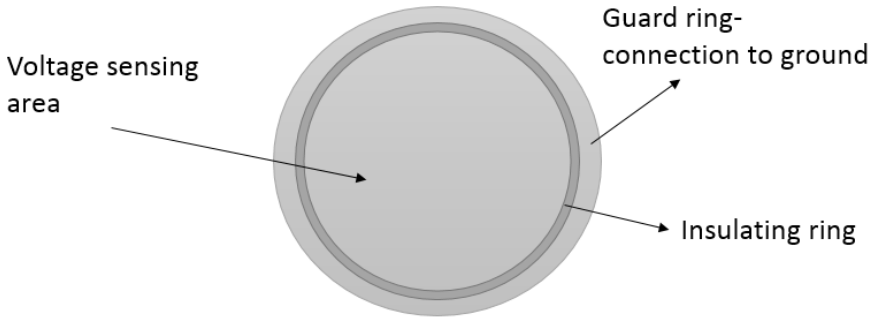

Figure 3. 4: Through-thickness measurements electrode configuration

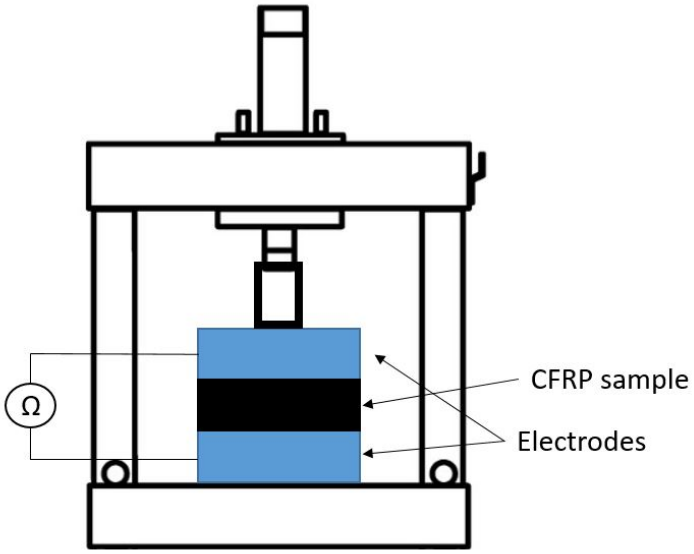

Figure 3. 5: Through-thickness resistance measurements setup.

3.3.2 Uncertainty of measurements

The main source of systematic errors in the electrical resistance measurements arise for the measuring device if this is not calibrated. For the particular ohm-meter used in this study, AIM TTi BS-407, the typical accuracy as stated by the manufacturer was 0.1%. Prior to the measurements conducted on the CFRP samples, a reference resistor of 1 Ω was used to verify the accuracy of the test setup (ohm-meter and test leads). The obtained resistance values were exhibiting deviation lower than 0.1% of the resistor's nominal value of 1 Ω.

In addition, electrical resistance measurements are influenced by the resistance of the actual electrical contact/electrode, also known as contact resistance R_c and the applied pressure in the electrical contact area [179].The total measured resistance, R_{tot}, can be expressed as the sum of contact resistance, which is dependent on the type of electrode/connection, and the actual resistance of the sample R_s, eq. 3.1.

$$R_{tot} = R_s + R_c \qquad \text{eq. 3.1}$$

Estimations of the R_c can be achieved by measuring the resistance of samples with the same width and thickness and varying the length of the sample. Assuming that the conductivity of the sample/material and the contact resistance are independent of the length of the sample, a linear behaviour is expected as presented in the plot below, Fig. 3.6. Deviations from an ideal linear behaviour can be estimated from the quality of the fitted linear equation on the experimental results leading to estimations of the uncertainty of the measured resistance as well as contact resistance. This approach has been utillised also by Lin [74] in CFRP measurements, and can be used to validate the hypothesis.

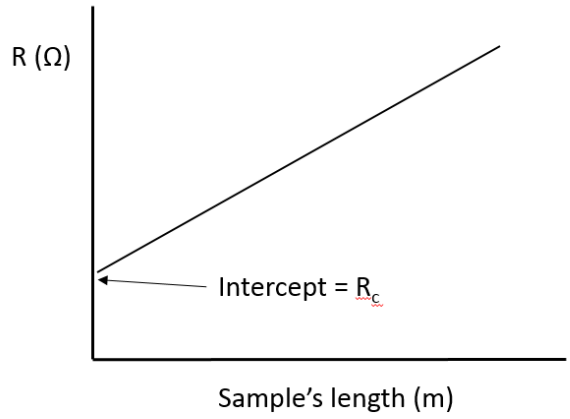

Figure 3. 6: Total measured resistance versus sample's length.

As already mentioned, a parameter that can also introduce uncertainty in the resistance measurements is the applied pressure at the electrical contact. Air gaps between the electrodes and the sample can be formed due to surface roughness, leading to poor ohmic contact [179]. As explained in the previous section, a screw actuator was incorporated in the test cell to control the applied pressure in the electrical contact area. Resistance measurements were conducted for a 5-ply CFRP laminates, with a width of 39.9 mm and thickness of 4.07 mm, in the fibre direction, where the amount of applied torque in the bolt was varied by the use of a torque wrench. The axial force generated from the bolt was calculated as well as the corresponding applied pressure at the electrical contact. The applied pressure dependency of the measured resistance in the fibre direction for the 5-ply CFRP laminates is depicted in Fig. 3.7. It is seen that a decrease in the resistance values is observed with increasing applied pressure. A saturation value is observed for applied pressures above 5MPa, and thus pressures above 5MPa will be used during the measurements that will be conducted in this study. The fact that the decrease in resistance is only about 14% proves the efficiency of the electrode attachment concept developed in this study to obtain ohmic contact over the surface of the electrical contact.

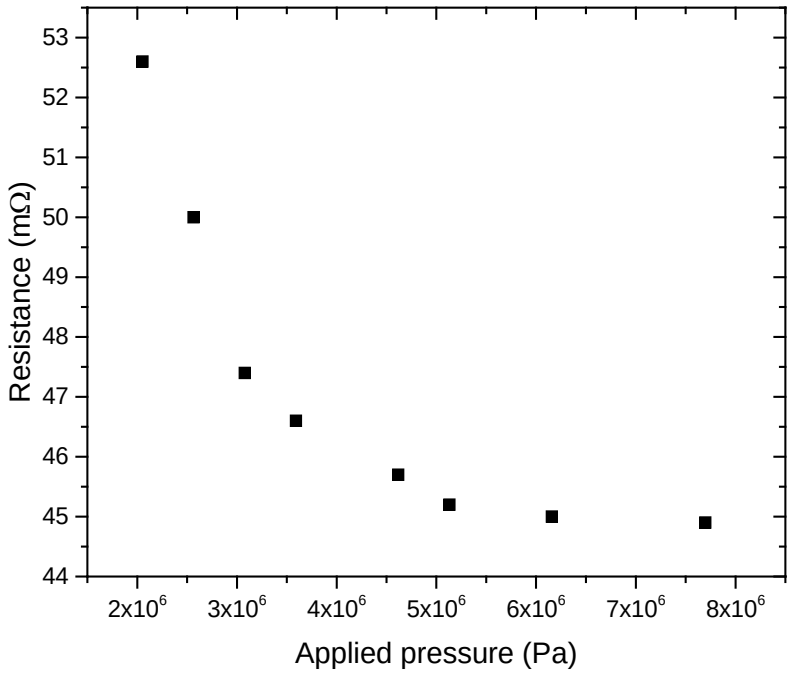

Figure 3. 7: Total resistance measured as a function of applied pressure in the electrical contact area in the fibre direction for a 5-ply CFRP.

For the particular case of measurements in CFRP composites, the main source of random error arise from the samples themselves, and specifically from variability in their manufacturing process. Initially, the case of unmodified CFRP laminates is considered. All of the laminates in this study were manufactured by means of the vacuum infusion method. Although this method is widely used by industry for the manufacturing of large structures, it exhibits sizable variations with regard to the fibre volume content of the laminates. As the liquid polymer matrix infiltrates the dry fibre layers, some movement of the fibre tows can occur causing misalignment. Considering that measurements are conducted on samples that are significantly smaller than the produced laminates, localised fibre volume variations can affect the measurements. In addition, for laminates containing conducting nanofillers, the state of dispersion of the filler as well its distribution through the bulk of the laminate add to the random error of the measurements. For example, a high concentration of filler close to the resin inlet side can provide high through-thickness conductivity values that do not describe accurately the apparent conductivity of a laminate with well distributed nanofiller. To account for potential discrepancies, measurements were conducted in samples that were obtained from both close to the resin inlet side as well as close the vacuum suction side. A total of 2 samples per manufactured plate were utillised in the measurements, each sample was tested 5 times and the average value along with its standard deviation was considered, after the contact resistance value was subtracted from the measured value. Then the values from the inlet and suction sides were compared and if the percentage of deviation was below 5% the sample was considered to have a satisfactory distribution.

3.4 Thermal conductivity measurements

Unlike electrical conductivity measurements, thermal conductivity measurements are more challenging in CFRP materials, as the samples need to be designed in a manner to allow optimal heat flow depending on the direction as well as the technique used. In this work, a steady-state technique was developed to characterize the thermal conductivity in the through-thickness and transverse directions. Considering that the thermal conductivity of the composite along the fibre direction is of similar order of magnitude as the thermal conductivity of the fibres themselves along their length axis, i.e. between 3 W/mK and 10 W/mK for PAN-based fibres [46], [104], [180], and that the addition of GO is not expected to affect the heat conduction in this direction, it was decided not to conduct measurements in this direction, as the main focus is the investigation of the through-thickness and transverse properties.

For the characterization the through-thickness direction, disc shaped specimens with a diameter of 50 mm and thickness of approx. 5mm were waterjet-cut from the manufactured laminates. Measurements in the transverse direction required specific specimens to be manufactured to achieve heat flow transverse to the fibres; Figure 3.8 shows how this was achieved. CFRP strips, approx. 7 mm and 9 mm wide, were cut from the manufactured laminates and bonded together using an epoxy-based adhesive to form discs of 50 mm diameter such that the transverse direction of the laminate was aligned with the heat flow direction (i.e. through the thickness of the disc). Since the epoxy bond line, approx. 100 µm, was parallel to the heat flow direction, it was assumed that the adhesive did not affect the measurements as the total area of the bonding is about 1.5% of the total cross sectional area of the samples.

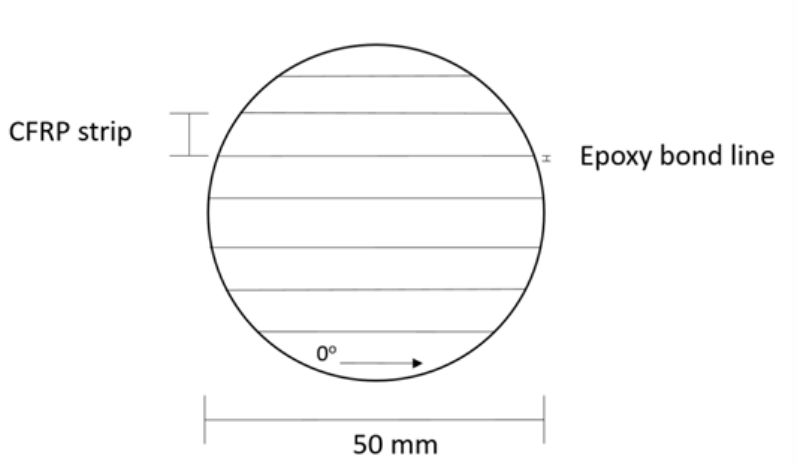

Figure 3. 8: Schematic of the sample used for the transverse thermal conductivity measurements.

3.4.1 Description of apparatus

A guarded hot plate apparatus consists of two main components, a substrate which introduces the heat flux to the sample or hot plate, and a heat sink to promote heat flow through the sample, the cold plate, Fig. 3.9. To mitigate lateral heat losses thermal insulation is applied following different approaches, where the apparatus is placed in an environment that minimizes the heat exchange such as vacuum or a water bath [39], [104], [180].

In this study disk shaped Brass substrates, 50mm in diameter and 15mm in thickness, were utilized as hot and cold plates, respectively. The brass disks were sanded to obtain a surface roughness of 5μm. A heating element, rated at 2W at 12V, was attached to the base of the hot plate substrate. In both of the substrates, 1.5mm holes were drilled to allow the installation of K-type thermocouples for temperature sensing purposes. An aluminium block was milled to create a circuit to allow cooling fluid to flow through it and to act as a heat exchanger. The temperature of the cooling block was monitored using a K-type thermocouple placed in the block. An Ethylene Glycol mixture was circulating through the cooling block via the bath/circulator, Huber Minichiller 280 OLÉ. The temperature of the cooling fluid was controlled through the built-in thermostat.

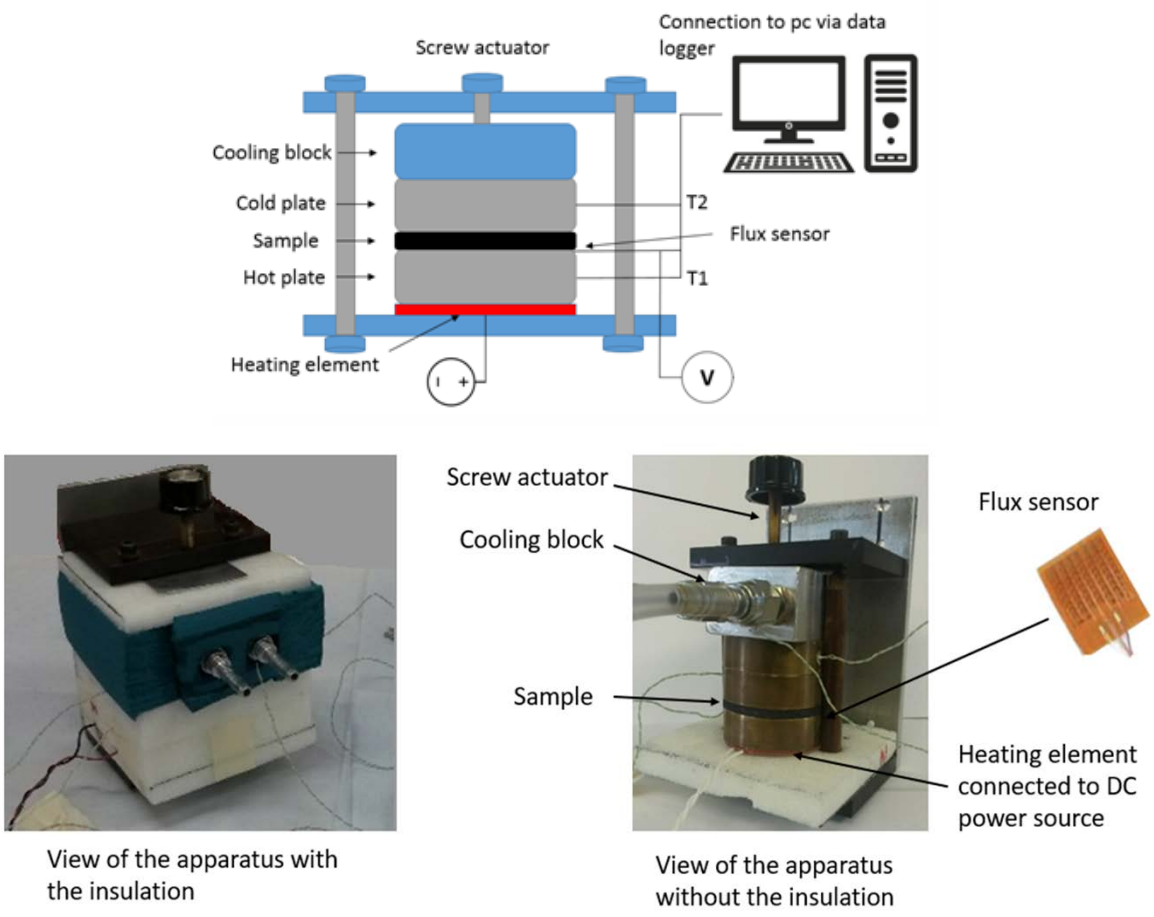

Figure 3. 9: Schematic representation of the apparatus without the insulation (top) and view of the apparatus (bottom).

To assure reproducibility an M6 bolt actuator was employed. By applying a torque of 1Nm, and assuming the friction coefficient between polymer and metal to be 0.3, an axial force of approximately 555N was generated from the bolt leading to a total of 0.28MPa of applied average pressure. This level of externally applied pressure was sufficient to ensure that surface air gaps were avoided in the interfacing materials, as it comes in paste form, Electrolube HTSP, with a thermal conductivity of 3 W/mK. To accurately obtain the heat flux through the surface of the sample a thin film flux sensor, HFS-4 OMEGA Engineering, was incorporated in the apparatus. Readings of the DC voltage signal of the sensor were achieved with the use of an Agilent, technologies 34401A Voltmeter. The heat flux was calculated by dividing the output signal of the sensor, in the mV range, with the sensitivity of sensor, 1.6 μV/W/m^2 As follows:

$$q = \frac{V}{S} \qquad \text{eq. 3.2}$$

Where q is the heat flux, V is the sensor's output voltage and S is the sensor's sensitivity.

Temperature readings from the thermocouples were recorded with the Pico Technologies TC-08 data logger. Thermal insulation was achieved with the use of PMI foam, Polymethacrylimide, Rohacell 51 IG-F, with thermal conductivity values of 0.033 W/mK (data sheet value).

3.4.2 Validation of the measurement technique and measurement uncertainty

To validate the measuring accuracy of the apparatus, measurements were carried out on sample materials with well-defined thermal conductivity values. Measurements were conducted by applying a heat flux from the hot plate, while heat was constantly being removed from the cold plate. The heat flux values and their variation over time were monitored using an Agilent 34401A multimeter. Equilibrium conditions, i.e. steady-state, were assumed when the temperature difference between the hot and cold plate was not exhibiting variations higher than 0.5 ^{o}C for a time period of 30 min.

In this study, two reference materials were used to obtain a two point calibration: PTFE (Polytetrafluoroethylene), supplied by RS Components, and Fused Silica (quartz glass), supplied by UQG Optics, Cambridge, UK. Disk shaped samples with a diameter of 50 mm and different thicknesses were tested for both reference materials, see Fig. 3.10.

Estimation of the true thermal conductivity value without the influence of the interfaces can be achieved by plotting ΔT/q versus Δx. Assuming a linear relation, the conductance can be extracted from the intercept of the fitted line and the thermal conductivity from the slope. Estimations regarding the measurement uncertainty were based on the quality of the fitted equation on the experimental values, as presented in Fig.3.10, the OriginLab 2018 software was used for all of the

calculations. Based on this method the uncertainty for both thermal conductivity and interface conductance was estimated. From the obtained results listed in Table 3.4, it is seen that the measured values agree well with the values stated by the suppliers and found in literature [60], [173], [181].

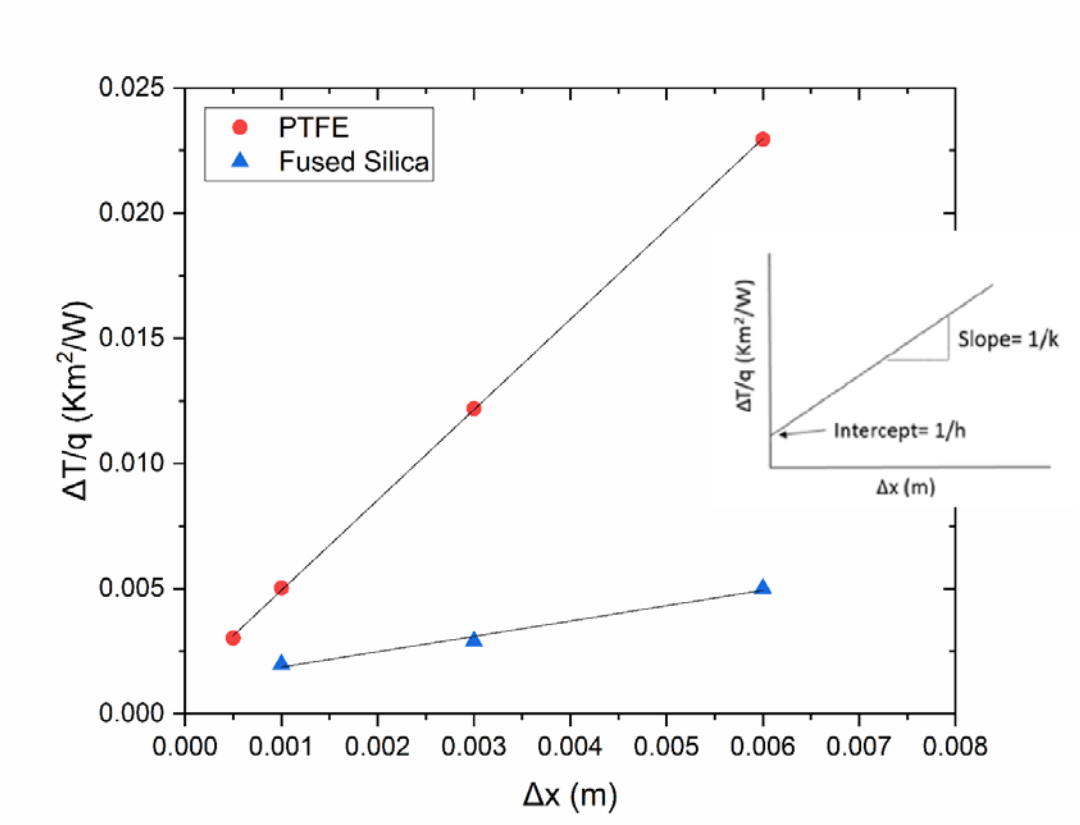

Figure 3. 10: Ratio of temperature gradient (ΔT) to flux (q) versus sample thickness (Δx) for the PTFE and Fused silica samples examined in this study.

Table 3. 4: Thermal conductivity values of reference materials at 20°C

Material	Thermal conductivity W/mK	Thermal conductivity (Measured) W/mK	Interface conductance h (W/m^2K)
PTFE	0.2- 0.3 [59], [60], [182]	0.277 ±0.0015	754 ±37
Fused Silica	1.38 [173], [183]	1.428 ±0.05	1234 ±50

The observed discrepancy for the fused silica is associated with the guarded hot plate (GHP) method. Thermal conductivity values similar to that of fused silica are usually close to the upper limit of the measuring capabilities for this method [60].

The main sources of systematic errors were identified in the flux sensor used to measure the heat flux during the measurements, and the temperature readings recorded in the data logger. In both cases the accuracy was 1% and 0.2% respectively according to the manufacturers.
To mitigate possible false readings from the thermocouples due to poor contact within the brass substrates, the same heat transfer compound used to interface the sample with the hot and cold plates was utillised for mounting the thermocouples.

Each sample was measured two or more times, and corrections to the conductivity values were made using an analogue of resistances connected in series as follows (see also Fig. 3.10):

$$\frac{\Delta x}{k_{meas}} = \frac{\Delta x}{k_{true}} + \frac{1}{h} \qquad \text{eq.3.3}$$

Where the ratio Δx/k is the thermal resistance of the sample, 1/h is the thermal interface resistance, Δx is the sample thickness, k_{meas} is the measured thermal conductivity, k_{true} is the corrected value of thermal conductivity and h is the interface conductance.

Akin to the electrical resistance measurements, an identical measuring protocol was followed for the characterization of the thermal conductivity and to account for random errors associated with the manufacturing process. Specifically, since the thermal conductivity measurements required circular disk shaped samples, the samples that were used for the measurements of the through-thickness electrical conductivity were utillised in the thermal measurements.

3.5 Interlaminar shear strength - ILSS

In unidirectional laminates the ILSS is a function of fiber/matrix adhesion, the fracture resistance of the matrix and the level of porosity [110], [184]–[186]. Thus, information regarding the effect of adding GO to the resin system can be estimated by measuring the ILSS, assuming that the fibre volume fraction of the different laminates is comparable. The ILSS was evaluated using an easy to use short beam shear test method (three-point bending). The tests were performed in accordance with the ASTM D2344 test standard [187]. The span to width ratio was set to 4:1 and the crosshead movement of the electro-mechanical testing machine used rate was 1 mm/min. To account for manufacturing variabilities, fibre volume fraction variations due to the infusion process and possible inhomogeneous dispersion of the filler, test specimens were cut along the resin flow direction. The mechanical tests were conducted using an Instron 5569 universal electro-mechanical testing machine with a load capacity of 50 kN, and the Bluehill software from Instron was used for logging the load/displacement data. The results are presented as mean values with standard deviations based all of the tested samples of each of the examined laminates, at least 5 sample per

laminate type and they were cut from both close to the resin inlet and vacuum suction sides. The ILSS was calculated using the following expression:

$$ILSS = 0.75 * \left(\frac{P}{b*h}\right) \quad \text{eq. 3.4}$$

Where P is the maximum load observed during the test, b the specimen width and h the specimen thickness.

3.6 Raman spectroscopy

Spectroscopic methods have been used for the identification and study of various substances for several decades. All of them are based on the interactions between light and matter. Raman spectroscopy is a branch of vibrational spectroscopy and is based on the inelastic scattering of photons from a monochromatic light source, a laser, by a molecule [188]. When a certain molecule is excited by a scattered photon from its ground state to a higher energy state, during the 99,999999% of the time it will return to its original energy state emitting a photon with the same intensity as the original incident photon, this process is known as Rayleigh scattering, Fig.3.11. However, when the excited molecule does not return to its original ground state, a photon with a different energy to the incident photon is emitted. This provides an energetic gain or loss and a shift on the wavelength. This type of scattering is known as inelastic scattering or Raman scattering. This Stokes shift is a unique signature of each molecule and for the case of GO is given in Fig. 3.13.

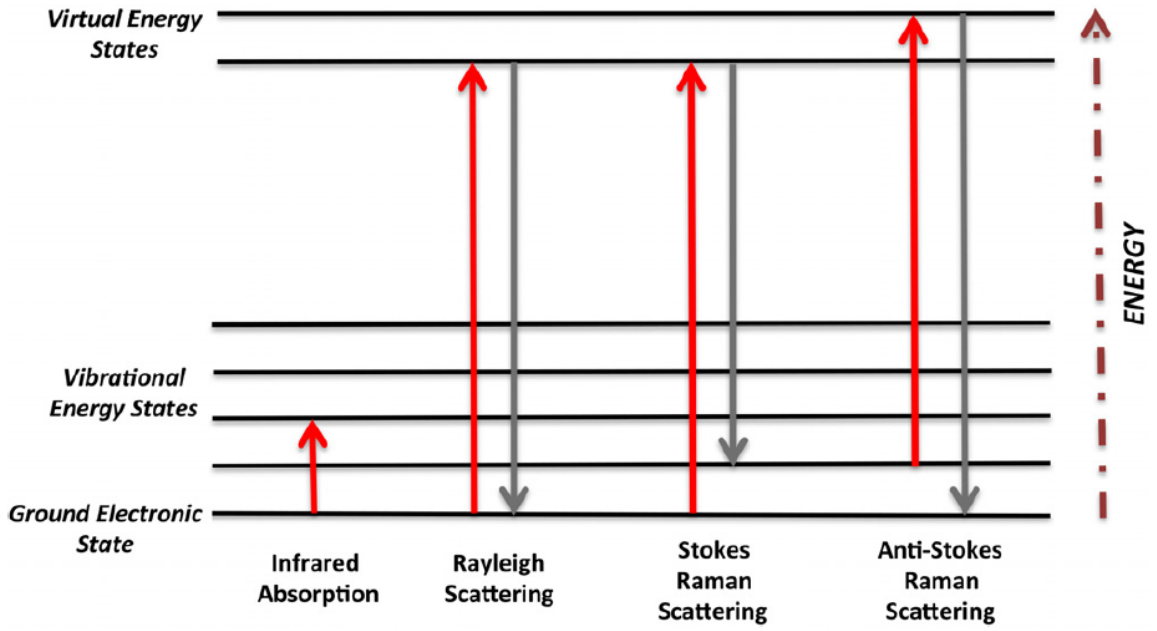

Figure 3. 11: Energy state diagram describing the transition occurring during different light scattering processes [188].

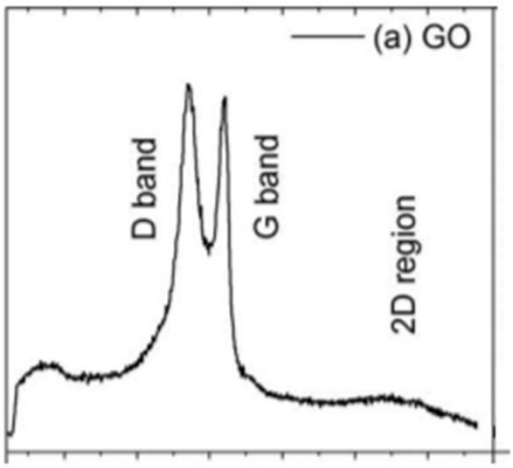

Figure 3. 12: Raman spectrum for GO in powder form [189].

In this study a Renishaw RM100 confocal microprobe system was used, Fig.3.12. A near-infrared (NIR) diode laser operating at 6.25 mW power with 780 nm laser excitation was utillised. This wavelength was chosen to inflict less damage to surface of the sample as well as minimize fluorescence that can occur and make the detection of the weak Raman shifts untraceable. The magnification of the objective lens was x50, giving a beam spot diameter of approx. 5 µm.

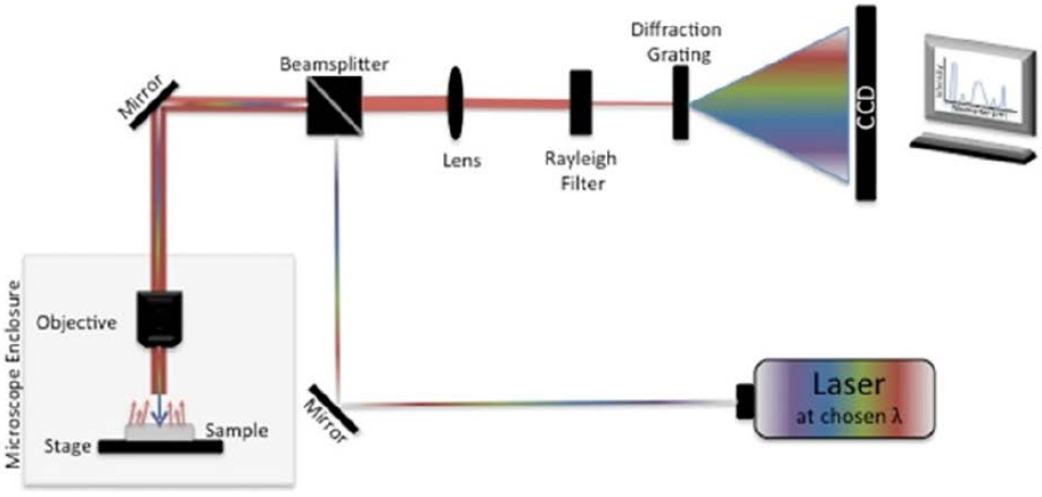

Figure 3. 13: Schematic representation of a Raman spectrometer with a confocal microscope[188].

Chapter 4 Benchmark electrical and thermal conductivity

To establish a set of reference data for comparative purposes, the anisotropic electrical and thermal conductivities of neat CFRP laminates was measured followed the procedures described in the previous chapter.

4.1 DC electrical conductivity

Initially an approximate assessment of the contact resistance needs to be realized to estimate its influence in the CFRP measurements. This can be achieved by measuring the resistance of samples with the same width and thickness and varying the length of the sample. Assuming that the conductivity of the sample/material and the contact resistance are independent of the length of the sample a linear behaviour is expected. Contact resistance measurements in the fibre and transverse directions of CFRP were conducted. For the fibre direction samples a width of 39.9 mm and thickness of 4.07 mm were employed. The length of the samples was ranging from 29.75 mm to 180 mm, Fig. 4.1. Two samples were tested for each length, all samples were cut from the same plate and measured at least 3 times. As it is seen in the figure below, a linear relation between the measured resistance and the sample length is observed. The R_c value was found to be approx. 12±2 mΩ from the intercept of the fitted line.

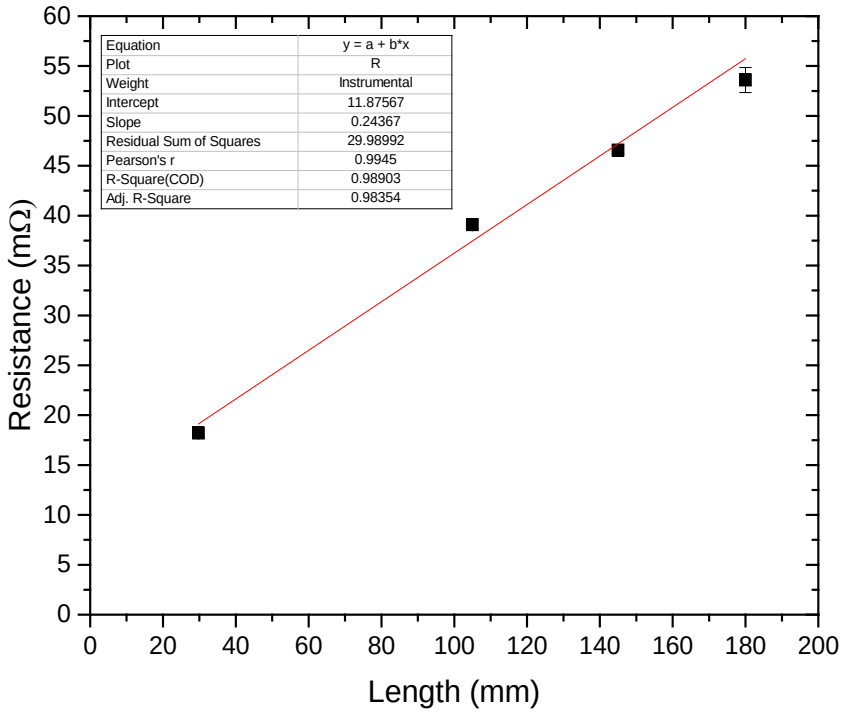

Figure 4. 1: Resistance along the fibre direction versus sample length.

A similar process was followed to determine the contact resistance in the transverse direction, Fig. 4.2. Samples with width of 39.5 mm and thickness of 4.1 mm were employed. A linear relation was observed, as expected, and the contact resistance was found to be approximately 0.24 Ω.

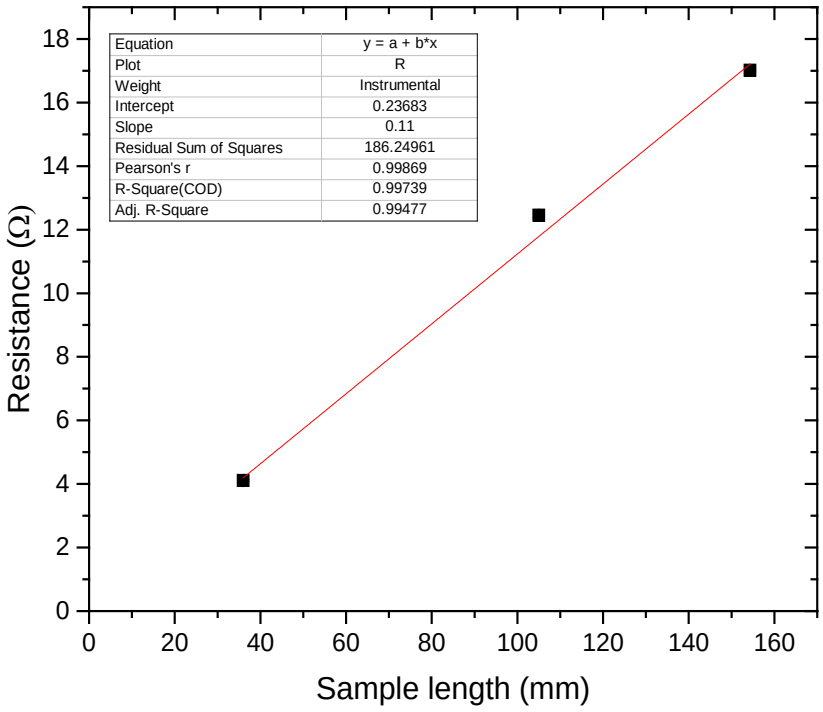

Figure 4. 2: Transverse resistance versus sample length.

Based on the investigation of the electrical contact resistance it can be concluded that the longer the sample, in the fibre and transverse directions, the less is the influence of contact resistance in the measurements, as the total resistance of the sample dominates the measurement. The different contact resistance values between the fibre and transverse directions can be mainly attributed to the intrinsic resistance of the electrical contact area and it is heavily influenced by the orientation of the fibres. As mentioned in section 2.2.1, the anisotropic structure of PAN-based fibres is reflected on their electrical properties. Hence, during the along the fibre resistance measurements, the electrical contact consists of fibres that are oriented with their highest conductivity axis perpendicular to the contact area. Consequently, a lower contact resistance can be realized. On the other hand, during transverse resistance measurements, the different fibre orientation, fibres are positioned in parallel with the electrical contact, contributes to increased resistance in the electrical contact area.

The calculation for the through-thickness direction were realized according to ASTM D 257-14 standard [190]. To reduce the uncertainties from the manufacturing process, i.e. variations of fibre volume content, three samples were cut from each of the manufactured plates. The measured values, including the contact resistance contribution are listed in Table 4.1.

Estimations of the uncertainty of the conductivity values listed in Table 4.1 were based on the influence of the contact resistance R_c, and its uncertainty, on the sample resistance R_s. Then the conductivity was calculated based on the dimensions of each sample as follows:

$$\sigma = \frac{l}{R_S * A} \qquad \text{eq.4.1}$$

Where l is the length of the sample, R_s is the resistance of the sample and A the cross sectional area.

Table 4. 1: DC conductivity values for the manufactured laminates, including contact resistance corrections

Laminate	Longitudinal direction (S/cm)	Transverse direction (S/cm)	Through-thickness direction (S/cm)
$[0^o]_5$	220 ±14	0.561 ±0.01	0.0543 ±0.0027

Discussion

The anisotropic behaviour of unidirectional CFRP was quantified from the DC electrical conductivity measurements. The conductivity in the fibre direction was found to be approx. 3 orders of magnitude higher than in the transverse direction, and 4 orders of magnitude higher than in the through-thickness direction. The obtained values for the fibre direction agree well with published values for unidirectional laminates with similar fibre volume contents, approximately 58%, as reported by Hirano [81] and Lin [74], 360 S/cm and 450 S/cm, respectively. It has to be pointed out that differences in the electrical conductivity in this direction are directly linked with the intrinsic electrical conductivity of the fibres themselves. Similarly by comparing the conductivities in the transverse and through-thickness directions with the results reported by Hirano [81], 2.07×10^{-1} S/cm and 2.4×10^{-2} S/cm, respectively, a reasonable agreement was obtained. However, these measurements correspond to aerospace grade prepregs that usually incorporate toughened interlayers to prevent delaminations, thus increasing the through-thickness resistance.

The observed discrepancies are directly linked with the contact resistance values, hence the lower deviation in the transverse direction, which can be neglected. The higher deviations observed in the longitudinal direction are due to the fact that the contact resistance is of the same order of magnitude as the actual resistance of the CFRP sample. Whilst the procedure and the materials used were identical in both cases, it appears that the fibre alignment in the electrical contact area dominates the contact resistance.

4.2 Thermal conductivity

Due to the increased complexity needed to characterise the thermal conductivity in the fibre direction, and since this is not an objective of this study, the thermal conductivity of the manufactured laminates was only determined for the transverse and through-thickness directions. Measurements of the through-thickness thermal conductivity were conducted in UD CFRP samples consisting of 2, 5 and 10 plies according to the methodology described in section 3.4. Three samples were cut from each of the manufactured plates to eliminate any influence from variations of the fibre volume content due to the infusion process, and each sample was tested at least twice. From the obtained results, see Table 4.2, it is seen that the measured thermal conductivity values were consistent for all the considered thicknesses with only minor variations. The mean heat flux during the measurements was 1380 W/m^2. As described in the section 3.4, based on the intercept of the fitted equation in the plot depicted below, Fig. 4.3, the conductance was found to be 1.1 kW/m^{2}K which is consistent with the obtained results for the examined reference materials.

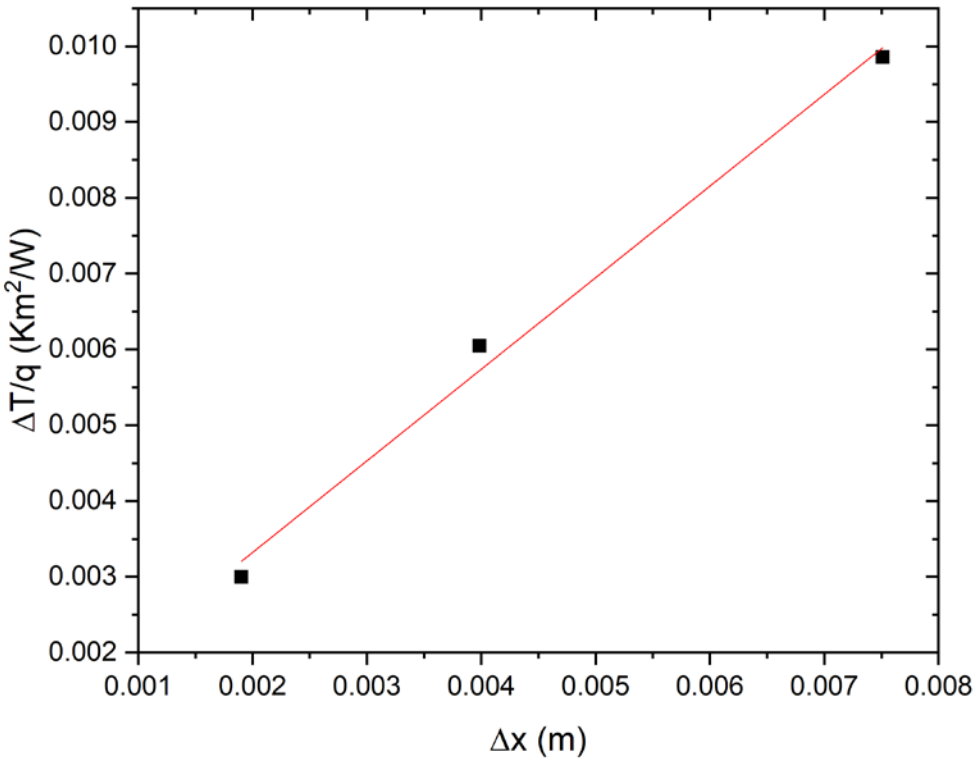

Figure 4. 3 Plot of ΔT/Q versus Δx for three difference sample thicknesses.

Table 4. 2: Through-thickness thermal conductivity of manufactured CFRP laminates

Sample	Apparent thermal conductivity (W/mK)	Thermal conductivity-with correction (W/mK)
$[0^o]_2$	0.633	0.894
$[0^o]_5$	0.655	0.770
$[0^o]_{10}$	0.695	0.768

A similar procedure was followed for the characterization of the transverse conductivity. However since a different type of sample was used for these measurements, instead of number of plies the thickness is expressed in mm. The interface conductance was found to be 1391 kW/m^{2}K. The results are listed in the table below, Table 4.3.

Table 4. 3: Transverse thermal conductivity of manufactured CFRP laminates

Sample thickness	Apparent thermal conductivity (W/mK)	Thermal conductivity-with corrections (W/mK)
7.226 mm	0.802	0.871
9.218 mm	0.815	0.871

Similar trends as for the electrical conductivities were observed for the thermal conductivities in the transverse and through-thickness directions. Epoxy-rich interlaminar regions decrease the through-thickness thermal conductivity relative to the transverse thermal conductivity by approximately 12%.

Table 4. 4: Measured thermal conductivity values

Direction	Thermal properties	
	Thermal conductivity (W/mK)	Interface conductance (W/m^{2}K)
Longitudinal	N/A	N/A
Transverse	0.87 ±0.01	1391 ±43
Through-thickness	0.77 ±0.02	1100 ±49

Discussion

The large discrepancy observed in the 2-ply sample is due to the aspect ratio of the sample itself, which means that a large surface area is exposed to the heat flux relative to the small thickness. Identical values were obtained for the 5 and 10-ply samples after applying the corrections, thus samples with a minimum thickness of 5 plies will be used onwards. Direct comparison of the

obtained thermal conductivity values with values available in open literature cannot be conducted, since the thermal properties of CFRP are affected by factors such as the thermal conductivity of the different types of carbon fibres, the conductivity of the matrix, the fibre volume fraction and the manufacturing process to name some. However, differences in the carbon content of PAN-based fibres can also influence the thermal conductivity, Toray's T300 (93% carbon) exhibit a thermal conductivity value of 10.4 W/mK, unlike the M50J (>99% carbon), also from Toray, with 97.9 W/mK. Although these values concern the fibre direction, the difference in carbon content also can affect the transverse thermal conduction [41]. Results reported by Ogasawara [18] suggest a through-thickness value of 0.609 W/mK, but without specifying the fibre content. Results presented by Sweeting [104] showed a thermal conductivity value of 0.5 W/mK for a UD laminate with 49% fibre volume content. Measurements by Han [12] for higher fibre volume content UD laminates, approx. 63%, showed a through-thickness value of 1.04 W/mK. However, these measurements were conducted at elevated temperatures. When the measured thermal conductivities obtained in this research, and considering variability due to manufacturing process and constituent materials (especially the thermal conductivity of the polymer matrix), it is assessed that the results of this research are in good agreement with the data reported in literature.

For the case of transverse measurements there is a lack of available literature to compare the values from this research against. However, it is assumed that the result obtained here are sufficiently accurate and reliable for the following reasons. Since the fibre volume fraction is relatively high, approx. 57%, and with the only difference between the transverse and through-thickness directions being the characteristics of the interlaminar regions, the thermal conductivity should not be considerably higher for a vacuum infused laminate. Furthermore, as the fabric used in this study contained a certain percentage of glass fibres, for stitching purposes, that were located both parallel and transverse to the carbon fibres, the heat conduction mechanism in the transverse direction can be expected to be affected, as glass fibres exhibit thermal conductivity similar to that of the epoxy matrix, approx. 0.3 W/mK [191].

Chapter 5 Randomly oriented GO/CFRP laminates[2]

5.1 Development of GO reinforced CFRP laminates

The GO nanoparticles were added into the epoxy matrix in prespecified quantities, as shown in Table 5.1. The dispersion of GO into the epoxy was realised by means of high speed planetary mixing, in a dual asymmetric centrifuge configuration, Flacktek Speedmixer™ DAC 150.1 FV, for 10 min at 3000 rpm at ambient temperature. This method introduces high shear forces into the mixture, and has been proven to provide good dispersion of carbonaceous nanoinclusions in epoxy [141], [192], [193]. After mixing, the curing agent was added and the mixture was hand stirred for 5 min followed by degassing at ambient temperature for 10 min, Fig.5.1. The resin inlet channel was positioned parallel to the fibre direction, Fig. 5.2. After the infusion process, the laminates were cured for 6 h at 70 ^{o}C, as specified by the resin manufacturer.

Additionally to the GO filler contents listed in Table 5.1, trials with higher filler contents of up to 10 vol% GO were made. The outcome was partially infused laminates, as the resin viscosity increased significantly with the higher volumes of filler, indicating that the mixture was at a percolating stage. Thus, the optimum GO filler content for infusion purposes will be below the percolation threshold of that of the GO/epoxy system.

[2] The content of this chapter is roughly equivalent to the content of the paper:
E. C. Senis, I. O. Golosnoy, J. Dulieu-Barton and O. T. Thomsen, “Enhancement of the electrical and thermal properties of unidirectional carbon fibre/epoxy laminates through the addition of graphene oxide”, Journal of Materials Science, https://doi.org/10.1007/s10853-019-03522-8

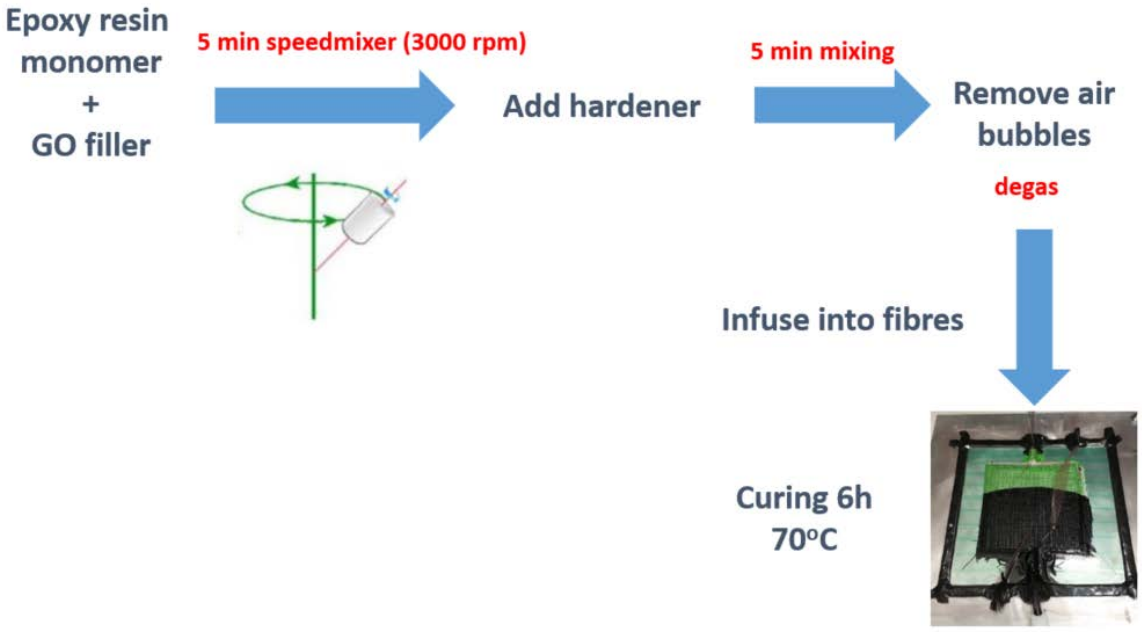

Figure 5. 1: GO-reinforced laminates manufacturing route.

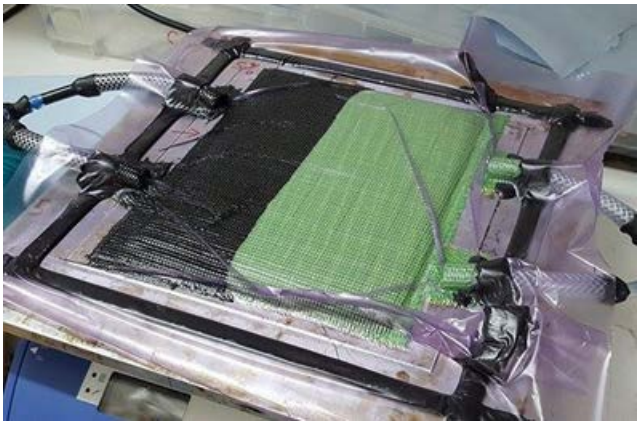

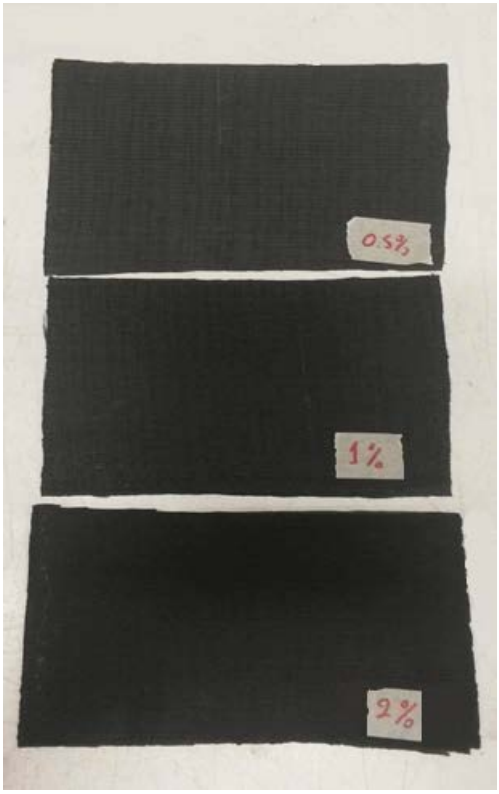

Figure 5. 2: (left) Infusion of a GO modified laminate (laminate dimensions: 25x25cm) and (right) cured GO/CFRP laminates (laminate dimensions 12x20cm).

Table 5. 1: Composition of manufactured GO reinforced CFRP laminates. (Matrix volume V_m% and V_{GO}% are estimated based on the volume of GO dispersed into the matrix).

Sample	V_f%	V_m%	V_{GO} %
Neat	57	43	0
0.32 vol%	57	42.87	0.14
0.63 vol%	57	42.73	0.27
1.26 vol%	57	42.46	0.54
2.52 vol%	57	41.92	1.08
3.78 vol%	57	41.37	1.63
6.3 vol%	57	40.29	2.71

5.2 Sample morphology

The morphology of the manufactured CFRP samples was examined by means of optical microscopy with the use of an Olympus BX 51 microscope and a Carl Zeiss EVO 50 SEM. This technique was used also used to produce micrographs to obtain the fibre volume content of the manufactured laminates as well as to assess the distribution of the GO nanofiller.

To estimate the fibre volume content of the manufactured laminates a series of steps were followed. Small samples were cut randomly from the manufactured plates. The samples were then polished with the use of Silicone Carbide surfaces varying the grit number. Water was used as lubricant up to the 1200 grit sandpaper, and the speed of the polishing apparatus was 300 rpm. For the last stage of the polishing process, a solution containing 1μm diamonds was used. The polishing procedure followed is listed in the table below, Table 5.2.

Table 5. 2: Polishing steps

Surface	Force (N)	Time
SiC 400	35	30sec
SiC 800	35	2min
SiC 1200	40	2min
SiC 4000	40	2min plus 2min with change of surface

The determination of the fibre volume content was realized with the use of the Olympus Stream Essentials software. By applying a threshold, Fig. 5.2 (right), to an already taken image (greyscale), Fig. 5.2 (left), a segmentation that isolates objects can be achieved, thus enabling distinction between the two different phases, i.e. the fibres and the matrix. This is realized by converting

greyscale images to binary data, setting all pixels below some threshold level to zero and all pixels about that threshold level to one. The fibre volume fraction can then be estimated by calculating the surface area of each phase.

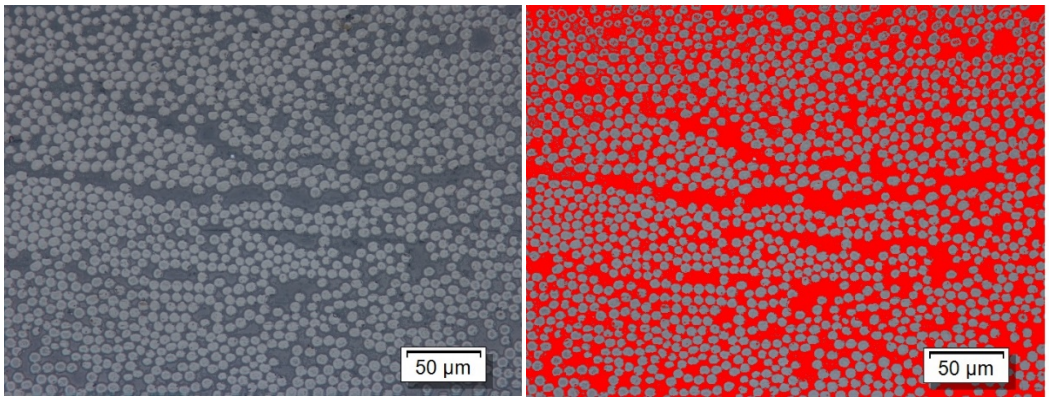

Figure 5. 3: (left) Initial image and (left) image after applying threshold. Fibre volume content approximately 55%.

A collection of produced micrographs, including the estimates of the fibre volume fractions, can be found in the Appendix B. From the obtained micrographs the estimated fibre volume content values ranged between 55% up to 58%, which it is in good agreement with the 57% which was the target. The slight variation is attributed to the manufacturing process, and it is a characteristic of the vacuum infusion process since the resin flow can alter the fibre distribution through the sample, hence the variation.

Due to the large number of samples manufactured in this study, an additional method for assessing the volume fraction of the laminates was also employed. By measuring the thickness of the manufactured CFRP plate it is possible to estimate the fibre volume fraction using the cured ply thickness equation (cpt), eq. 5.1 [194] as follows:

$$cpt = \frac{W_f}{10\rho_f V_f}, \qquad \text{eq.5.1}$$

where W_f is the aerial density of the fabric used for the laminates, ρ_f is the density of the fibres used and V_f is the fibre volume fraction.

This simple relation is used by routinely by industry to estimate the fibre volume content of laminate. For the purposes of this study, laminates with an approximate carbon fibre volume content of 57%, the parameters of the cured ply thickness equation had the values listed in Table 5.3.

Table 5. 3: Cure ply thickness equation parameters for the CFRP laminates manufactured in this study.

Parameter	Input value
CPT	0.85 mm
W_f	882 g/m^2
ρ_f	1.81 g/cm^3
V_f	57%

To assess the morphology of the samples containing GO, observation under the optical microscope were initially conducted. The samples were sliced open to expose the surface of the fibres. The samples under examination were then submerged in acetone to remove any remaining dust or by-product of the slicing/cutting process. This procedure has been carried out for both the CFRP infused with neat epoxy and GO-reinforced CFRP to compare their morphology. In Fig. 5.3 (a), the surfaces of individual fibres of unmodified CFRP is depicted. Similar images for a GO-reinforced CFRP are presented in the Fig. 5.3 (b), (c), (d). By comparing the figures, it is seen that GO particles are observed on the surfaces of the fibres for the GO-reinforced CFRP. The difference in the image color is attributed to the different filters used in the optical microscope as a means to enhance the contract between the fibres and the GO particles.

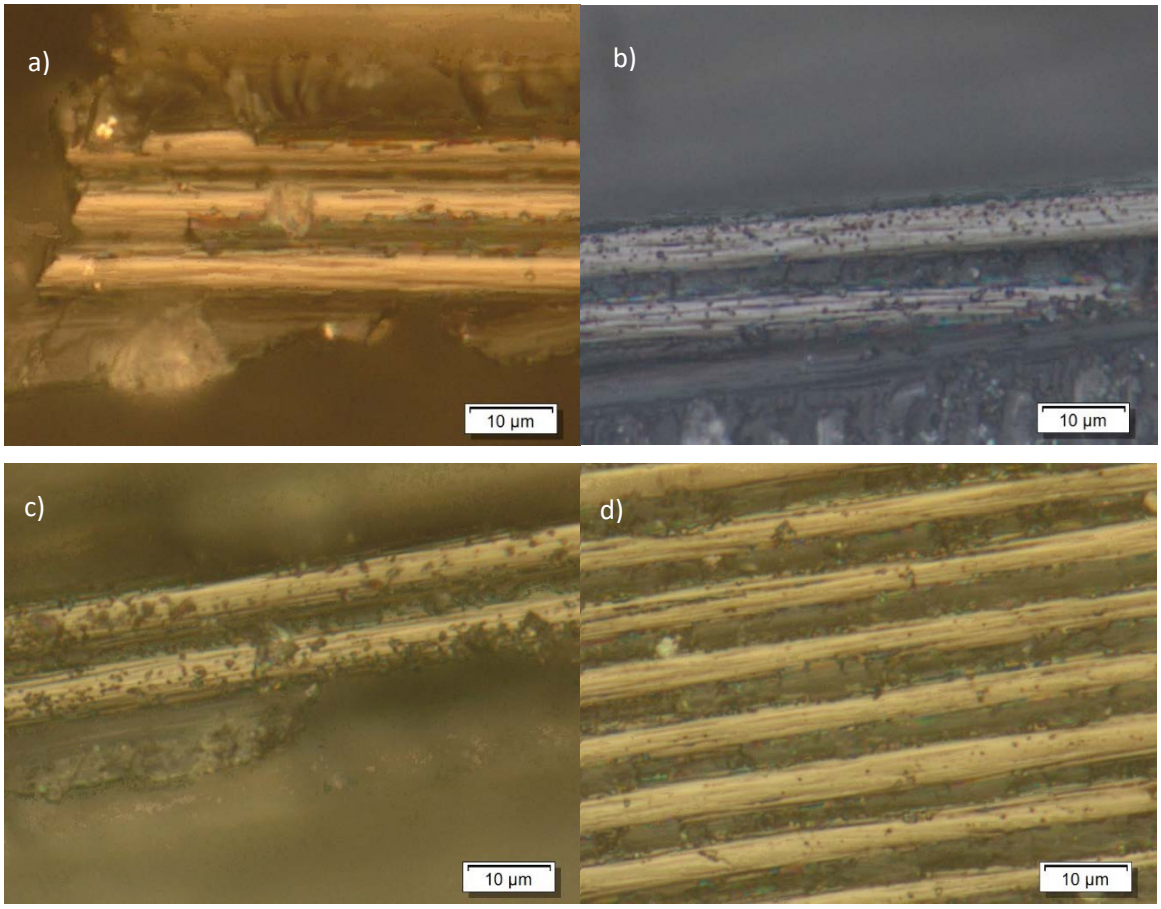

Figure 5. 4: a) fibre surface of neat CFRP, b) and c) 6.3 vol% GO/CFRP laminate and d) GO 0.63 vol% GO/CFRP laminate.

Further investigation with the use of a Scanning Electron Microscope (SEM) was conducted to obtain clear images of the morphology of the sample surfaces and to provide further information regarding the addition of GO. The images are presented in Fig. 5.4.

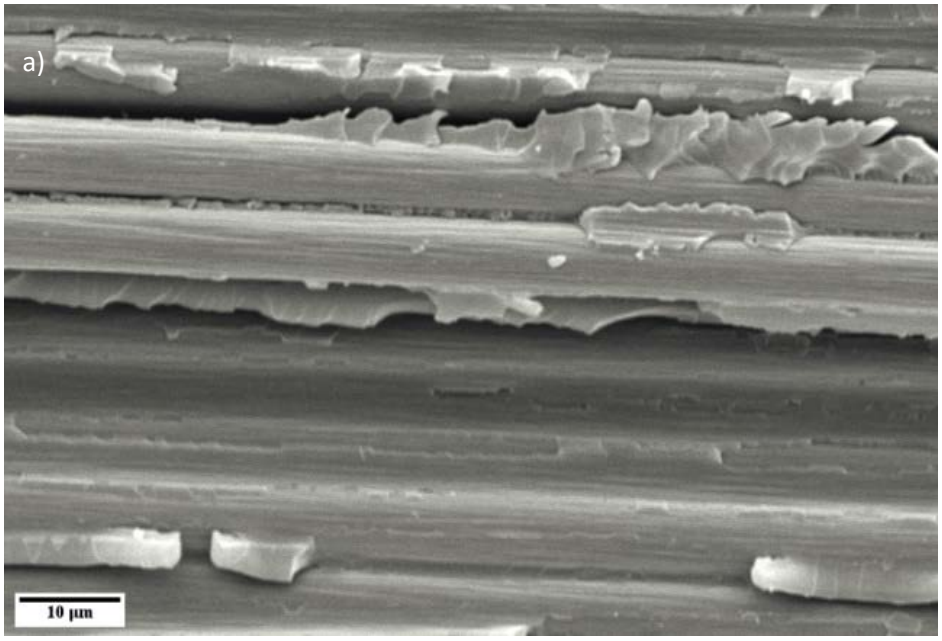

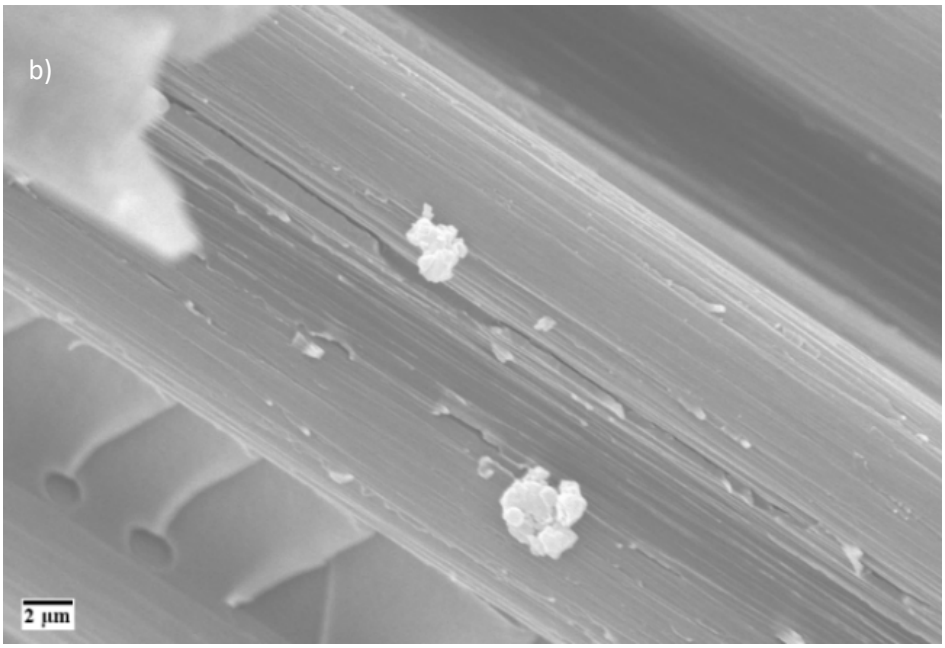

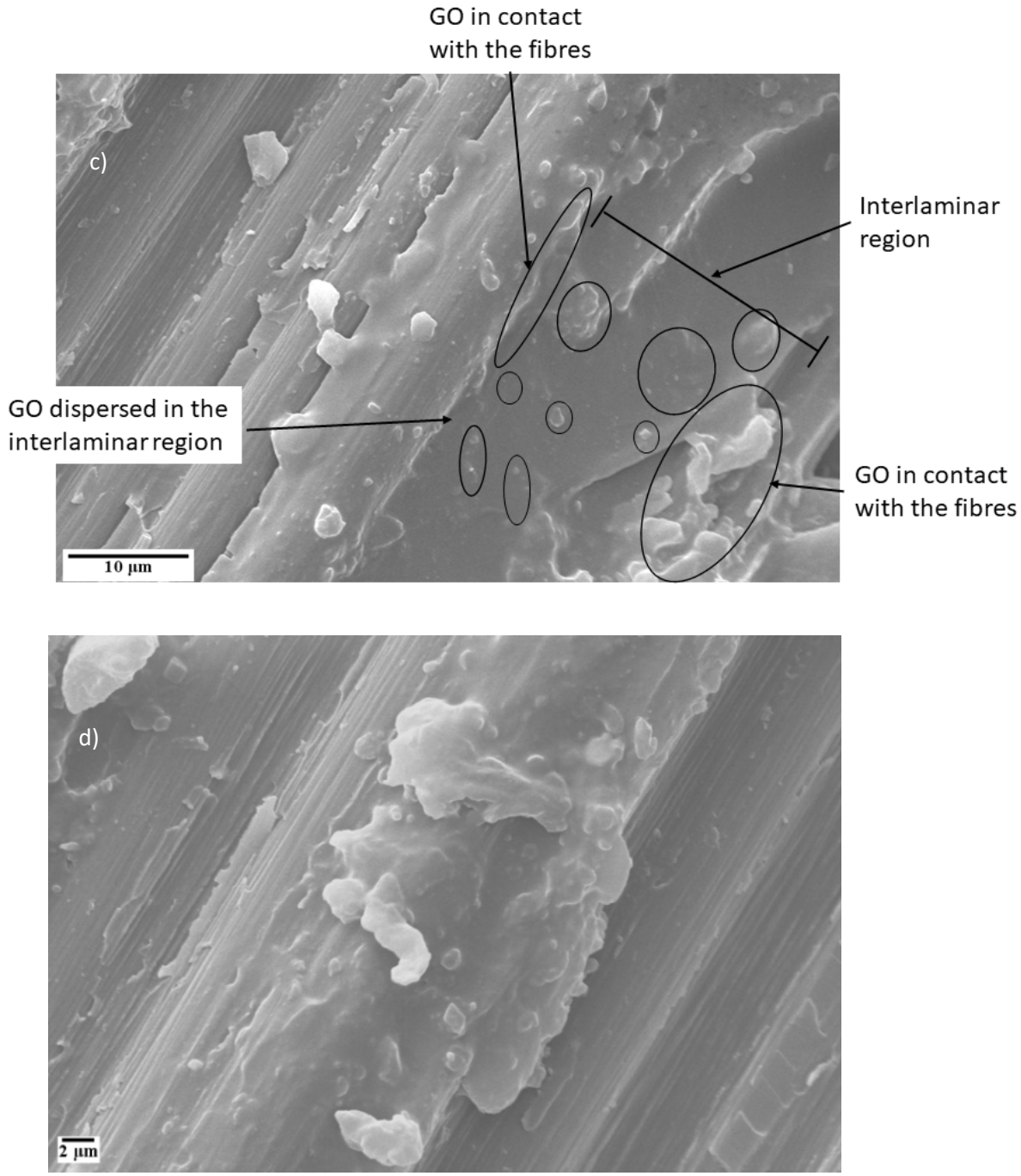

Figure 5. 5: Scanning electron microscopy images for the samples containing: a) neat CFRP, b) 0.63 vol% GO (fibre surface view), c) 6.3 vol% GO (interlaminar region) and d) 6.3 vol% (fibre surface view).

Discussion

From the SEM images it is seen that the morphology of the inclusions dispersed into the CFRP laminates appear to be similar to the dimensions stated by the supplier, see Fig. 5.4 b). As expected, inclusions in the form of aggregates are observed for high filler contents, but they cannot be considered as a case of severe aggregation. Aggregates with dimensions similar to the fibre

diameter will significantly affect both the infusion process and the mechanical response of the laminate. This is because of the oxygen groups that exist in GO that contribute to larger intramolecular distances, thus creating weaker bonds, making it easier for exfoliation from thicker graphene stacks into small platelets, even using simpler methods such as planetary mixing [140], [192]. Furthermore, the GO particles are seen be located in the close vicinity of the fibre surfaces, which is indicative of good compatibility of the filler with the epoxy matrix and the epoxy-based sizing of the fibres. In the case of high GO filler loading, i.e. 6.3 vol%, it is worth noting that the concentration of filler adjacent to the fibres, see Fig. 5.4 d), where GO appears to be attached to both the epoxy and the fibres forming an interfacial region. This particular feature suggests compatibility between GO and epoxy resin as suggested in the literature [154], and can be expected to provide improvements of the electrical and thermal conductivities as well as the mechanical stress transfer capability.

5.3 DC electrical conductivity

As already mentioned in Chapter 3, to mitigate any influence of unsatisfactory distribution of the nanofiller because of the infusion process, measurements were achieved both in the resin inlet side and the vacuum suction side, along the resin flow. For this reason a laminate type, as depicted in Fig. 5.5, was devised. The samples were initially cut in half, perpendicular to the infusion line. Measurements were carried out first for the transverse direction, sample annotation TR-1 and TR-2, before being cut to form samples TT-1 and TT-2 for through-thickness measurements. The rest of the samples was used to conduct ILSS tests.

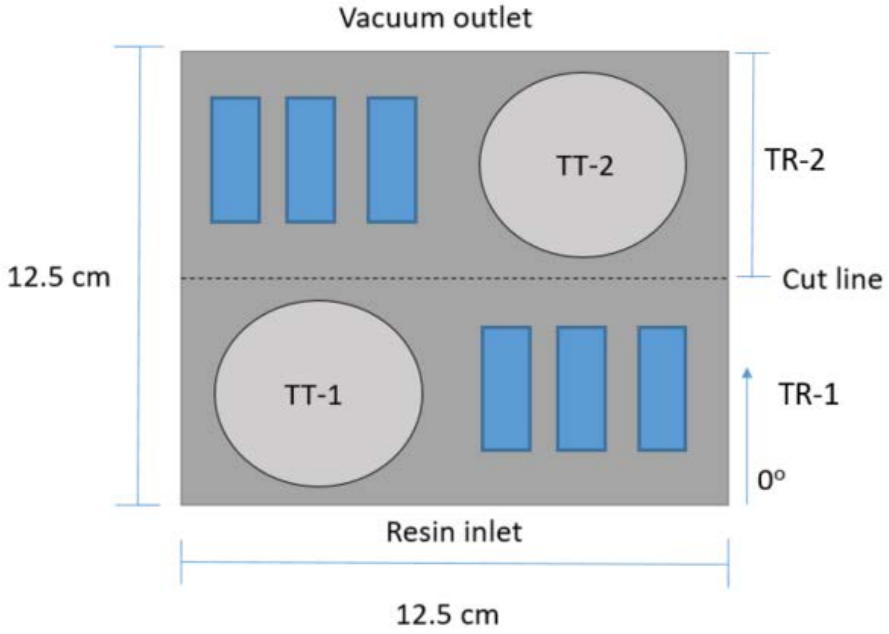

Figure 5. 6: Schematic of the position the samples were cut off, measurement areas (TR: transverse, TT: through-thickness, blue shade samples were used for ILSS testing).

5.3.1 Transverse electrical conductivity

The influence of GO filler content on the electrical conductivity in the transverse direction is shown in Fig. 5.6. It is seen that the addition of GO leads to a slight increase of the conductivity values. No substantial increase was observed for low filler contents, i.e. below 1.26 vol%, but the effect becomes more pronounced at filler contents above 2.52 vol% where a non-linear increase occurs with further addition of GO reaching its maximum value of approx. 0.7 S/cm at 6.3 vol%.

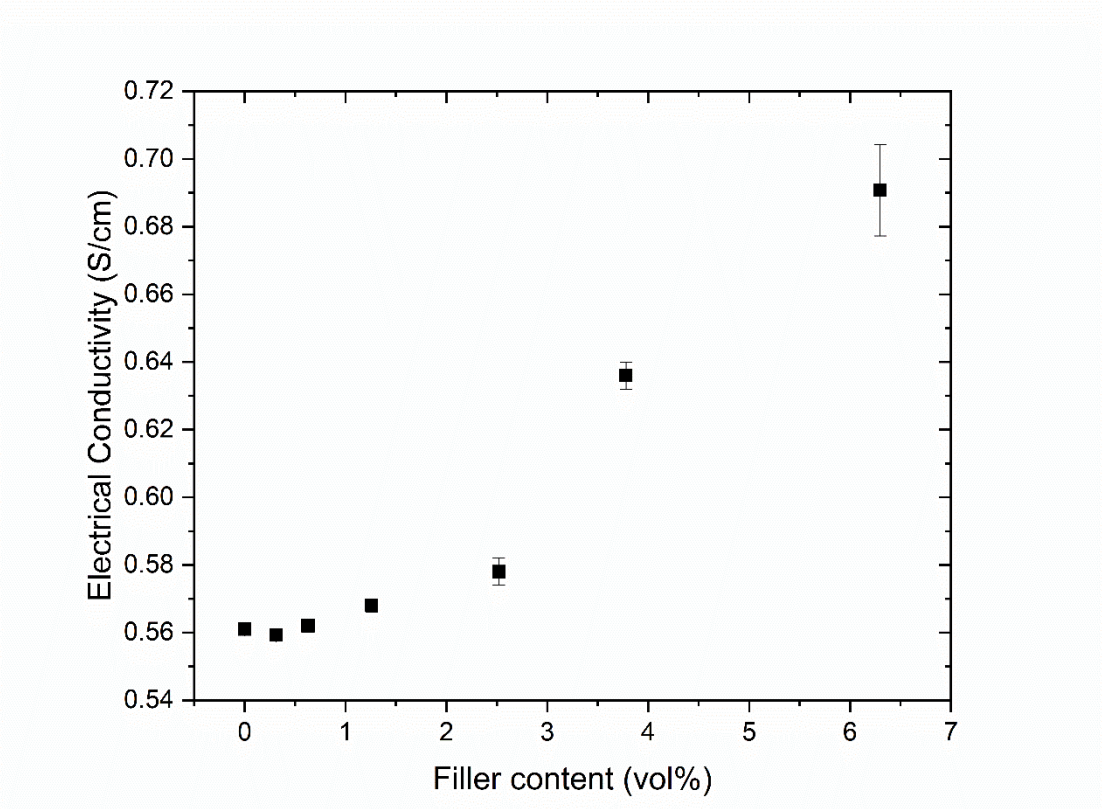

Figure 5. 7: Transverse electrical conductivity as a function of GO vol% dispersed into the polymer matrix.

Discussion

For the transverse electrical conductivity, the measurements (see Fig. 5.6) show that the low contents of GO up to 2.52 vol% do not have a significant effect, exhibiting values that are very similar to the neat CFRP properties. However, at high filler contents, 6.3 vol%, an increase of the electrical conductivity is observed. Although this increase cannot be described as substantial, it is not expected that drastic increases in the transverse direction will occur since current conduction is dominated by fibre-to–fibre contact points [195]. Considering that the laminates manufactured in this study have fibre volume fractions well above the percolation threshold, which is approx. 40 vol% [73], the addition of high contents of GO can only decrease the contact resistance between

the fibres or interconnect adjacent fibres at multiple points along the bulk of the laminate. Thus, by reducing the intra-lamina resistance, combination of fibre to fibre contact resistance and volume resistance of the polymer between the fibres, the composite behaves similarly to a laminate with a higher fibre volume fraction. Less space between the fibres is occupied by the insulating epoxy matrix. Hence, the observed non-linear increase for high GO contents, in this case above 2.52 vol%. The above mechanism is supported by the SEM characterization (see Fig. 5.4 (c)), where GO flakes appear to interconnect adjacent carbon fibres, within the same lamina.

5.3.2 Through-thickness electrical conductivity

From the through-thickness direction measurements (see Fig. 5.7), it is seen that the GO filler content does have significant influence on the electrical conductivity, and a nonlinear increase can be observed with the addition of GO. At low GO contents, i.e. 0.32 vol% and 0.63 vol%, a modest increase of the conductivity is seen. Further increasing the GO content, i.e. to 1.26, 2.52 and 3.78 vol%, leads to a more substantial rise of the conductivity as the higher volume of conducting inclusions dispersed into the interlaminar region polymer facilitate the current flow through the laminate bulk. Since interlaminar regions are dominated by the polymer matrix, the associated conduction mechanism, in this case tunnelling through the dispersed GO flakes, can be treated as in a polymer composite, where the dependency of the electrical conductivity from the filler content is non-linear [196]. For the highest GO filler content, i.e. 6.3 vol%, a threefold increase of the electrical conductivity is observed, where the conductivity reaches the same order of magnitude as in the transverse direction, i.e. 0.18 S/cm and 0.56 S/cm, respectively. The explanation for this behaviour is supported by the SEM images, see Fig. 5.4 (c), which indicate that GO inclusions interconnect the adjacent laminae by forming conducting paths through the interlaminar region.

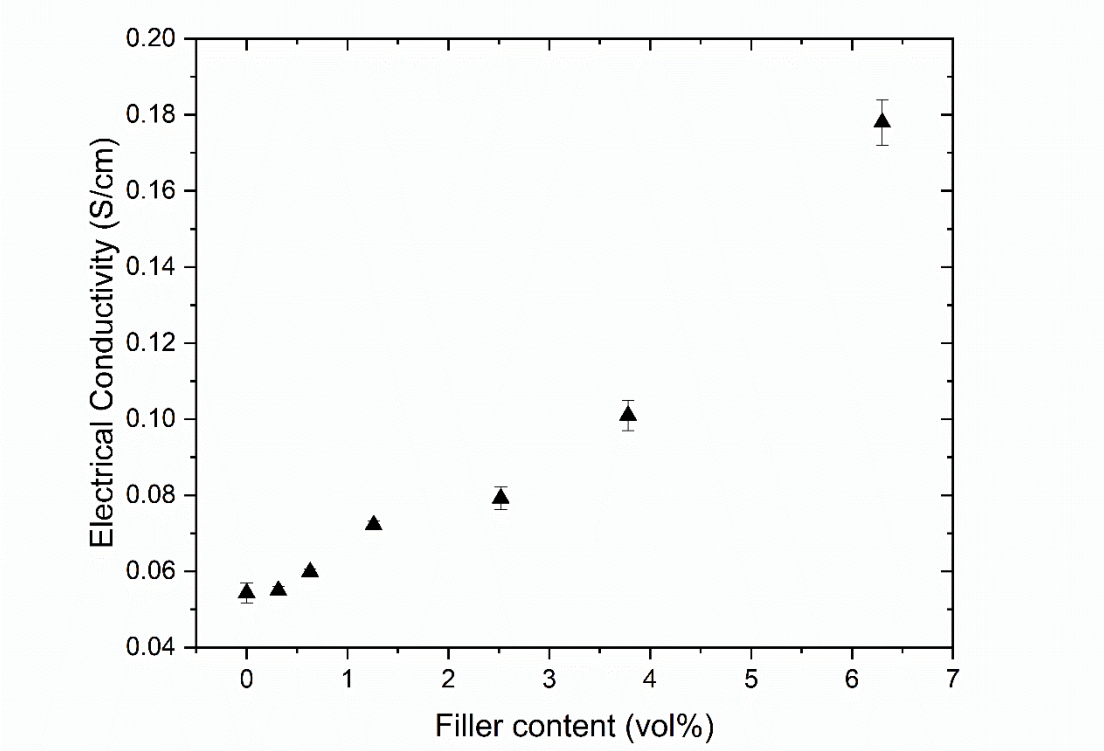

Figure 5. 8: Through-thickness electrical conductivity as a function of GO vol% dispersed into the polymer matrix.

Discussion

It has been reported that different fillers and filler incorporation methods can also provide improvement in electrical conductivity for comparable material and processing systems suitable for large volume manufacturing. For instance, the use of GNPs in the fibre's sizing has led to improvements with values up to 0.07 S/cm [110], which is less than the improvement reported here. The incorporation of several types of CNTs has shown its potential with achieved through-thickness electrical conductivity values ranging from ~10^{-3} S/cm [80], [197] up to 0.089 S/cm [125], which is similar to that reported here for the lower filler contents. However, it should be noted, that it is difficult to increase the content of CNTs due to the increase in viscosity of the polymer matrix and possible degradation of some of the mechanical properties. So far the highest reported value of through-thickness electrical conductivity for a CFRP laminate is 1.1 S/cm [13], but it should be noted that this was not achieved for an epoxy matrix but rather polyaniline (PANI) that exhibits considerably lesser mechanical properties than epoxies. Although the increase observed in this study is significant, it is clear that to produce a through-thickness conductivity identical to the conductivity in the transverse direction, significantly higher quantities of filler need to be infused into the laminate to deliver a high degree of percolation into the matrix material. Ideally, this would provide further increase in the conductivity since the physical current conducting paths are formed

prior to the infusion. However, higher levels of filler loading will make the matrix material difficult to handle as the viscosity increases drastically when percolation is observed, and it will prevent a good wetting of fibres and matrix consolidation during the infusion process. Also, higher GO filler contents are likely to have a degrading effect on the ILSS.

Regarding the bulk matrix modification method of incorporation of the nanofiller into the laminate, it should be pointed out that this this research represents one of the first studies in which the nano/modified polymer matrix has been infused into the continuous fibre carbon fabric, since the majority of the published studies involve hand layup processes [54], [80], [144], [198]. Only recently Gaztelumendi [131] and Umer [199] presented infusion processes of MWCNT/epoxy into CFRP and GO/epoxy in GFRP, respectively.

An aspect that is critical in the case of nanoreinforced CFRP made with infusion processes is to avoid the filtration of the inclusions by the fibre network. Although this is a valid statement or claim, parameters such as filler shape/size and the state of dispersion within the epoxy matrix prior to the infusion can greatly affect the distribution of the filler into the laminate bulk. To assess this, as stated in the introduction of the section, measurements of the through-thickness and transverse electrical conductivity were conducted along the infusion direction, see Fig. 5.5. Potential discrepancies between the measured values can be considered as an indication of unsatisfying dispersion of filler. As seen in Fig. 5.7, the scatter of the measured values is small and can be considered negligible. It is thus assumed that the filtration effects were mitigated for two distinctive reasons: unlike other commercially available platelets (GNPs etc.), the GO used in this study had a mean diameter of 500 nm compared to 2-5 µm that is commonly found. Secondly, the method of dispersing the filler into the epoxy, planetary mixing, has shown great results in achieving homogenous dispersion of graphitic fillers within polymers [141], [200], [201].

5.4 Thermal conductivity

5.4.1 Transverse thermal conductivity

Fig. 5.8 shows that different GO filler contents do not have any significant influence on the measured transverse thermal conductivity, with only minor changes from the neat CFRP system value being observed. This is because, unlike the through-thickness direction, in the transverse direction, there are no interlaminar resin rich regions, which means that the heat flows mainly through the fibres passing small epoxy gaps between them. The main thermal resistance mechanism in this case would be heat flux funneling towards fibre contacts. Hence, the addition of GO filler cannot provide noticeable improvements as observed for the through-thickness direction

(next section). The marginal decrease with increasing GO filler content, although within the experimental measurement uncertainty, can likely be attributed to fibre contact topology changes caused by fibre volume fraction variations during the infusion process. In addition, considering that the volume of GO dispersed in the bulk of the laminate does not surpass 2.7 vol%, no significant increase was expected.

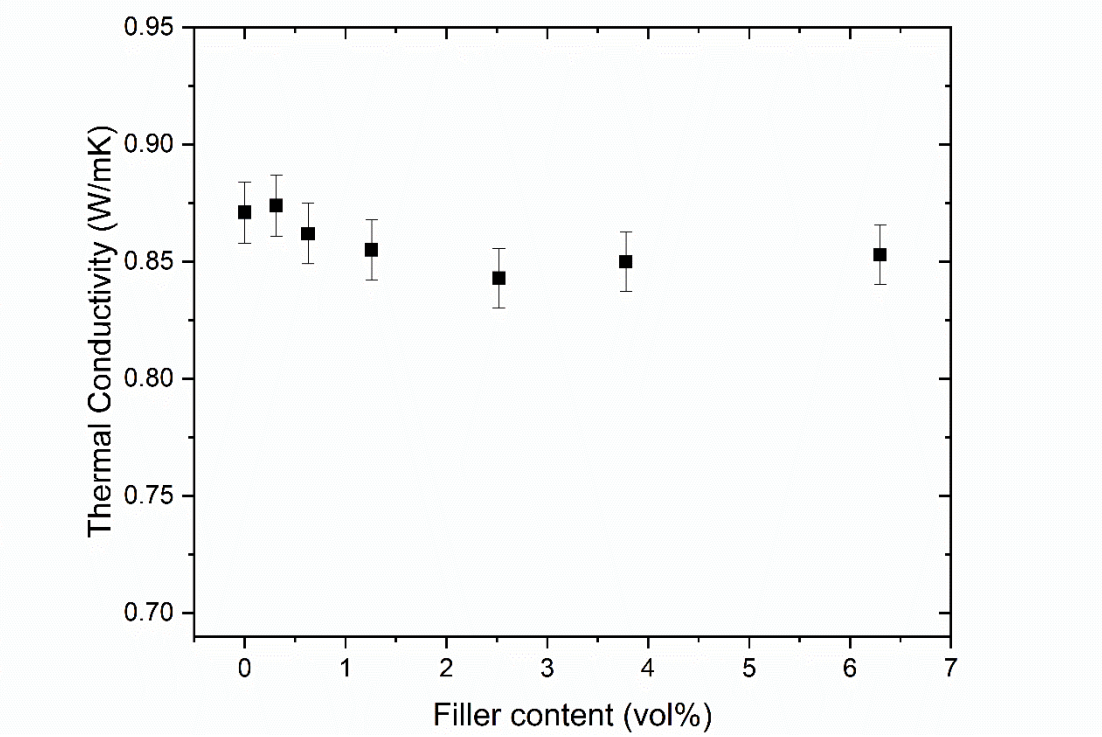

Figure 5. 9: Transverse thermal conductivity as a function of GO vol% dispersed into the polymer matrix.

5.4.2 Through-thickness thermal conductivity

The through-thickness thermal conductivity is presented in Fig. 5.9 as a function of the GO filler content dispersed into the epoxy matrix. When filler contents below 2.52 vol% are used, the thermal conductivity is not significantly affected by the addition of GO. Above 2.52 vol%, the thermal conductivity increases approximately linearly up to the highest GO filler content, i.e. 6.3 vol%.

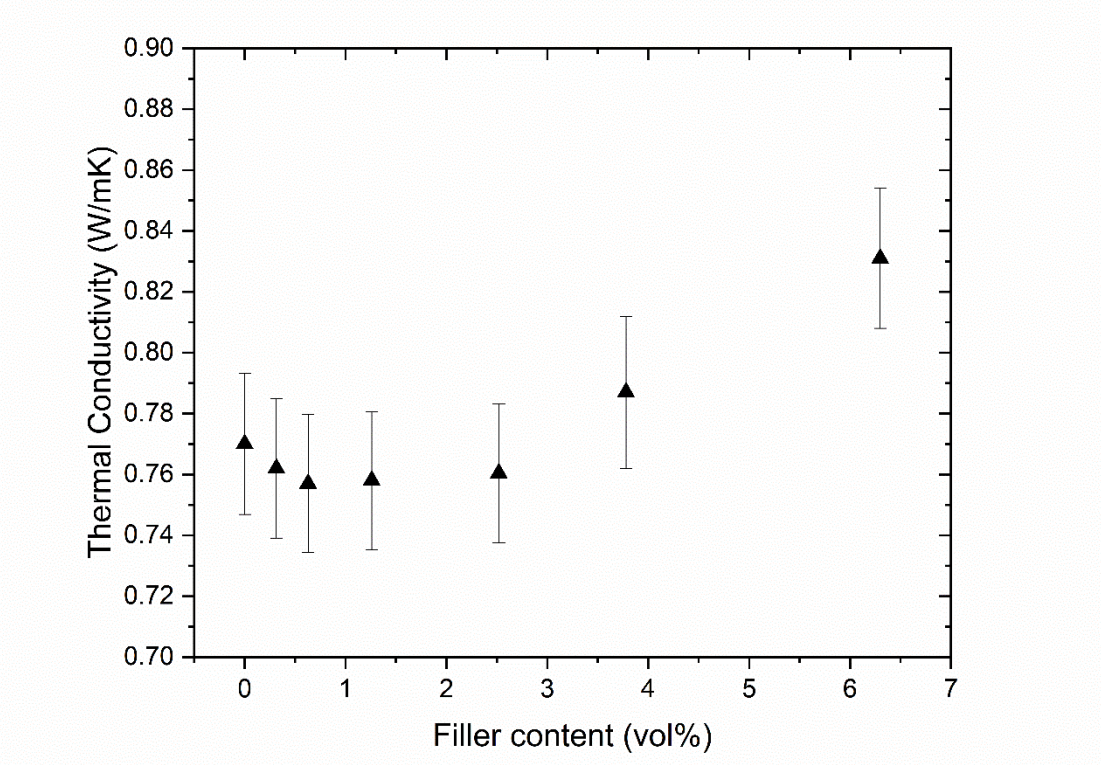

Figure 5. 10: Through-thickness thermal conductivity as a function of GO vol% dispersed into the polymer matrix.

Discussion

As indicated by the measurements, significant thermal conductivity improvements are only observed when high amounts of conducting filler are added to the epoxy matrix, i.e. 6.3 vol% GO. The associated mechanism hypothesized to be the enhancement of thermal conduction along the platelet shaped GO inclusions that occurs in the interlaminar regions of the thermally insulating polymer matrix. Unlike the electrical conductivity, improvements in thermal conductivity of a polymer require significantly higher filler loadings, which is not surprising since the values of thermal conductivities for GO and epoxy are only two orders of magnitude apart [61]. Hence, improved thermal conductivities can only be seen for 3.78 and 6.3 vol% filler content. Although the addition of a thermally conducting filler can assist the thermal conduction process, particular fillers and manufacturing/dispersion processes can further affect the rate of improvement, for example by aligning GO inclusions in a particular direction which is consistent with the conventional effective medium field theory [202]. For the case of GO filler, the oxygen content represents impurities in the crystalline structure of the filler, and can greatly affect the thermal conductivity of the filler itself [156], [157]. For the as-received GO used in this study, the oxygen content was between 5-10%, which can be considered as low, and, thus, the thermal conductivity of the filler will not be affected drastically. Molecular dynamic simulations have shown that the thermal conductivity of GO can be reduced down to 8.8 W/mK when the oxygen coverage is close to 20% [157]. Similar

results were reported after characterizing the thermal conductivity of free-standing GO films [156]. For low filler contents, up to 2.52 vol%, the added filler is insufficient to provide additional conduction in the interlaminar region, and the measured thermal conductivities are of the same magnitude as for the neat CFRP laminate. However, for 6.3 vol% filler content, the through-thickness thermal conductivity increased up to a point of reaching almost identical values as observed in the transverse direction of the neat CFRP. This is probably related to a non-uniform distribution of GO flakes, as at high GO vol% the flakes mainly accumulate in the interlaminar regions making the local vol% of GO higher than the average in the laminate bulk. The highest thermal conductivity measured in the present study is 0.83 W/mK, but even higher values have been reported in the literature [12]. However, many other factors have an effect on the thermal conductivity of nanoreinforced laminates such as the carbon fibre type, the fibre volume fraction, the thermal conductivity of the epoxy, the manufacturing method, the method of adding the nanofiller into the composite and the measurement temperature. Here the important factor is the suitability of the materials and the process for large volume manufacturing (as discussed in the previous section of the paper). Leaving that aside, similar values, 0.86 W/mK, have been reported for laminates containing GNPs, for the same filler content [147], but also for a significantly lower filler content of 0.5 wt%, 0.84 W/mK [102], but the GNPs were deposited directly onto the carbon fabric, adding both to cost and the complexity of the manufacturing process. Significantly lower values, approx. 0.53 W/mK, were observed in laminates containing both GNPs and SNPs, however, at a much lower fibre volume fractions [109].

5.5 Interlaminar Shear Strength

The ILSS results are shown in Fig. 5.10. It is seen that the addition of relatively low GO contents, i.e. 0.315 vol% and 0.63 vol%, provide significant improvements of the ILSS relative to the CFRP neat system; with increases of 29.7 % and 58.4 %, respectively. For higher GO filler contents, i.e. 1.26 vol% and 2.52 vol%, respectively, no significant effect on the measured ILSS is observed relative to the neat CFRP, albeit a except for modest improvements by 9.5% and 17.6% are see. The CFRP with 6.3 vol% GO displayed an ILSS that is 37 % higher than the neat CFRP system.

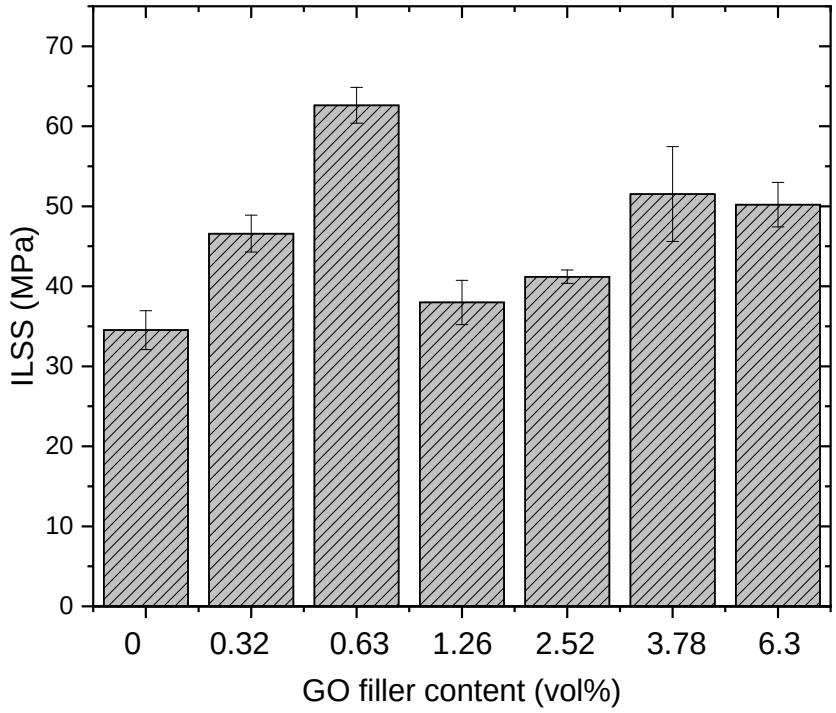

Figure 5. 11: Interlaminar shear strength as function of GO filler content dispersed in the polymer matrix.

Discussion

In general the ILSS of epoxy/carbon fibre composites can show large variations, with values ranging from 40 to 100 MPa [185], mainly affected by the surface treatment of fibre and the fibre volume fraction. The ILSS of neat CFRP is dependent from the shear properties of the polymer matrix and the fibre-matrix adhesive properties assuming the fibre volume fraction remains the same throughout the investigation [110]. Thus, ILSS can provide a good indication about whether the addition of a filler affects the matrix-fibre stress transfer properties.

From the ILSS tests conducted for varying GO filler contents it is observed that the addition of GO into the epoxy matrix leads to increased ILSS values, i.e. to improved matrix-fibre stress transfer. For low GO filler contents, i.e. 0.32 vol% and 0.63 vol%, a sharp increase in the ILSS is seen. The observed improvement can be attributed to the planar geometry of the GO filler agglomerates (flakes), with large surface areas, leading to enhanced filler/matrix adhesion [153], [203]. At low filler contents, it can be assumed that the filler is homogenously dispersed in the bulk of the laminate, which enables the GO flakes to effectively act as crack deflectors, thus suppressing further crack propagation into the epoxy matrix. In addition, as observed in the SEM images (Fig. 5.4 (b)), the rough or wrinkled GO flake surfaces contribute to the interlocking of the polymer matrix onto the GO. Moreover, the oxygen and hydroxyl functional groups of GO effectively bond the filler with

the epoxy matrix since Bisphenol A type of resins (similar to the one used in this study) contain epoxy and hydroxyl groups in their structure [132]. For intermediate filler contents, i.e. 1.26 vol% and 2.52 vol%, some aggregation is observed, and this can cause the formation of local stress concentration zones leading to decreased ILSS values compared to the samples containing finely dispersed GO flakes, while still providing improved behaviour in comparison to the neat CFRP. By further increasing the GO filler content, i.e. 6.3 vol%, notwithstanding the aggregation of the fillers, the higher dispersed volume of GO flakes provides a secondary reinforcement and strengthens both the epoxy/carbon fibre interphase and polymer interlaminar regions [204]. This explains the substantially increased ILSS value relative to the values obtained for the intermediate GO filler content samples, and is supported by the literature where improvements in ILSS are reported for other means of filling, including the incorporation of GO into the sizing and depositing GNPs directly onto the carbon fabric. Similar results to those found in this report are reported [102], [107], thus confirming the efficiency of incorporating GO filler directly in the bulk matrix.

Chapter 6 Aligning GO with an external applied electric field[3]

6.1 Introduction

For the development of CFRP laminates containing aligned GO, the GO filler contents listed in Table 6.1 were added to the epoxy matrix prior being infused to the dry fibres. Although the same carbon fibres and GO was used for the manufacturing of the aligned GO-CFRP laminates (A-GO/CFRP), a different epoxy resin was used, as the previous resin system (BASF Baxxores) was stopped from production. As stated in section 3.2.1, the replacement epoxy was provided by a different supplier that was licenced to produce the previously used epoxy according to the same chemical formulation.

Table 6. 1: Composition of the manufactured laminates

Wt_{GO}% (matrix)	V_{GO}% (matrix)	V_{GO}% (laminate)	V_f%
0.5	0.32	0.14	57
1	0.63	0.27	57
2	1.26	0.54	57
3	1.89	0.81	57
4	2.52	1.08	57
5	3.15	1.35	57

6.2 Methodology/Experimental setup

The theory describing the mechanism of the electric-field-induced alignment of a filler in a polymer medium is well documented in the literature for a wide variety of fillers [148], [201], [205]–[210]. Briefly, when a sinusoidal alternating field is applied to a conductive rod or platelet-like inclusion located in a dielectric liquid, a dipole moment is created due to charge accumulation around its edges, Fig.6.1 [201], [211], [212]. This polarization is generated due to the difference in electric

[3] The contents of this chapter is roughly equivalent to the contents of the paper:
E. C. Senis, I. O. Golosnoy, T. Andritsch, J. Dulieu-Barton and O. T. Thomsen, "The influence of graphene oxide filler on the electrical and thermal properties of unidirectional carbon fibre/epoxy laminates: effect of out-of-plane alignment of the graphene oxide nanoparticles", Polymer Composites, https://doi.org/10.1002/pc.25637

conductivity between the dielectric liquid and the inclusion creating a moment acting to the inclusion. Due to their shape, platelet inclusions exhibit higher polarization parallel to the platelet surface over the normal direction to their plane [211]. This allows platelets to be oriented with the lateral dimension parallel to the applied electric field. For the case of Graphene-based inclusions, this axis corresponds also with the axis of higher conductivity, as it is parallel to the graphene basal planes. In conjunction, the accumulation of opposing charges on the edges of the platelet favours the formation of chains-like networks as attractive forces between opposing charges interconnect adjacent inclusions, Fig.6.1, [212]. The main factor affecting the alignment process is the viscous friction that originates from the surrounding polymer, and it is responsible for balancing the field-induced torque. To calculate an approximate time (in seconds) for a flake shaped inclusion to be aligned with an E-field the following expression can be used [211]–[213]:

$$t_{flake} = \frac{1000}{\lambda\, \eta\, \varepsilon_0\, E^2}\ , \qquad \text{eq. 6.1}$$

where λ is the aspect ratio of the flake, η is the viscosity of the surrounding liquid in Pa s, ε_0 is the permittivity of free space (8.854 10^{-12} F/m) and E is the intensity of the field in V/m.

In this study where λ is 50, η is 0.275 Pa s and an applied field of 30 kV/m (30 V/mm), an approximate time of 0.58 sec is required for a flake to be oriented to the direction of the applied field.

In a similar manner the chain formation time can be estimated as follows [211] :

$$t = \frac{10\, \eta}{\varepsilon_0\, E^2}\,, \qquad \text{eq. 6.2}$$

where η is the viscosity of the surrounding liquid in Pa s, ε_0 is the permittivity of free space (8.854 10^{-12} F/m) and E is the intensity of the field in V/m.

Using the same input parameters as in eq. 6.1 the chain formation time was estimated to 344 sec, or approx. 6 min. Similar results have been recently obtained in a study concerning the alignment of graphene flakes within an epoxy [201]. As seen from the obtained results, even using a relatively low E-field (something that is preferable from a manufacturing perspective) a relatively short time is required to orient the filler and to start the formation of a chain-like network. The advantage of this mechanism/method is the formation of a percolating network without the necessity for the composite system to be already in the percolating phase. This can be beneficial for the processability of nanocomposite matrixes since percolating systems exhibit higher viscosity, thus hindering their use in infusion/moulding processes.

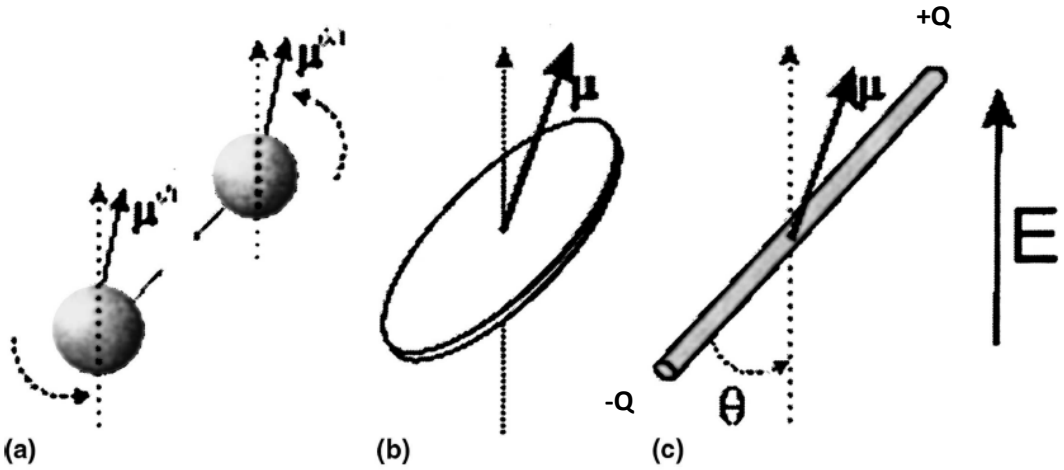

Figure 6. 1: a)Dipole-dipole attraction moves two inclusions towards each other and aligns them in the field direction; and b) and c) field-induced torque orients non-spherical inclusions along the field, μ represents the electric field-induced polarization. Figure adapted from [212].

To align the GO flakes into the bulk of the laminate a capacitor-like configuration was created based on the mould used for the infusion of each laminate, Fig. 6.2. A major concern when applying an electric field to an epoxy resin in liquid state is the higher permittivity/conductivity that epoxies exhibit compared to when they are in their solid state [214], [215]. Hence, current flow needs to be eliminated to avoid resistive heating phenomena. Thus, a PET tape was applied to the mould surface to electrically insulate the laminate from the mould. A second electrode was placed outside of the vacuum bag to avoid direct contact with the liquid matrix. The sin wave voltage signal was applied to the electrodes through a TTi TG1010A function generator connected to a TREK PZD 700A high voltage amplifier. The field parameters, 30 V/mm at 10 kHz, were chosen based on previous studies conducted in epoxy systems containing GNPs with similar Oxygen content, below 10%, [201] as well as other carbonaceous inclusions dispersed in polymer matrixes [148], [216]. The application time, 40 min, was determined based on the epoxy viscosity development with temperature during the curing process (information provided by the resin supplier).

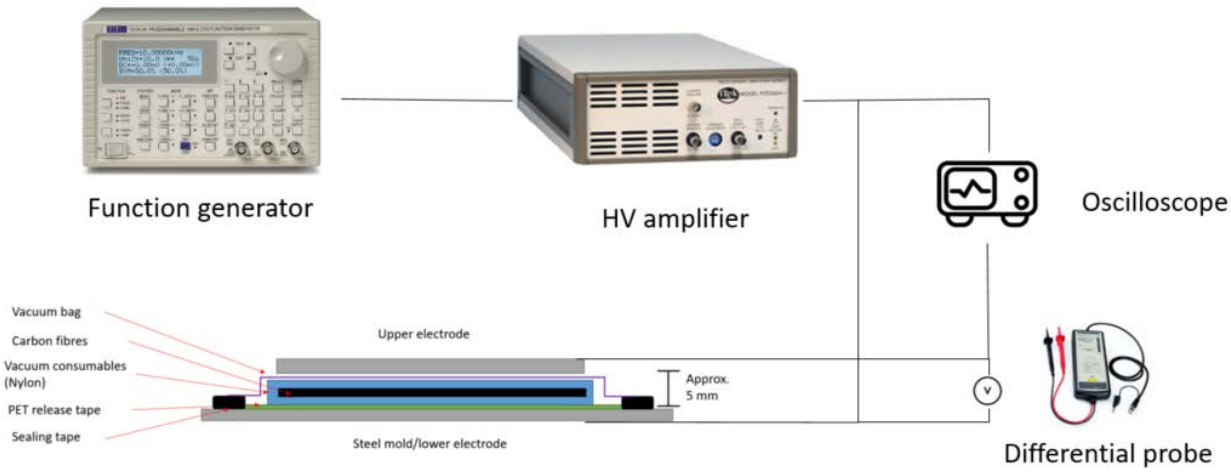

Figure 6. 2: AC field alignment setup.

6.3 Assessment of alignment/Morphology

To be able to clearly identify the contribution of each of the constituents of the composite, Raman spectra were obtained for the GO nanoflakes used in this study (when they were in a powder form as presented in [174]), for the Zoltek PX 35 carbon fibres as well as for the GO/CFRP laminates, Fig.6.3. Since a Raman microscope was used, it was possible to focus the laser beam to a specific area of interest (for the case of GO/CFRP) and obtain a spectrum from a specific spot. In Fig. 6.4 an optical micrograph of the interlaminar region of the sample containing 4 wt% A-GO/CFRP is presented. In addition to the carbon fibres, upper and bottom parts of the micrograph, smaller objects are observed dispersed within the interlaminar region. By focusing the laser beam to the spot (a) (see Fig. 6.4), an area with 4 visible features, a spectrum was obtained. Two characteristic bands are observed at 1307 and 1578 cm^{-1}, namely D and G, where D band is related to the induced disorder (sp3 hybridization) derived from powder processing while G band represents the in-phase, graphitic vibrations of the sp^2 carbon lattice and is associated with the first-order scattering of E_{2g} phonons [174], [217]–[219]. By obtaining a spectrum from spot (b) (see Fig. 6.4), which corresponds to an area with no visible features, a near amorphous behaviour was observed, with some indications of a crystalline structure to be present, possibly originating from GO flakes located deeper than the top surface.

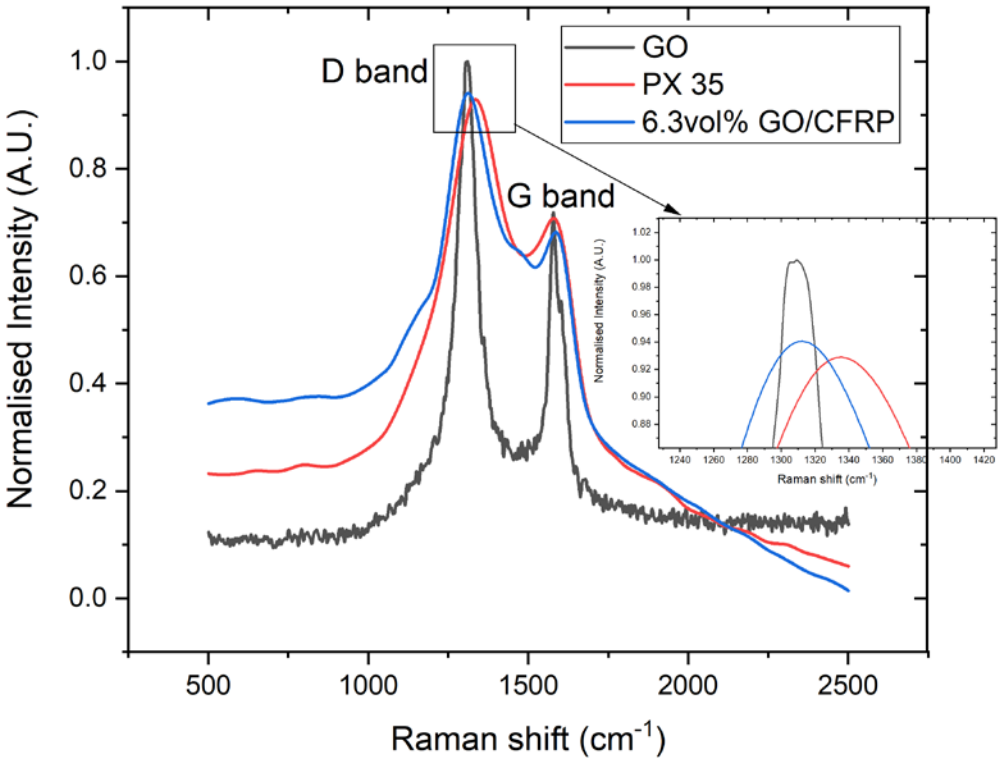

Figure 6. 3: Raman spectra for the GO used in this study, PX 35 carbon fibres and a CO/CFRP laminate.

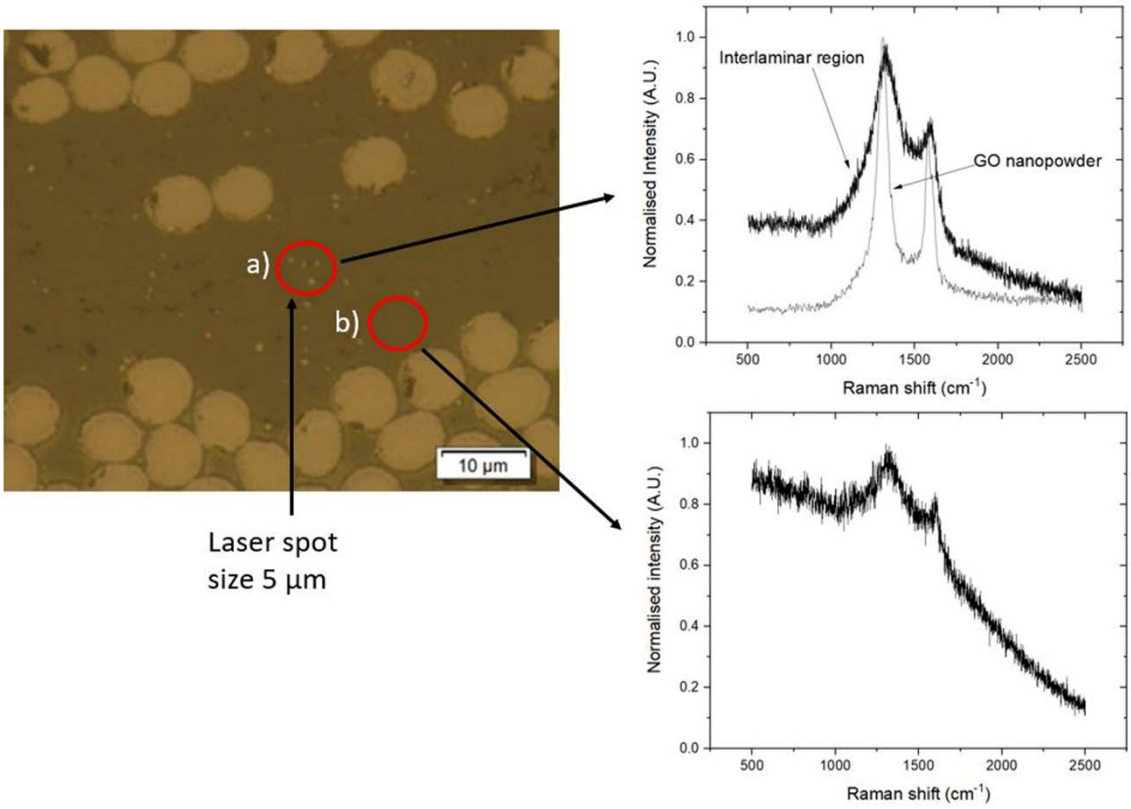

Figure 6. 4: Optical micrograph from the sample 4 wt% A-GO/CFRP and respective Raman spectra. Red circles denote the areas a) and b) where the Raman spectra were obtained from.

Discussion

As seen in Fig.6.3, all of the three examined constituents, carbon fibres, GO and GO/CFRP laminate, exhibit the characteristic G band at the same location. A variation is observed at the location of the D band between the GO-containing constituents and the carbon fibre samples. This is because PAN-based carbon fibre, like the Zoltek PX-35, exhibit their D band at around 1350 cm^{-1} and in this case is due to the A_{1g} vibrational mode of the graphite plane usually attributed to structural disorder [220]. Thus, an identification of the GO species was achieved based on the location of the D band peak. From the embedded Raman spectra, it can be observed that the features located in the interlaminar region (a) in Fig. 6.4) consist of GO. From the spectrum obtained from the area with no visible features (b) in Fig. 6.4) a near amorphous behaviour is observed, as expected for the epoxy matrix. However, an indication of the existence of GO was observed with the formation of weak D and G bands. This can be attributed to the existence of GO located further deeper under the surface that was excited by the laser ray as the penetration depth of such lasers can be in range of hundreds of nm [63]. In addition, due to the development of electrostatic attractive forces between the opposing charges of adjacent polarised GO flakes, a chain-like network is expected to be formed [201]. Although some indications of this network type can be observed in Fig. 6.4, they are not conclusive; firstly because optical micrographs provide information only about a specific plane and secondly the surface preparation route, surface polishing with abrasive sandpapers, have probably removed some of the GO that was located on that plane.

SEM micrographs are presented in Fig. 6.5, from which the formation of physical chain-like conducting paths between adjacent fibres is observed. The morphology of the observed features, a chain-like network, is similar to previously reported networks consisting of GNPs dispersed in epoxy [201], and clay dispersed in polydimethylsiloxane (PDMS) [205] that were subjected to out-of-plane alignment with an external AC field. In addition, a clear indication of a successful alignment process is evident as the GO flakes appear to be oriented perpendicular to the fibre plane, thus in parallel with the direction of the applied field. This is expected to have a significant influence on both the electrical and thermal conductivity for two distinctive reasons; the formation of such a percolating type of network is essential to promote the conduction process within the insulating epoxy matrix, but also and importantly since GO flakes are oriented with their basal planes positioned in parallel with the direction of applied electric current and heat flow, both conduction processes will be facilitated by taking advantage of the higher electrical and thermal conductivity of GO in this direction over perpendicular to the basal planes. This also becomes apparent in Fig.6.5 c) were ILSS fractured areas are observed, with individual GO flakes identified that are oriented perpendicular to the fibre axis, unlike Fig. 6.5 d), where an image from a laminate containing randomly oriented GO is depicted. There, GO flakes are arranged parallel to the fire axis.

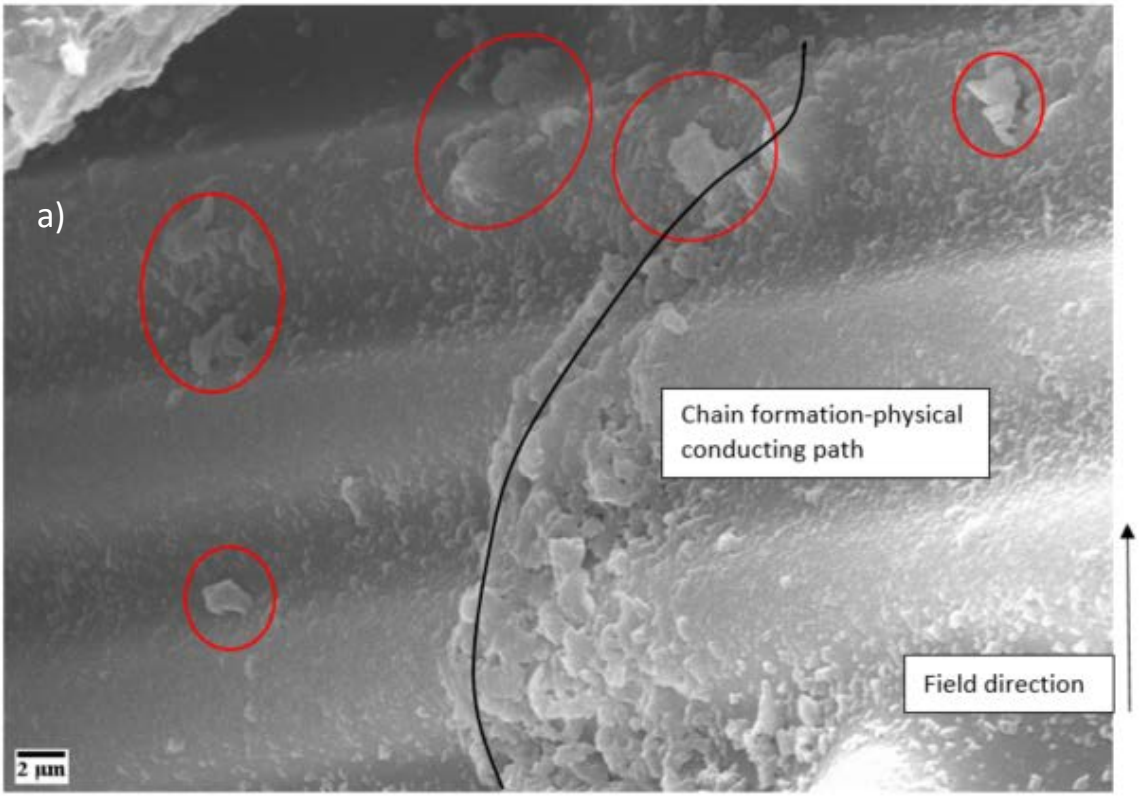
a)
Chain formation-physical conducting path
Field direction
2 µm

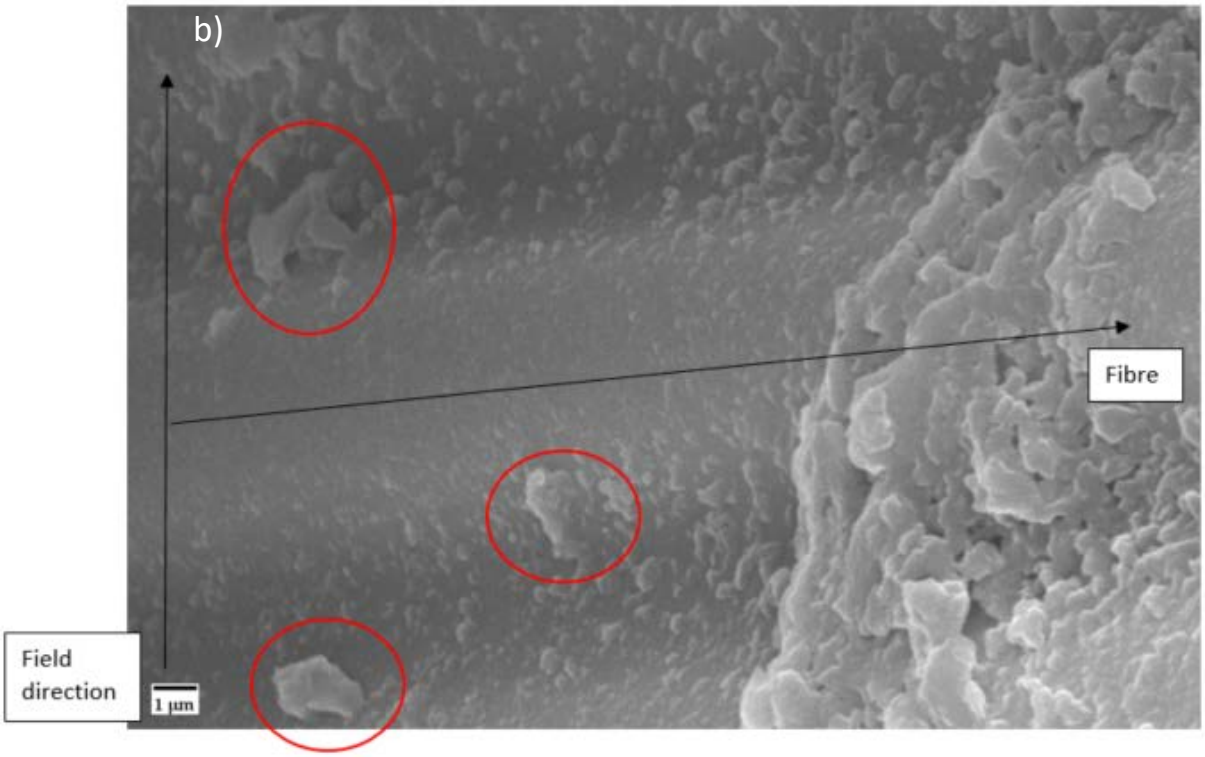
b)
Fibre
Field direction
1 µm

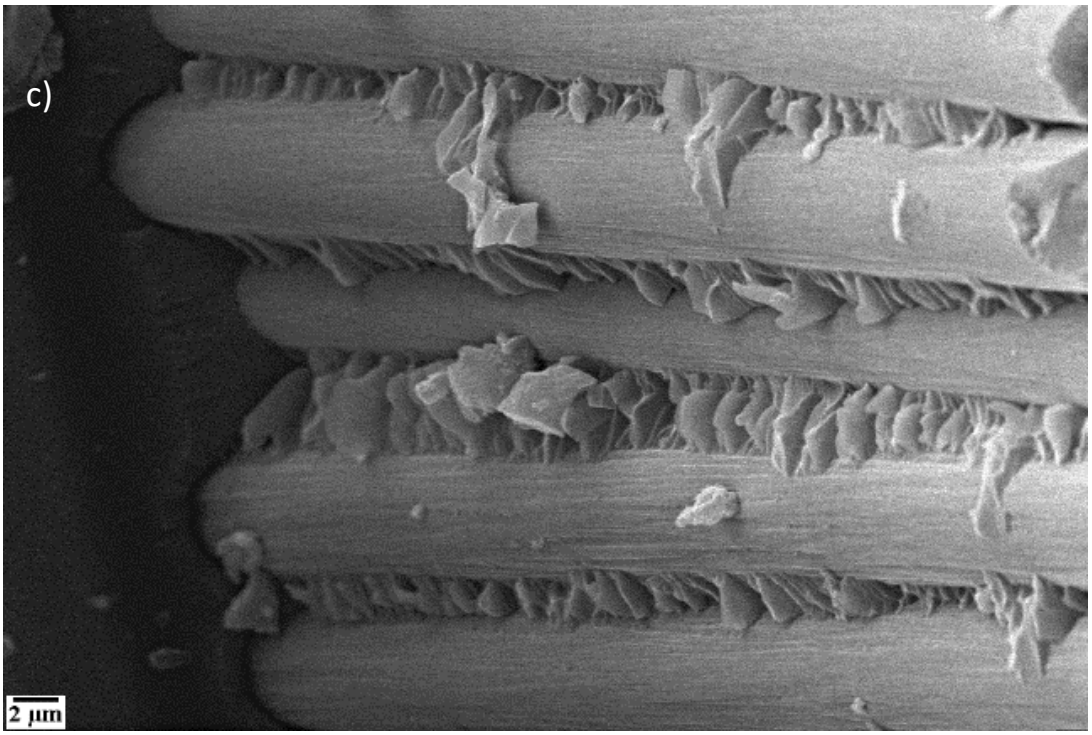

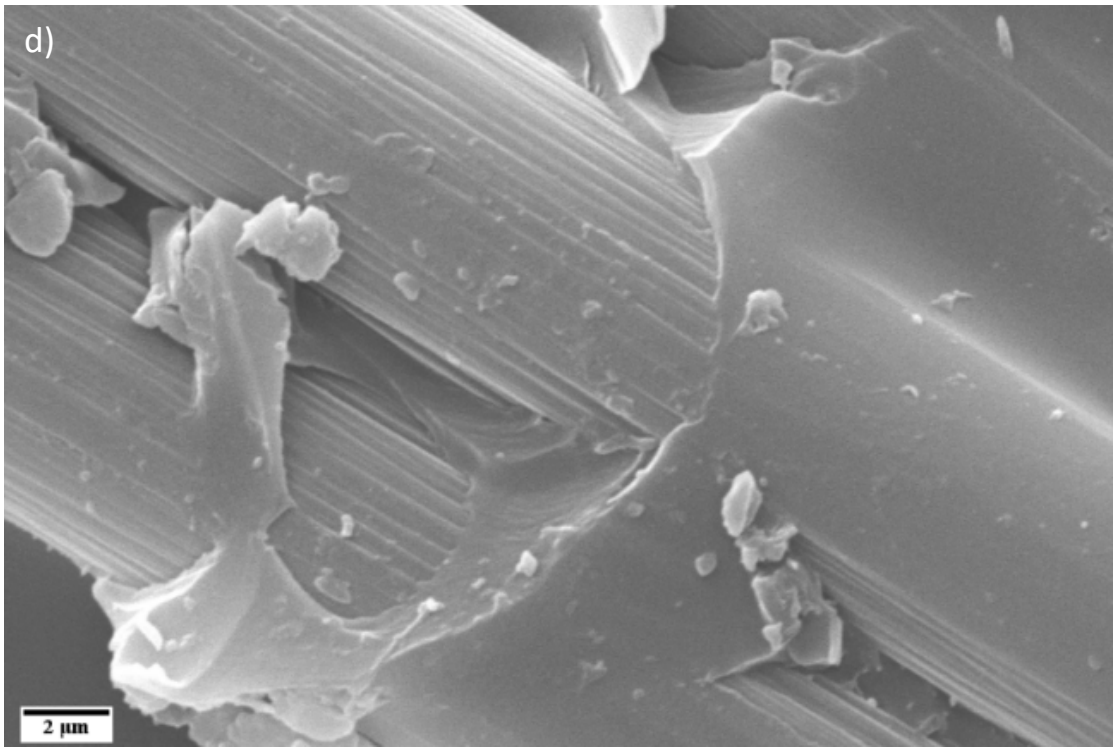

Figure 6. 5: Scanning electron microscopy images for the samples containing 4 wt% GO, a) and b) correspond to aligned, c) and d) (ILSS fractured areas) where c) is for A-GO/CFRP and d) for CFRP containing randomly oriented GO.

6.4 Electrical conductivity

Fig. 6.6 presents the dependency of the through-thickness electrical conductivity on the GO filler content for CFRP laminates containing randomly oriented GO and GO aligned perpendicular to the fibre direction. Noticeable improvements are observed for the laminates where the AC field is applied compared to the laminates containing randomly oriented GO. By comparing samples featuring the same GO filler content the influence of the E-field alignment can be assessed. Although the effects of out-of-plane alignment seem to be pronounced from filler contents above 1 wt% a 14%, an increase is observed even for the sample containing 0.5 wt% GO dispersed into the epoxy. For higher filler contents, the response of the A-GO/CFRP shows improvements ranging from 52% for the 1 wt% sample, 34% for 2 wt%, 68% for 4 wt% and 67% for the 5 wt% sample respectively. As seen the highest observed value, for the 5 wt% sample, of 0.16 S/cm shows a threefold increase over the neat CFRP laminate. This is directly linked with the ability to form a network among the dispersed GO flakes as the filler content gets higher.

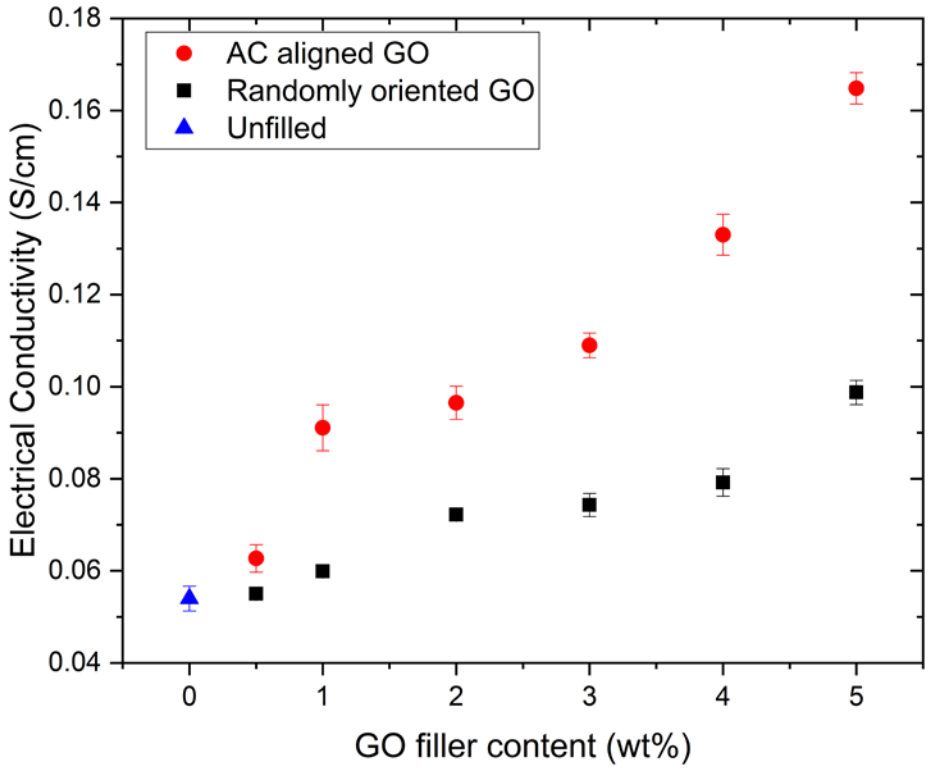

Figure 6. 6: Through-thickness electrical conductivity as a function of GO content dispersed in the matrix.

Discussion

The conduction process in polymer composites filled with a conducting reinforcing phase can be described by two distinct mechanisms. Depending on the spatial arrangement of the filler and the distance between adjacent inclusions the mechanism can be associated with percolation, tunnelling or a combination of them. However, percolation has a greater influence on the electrical conductivity of the composites since physical contact between the filler particles dominate the conduction process [71], [72], [221]. From Fig.6.6 a significant increase is observed in the electrical conductivity of the laminates that they were exposed to the AC field. The increase can be attributed to a combination of percolation and tunnelling. Regarding the tunnelling process, electrons travelling within GO can tunnel through the insulating polymer matrix to an adjacent GO flake or carbon fibre, depending the location within the laminate, facilitating the conduction process. At low filler contents, up to 2 wt%, the number of GO flakes/particles in not sufficient to initiate the formation of a network due to long distances between the particles allowing only a small amount of paths/segments to be created, there tunnelling conduction is a more relevant representation of the conduction process. However, as the filler content increases the interparticle distances are being reduced, and the assembly of a network/path is facilitated, thus a percolating type of conduction is present. Evidence of the formation of such network are present in SEM images, Fig.6.5. Although not conclusive, they can provide some justification for this claim always in conjunction with the electrical conductivity results. In addition, the formation of large aggregates is impeded due to repulsive forces between the GO flakes. It has to be pointed out that in previously reported results with identical constituent materials [222], to achieve through-thickness electrical conductivity values in the range of 0.18 S/cm, double the amount of GO had to be dispersed into the epoxy, around 10 wt%, showing the efficiency of the alignment method developed in this research over randomly distributed conducting particles. This in turns shows promising results for commercialising nanoreinforced laminates, as reducing the filler content required equates to lower production costs and improved processability. Since the polymer matrix does not have to be in a percolating state, a lower viscosity can be achieved aiding large scale production of components.

6.5 Thermal conductivity

The through-thickness thermal conductivity of both GO/CFRP and A-GO/CFRP is presented as a function of the GO filler content in Fig. 6.7. The addition of GO provides significant improvements of the thermal conductivity for both laminate types. Specifically, a linear increase is observed for low filler contents, 0.5 wt%, 1 wt%, 2 wt% and 3 wt%. Further increase of the filler content provides some marginal improvements with the values appearing to stabilize, reaching a plateau at around 4 wt%, with the exception of the sample containing 5 wt% where a slight decrease is observed.

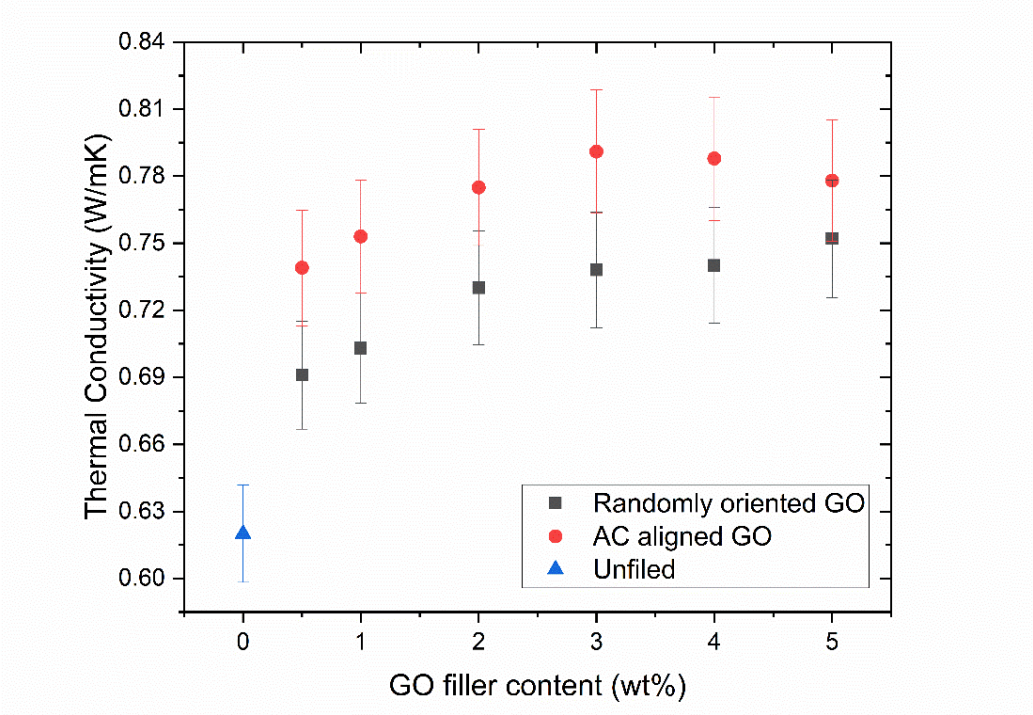

Figure 6. 7: Through-thickness thermal conductivity as function of GO content dispersed in the matrix.

Discussion

The main mechanism describing the enhancement in the through-thickness direction is the faster heat dissipation through the polymer dominated (resin rich) interlaminar laminate regions due to the higher thermal conductivity of GO [222]. Albeit the addition of a thermally conductive filler can contribute to higher thermal conductivity values, platelet-shaped fillers exhibit a certain degree of anisotropy, with their conductivity to be considerably lower in the out-of-plane direction [60], [223]. In addition, it has been found that the processing/manufacturing procedure have an effect on the filler orientation, i.e. platelets have been found to be aligned parallel to the injection direction during the moulding process of polymer composites [60]. Based on previous studies [60], [201], [205], the thermal behaviour exhibited by randomly oriented platelets dispersed within a polymer matrix, closely resembles the behaviour of platelets aligned in-plane (platelets aligned perpendicular to the heat flow), thus explaining the lower values observed in the absence of the electric field. For the case of A-GO/CFRP further addition of GO contributes to possible irregular chain formation. This has been reported to not efficiently improve the thermal conductivity, as the formation of aggregates reduces the ability to conduct heat effectively through the bulk of the surrounding polymer [224]. Furthermore, one significant aspect affecting the thermal conductivity of graphene-filled polymer composites is the influence from the interface contact resistance between the filler and the epoxy matrix as well as between the filler particles when in contact [225].

Albeit the alignment facilitate the phonon transport along the GO basal planes the fact that the GO flakes are arranged in a chain-like network increase the number of interfaces along the heat flow direction indicating the diminishing effects of interface resistance.

6.6 Mechanical response- ILSS

The interlaminar shear strength results of the A-GO/CFRP are presented and compared with CFRP laminates containing randomly oriented GO in Fig. 6.8. It is seen that the addition of low filler contents of GO, 0.5 wt% and 1 wt%, leads to a sharp increase in the ILSS on both laminate categories. Although the obtained values for 1 wt% filler content are quite similar, the laminate containing aligned GO shows negligibly lower values, approx. 4%, but without surpassing the measurement deviation. For the lowest percentage of GO, 0.5wt%, a 20% increase of the ILSS is observed for the A-GO/CFRP laminate compared to the conventionally GO infused laminate. A similar behaviour is exhibited for filler contents of 2 wt% and 4 wt% with the laminates containing aligned GO seen to exhibit 56% and 30% improved ILSS values, respectively. Further increase of the GO content, 5 wt%, decreases the ILSS of the AC aligned laminates, while some minor improvements are seen for the laminates containing randomly oriented GO.

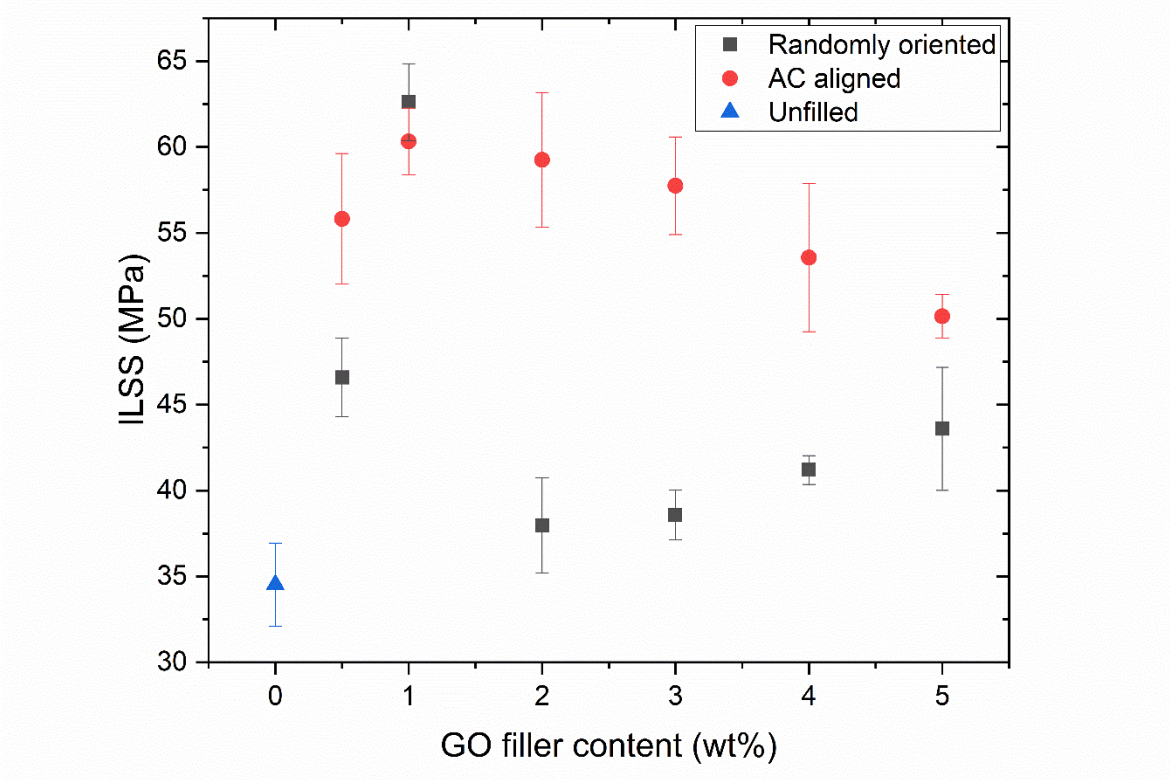

Figure 6. 8: ILSS as a function of GO content dispersed in the polymer matrix.

Discussion

The sharp increase of the ILSS at low filler contents, 0.5 wt% and 1 wt%, is attributed to improved fracture resistance and toughness of the interlaminar regions leading to higher loading capabilities for the GO reinforced laminates. Both the morphology/shape (combination of planar geometry and wrinkled surface) and chemical composition of GO, existence of oxygen groups that allow bonding with the epoxy matrix, have been highlighted as the predominant mechanisms for enhancing the mechanical properties of nanocomposites [153], [203], [226], [227]. Considering the polymer dominated interlaminar regions, the ILSS increases significantly by the addition of GO, as the matrix properties have a significant influence on the fibre/matrix stress transfer of the laminate [228]. In general, the addition of a high modulus filler into a low modulus matrix, like epoxy, enable the arrest or deflection of cracks initiated within the polymer [56]. Since the ILSS test method is can be used to assess the load transfer mechanisms in these polymer-rich regions, improvements of the ILSS indicates enhanced fracture strength and toughness of the polymer matrix. The different behaviour observed for the A-GO/CFRP at high filler contents, above 2 wt%, is attributed to the reduction of the agglomeration due to electrostatic repulsive forces between the GO flakes. As charge is accumulated on the edges of the GO flakes, adjacent flakes retract from forming aggregates and a chain-like network can be observed, see SEM Fig. 6.5. Hence, the A-GO/CFRP laminates retain higher ILSS values at high filler contents compared to the laminates containing randomly oriented GO. This type of network is reminiscent of the z-pinning method that has been introduced as a means of enhancing the through-thickness mechanical properties of FRP laminates, but without the need of adding metallic pins within the laminate [229].

Chapter 7 Conclusions and Future Work

7.1 Conclusions

The primary aim of the research was to develop CFRP laminates with enhanced electrical and thermal properties that can be used for the manufacturing of large composite structures. The motivation for the work has arisen from the issues observed in CFRPs when electrical current and thermal loads are introduced into the composite structure. The work has been carried out using low cost commercially available materials used in the manufacturing of wind turbine blades. The work in the thesis is divided into 4 main sections:

1. Characterize the anisotropic electrical and thermal conduction mechanisms by developing reliable experimental procedures.
2. Develop a manufacturing route for nanomodified that is applicable on an industrial scale.
3. Obtain a multiscale composite system with enhanced electrical and thermal conductivity with the possibility of achieving isotropic properties.
4. Optimize the manufacturing process to allow reduction of the required amount of filler while achieving improved electrical and thermal properties.

The work conducted in Chapters 3 and 4 has fulfilled the first objective, the anisotropic behaviour of CFRP was quantified. A measurement protocol was developed and presented for electrical measurements in all three principle directions of unidirectional laminates. Thermal conductivity measurements were realized, using a self-developed apparatus, in the transverse and through-thickness directions. The longitudinal electrical conductivity was found to be 3 orders of magnitude higher than in the transverse direction, and 4 orders of magnitude higher than in the through-thickness direction. A similar behaviour was observed with regards to the thermal conductivity, albeit less prominent, where the thermal conductivity in the transverse direction was found to be 13% higher than in the through-thickness direction.

The second objective of this study was to develop a manufacturing route for nanomodified CFRP laminates and it is presented in Chapter 5. It was demonstrated that GO reinforced CFRP laminates can be manufactured using VARTM and utilising bulk matrix modification. By employing a commercially available filler with smaller dimensions than of the conventionally used, 500 nm lateral diameter, homogeneous distribution of the filler can be achieved through the bulk of the laminate. Planetary mixing provided satisfactory dispersion of the filler within the epoxy matrix while at the same time being an industrially scalable process.

The development of a multiscale composite with enhanced trough-thickness electrical and thermal conductivity is presented in Chapter 5 and fulfills the requirements of the main objective of the PhD. The through-thickness electrical conductivity showed a threefold increase compared to reference sample, reaching a value of 0.18 S/cm. The transverse direction electrical conductivity although was found not be greatly affected, showed some marginal improvements reaching 0.7 S/cm. A similar behaviour was observed for the thermal conductivity, where GO/CFRP laminates exhibited near identical through-thickness and transverse thermal conductivities, 0.83 W/mK and 0.86 W/mK respectively. Albeit these improvements are promising they do showcase that it is not possible to achieve isotropic electrical and thermal conductivity in a nanomodified CFRP laminate using bulk matrix modification.

The final aim in this study was to optimize the manufacturing procedure to achieve improved performance but with lower amounts of GO added to the laminate and it is presented in Chapter 6. Altering the spatial arrangement of GO by applying a relatively low AC field (30 V/mm), to create a chain-like network proved to be effective in increasing both the electrical and thermal conductivities in the through-thickness direction. Specifically, the electrical conductivity of the laminates exposed to the alignment process, A-GO/CFRP, reached values approx. 0.18 S/cm that are identical to the values observed by laminates containing randomly oriented GO. However, with this method, a 50 % reduction in the required filler was achieved. By utilising less filler in the polymer matrix, a lower viscosity can be achieved, which in turn significantly improves the processability during infusion and injection processes.

In conclusion, the GO modified CFRP laminates developed in this study belong to a new class of composites, referred to as multiscale composites, where their properties can be tailored depending on the specific application and design requirements. The improved electrical (in particular) and thermal conductivities have the potential to improve the overall material performance by acting as a means of mitigation of electrically or thermally induced damage, for instance as seen for lightning strike event in aircraft or wind turbine blades.

7.2 Recommendations for future work

The addition of nanoinclusions into the CFRP structure, as described in this study, revealed the potential of tailoring the properties of CFRP (electrical, thermal and mechanical) according to specific requirements. Due to the wide range of available fillers, different nanomodified laminate combinations can be devised depending the application. Two-dimensional fillers such as boron nitride, with crystalline structure similar to GO, have shown promising results in improving the

thermal properties of polymer nanocomposites [230], thus an investigation of its addition into a CFRP laminate would be beneficial for applications where CFRPs are exposed to high thermal loads.

The work in Chapter 6 suggested that AC electric fields can be utilised to alter the orientation of a filler within a laminate. Based on the developed methodology, an investigation of an alignment on different directions, filler aligned parallel or transversely to the fibre axis, would be beneficial in revealing what improvements can be achieved in each direction.

Furthermore, the use of a DC field has shown great potential in electrophoretic deposition applications, as highlighted in section 2.4.1. Edge oxidized GO, like the one used in this study, is a suitable candidate for depositing a filler onto a carbon fabric for two distinct reasons, the negative charge of the hydroxyl groups makes it able to be polarized, in addition the fact that the carbon fibres used in this study were sized with an epoxy compatibilizer, thus oxygen groups were present on the fibre surface, allows the formation of chemical bonds between the oxygen groups of the carbon fibre surface with the GO.

Appendix A Publications

Journal articles

1. E. C. Senis, I. O. Golosnoy, J. Dulieu-Barton and O. T. Thomsen, "Enhancement of the electrical and thermal properties of unidirectional carbon fibre/epoxy laminates through the addition of graphene oxide", Journal of Materials Science, https://doi.org/10.1007/s10853-019-03522-8

Journal articles accepted for publication

- E. C. Senis, I. O. Golosnoy, T. Andritsch, J. Dulieu-Barton and O. T. Thomsen, "The influence of graphene oxide filler on the electrical and thermal properties of unidirectional carbon fibre/epoxy laminates: effect of out-of-plane alignment of the graphene oxide nanoparticles", Polymer Composites, https://doi.org/10.1002/pc.25637

Conference papers

1. E. C. Senis, O. Vryonis, S. F. Madsen, I. O. Golosnoy, J. M. Dulieu-Barton and O. T. Thomsen, (June 2017), "*Improved current conduction capability of nanomodified CFRP for lightning protection of wind turbine blades*". In Joachim Holbøll (chair) in the *Lightning protection of wind turbines*. Symposium conducted at the *Wind Energy Science Conference*, Copenhagen, Denmark.
2. E. C. Senis, I. O. Golosnoy, J. Dulieu-Barton, O. T. Thomsen and S. F. Madsen, "Characterization of through thickness thermal conductivity of wind turbine blade CFRP materials using a steady-state technique", *International Conference on Composite Materials*, 20-25 August 2017, Xi'an, China.
3. E. C. Senis, O. Vryonis, I. O. Golosnoy, J. M. Dulieu-Barton, O. T. Thomsen, L. Carloni and S. F. Madsen, "The Influence of Graphene Oxide on the electrical conduction in unidirectional CFRP laminates for wind turbine blade applications", *International Conference on Lightning and Static Electricity,*13-15 September 2017, Nagoya, Japan.
4. E. C. Senis, I. O. Golosnoy, J. Dulieu-Barton and O. T. Thomsen, "Assessing the dispersion of nanoinclusions in nanoreinforced CFRP laminates using electrical resistance measurements", *European Conference on Composite Materials*, 24-28 June 2018, Athens, Greece.

Conference papers (contributing author)

1. A. A. M. Laudani, I. O. Golosnoy, J. Kremer, E. C. Senis, O. T. Thomsen, P. L. Lewin, "Experimental characterization of contact resistivity of CFRP wind turbine spars' equipotential bonding", 65th IEEE Holm Conference, 15-18 September 2019, Milwaukee, USA

Poster presentations

1. E. C. Senis, I. O. Golosnoy, J. Dulieu-Barton and O. T. Thomsen, "Analysis of through-thickness thermal conductivity of wind turbine blade CFRP", Universities High Voltage Network Colloquium,16 January 2018, Winchester, UK

List of References

[1] M. Pasqualetti, R. Richter, and P. Gipe, “History of wind energy,” *Encycl. energy*, vol. 6, pp. 419–433, 2004.

[2] T. J. Price, “James Blyth—Britain’s first modern wind power pioneer,” *Wind Eng.*, vol. 29, no. 3, pp. 191–200, 2005.

[3] R. W. Righter, *Wind energy in America: A history*. University of Oklahoma Press, 1996.

[4] GWEC, “Global Wind Report,” *Wind energy Technol.*, p. 75, 2017.

[5] A. Arapogianni and J. Moccia, “Where’s the money coming from? Financing offshore wind farms,” *Eur. Wind Energy Assoc.*, 2013.

[6] “European Council Conclusions 29/30 October 2009.”

[7] P. Brøndsted and R. P. L. Nijssen, *Advances in wind turbine blade design and materials*. Elsevier, 2013.

[8] P. S. Veers *et al.*, “Trends in the design, manufacture and evaluation of wind turbine blades,” *Wind Energy*, vol. 6, no. 3, pp. 245–259, 2003.

[9] M. Rosemeier and M. Bätge, “A concept study of a carbon spar cap design for a 80m wind turbine blade,” in *Journal of Physics: Conference Series*, 2014, vol. 524, no. 1, p. 12039.

[10] L. Mishnaevsky, K. Branner, H. N. Petersen, J. Beauson, M. McGugan, and B. F. Sørensen, “Materials for Wind Turbine Blades: An Overview,” *Materials (Basel).*, vol. 10, no. 11, p. 1285, 2017.

[11] V. Girgiutiu, “Chapter 1 - Introduction,” V. B. T.-S. H. M. of A. C. Giurgiutiu, Ed. Oxford: Academic Press, 2016, pp. 1–23.

[12] S. Han and D. D. L. Chung, “Increasing the through-thickness thermal conductivity of carbon fiber polymer–matrix composite by curing pressure increase and filler incorporation,” *Compos. Sci. Technol.*, vol. 71, no. 16, pp. 1944–1952, 2011.

[13] V. Kumar *et al.*, “Effect of through-thickness electrical conductivity of CFRPs on lightning strike damages,” *Compos. Part A Appl. Sci. Manuf.*, vol. 114, pp. 429–438, Nov. 2018.

[14] K. Schulte and C. Baron, “Load and failure analyses of CFRP laminates by means of

electrical resistivity measurements," *Compos. Sci. Technol.*, vol. 36, no. 1, pp. 63–76, 1989.

[15] A. Todoroki, M. Tanaka, and Y. Shimamura, "Measurement of orthotropic electric conductance of CFRP laminates and analysis of the effect on delamination monitoring with an electric resistance change method," *Compos. Sci. Technol.*, vol. 62, no. 5, pp. 619–628, 2002.

[16] Y. Hirano, S. Katsumata, Y. Iwahori, and A. Todoroki, "Artificial lightning testing on graphite/epoxy composite laminate," *Compos. Part A Appl. Sci. Manuf.*, vol. 41, no. 10, pp. 1461–1470, 2010.

[17] Y. Wang, "Multiphysics analysis of lightning strike damage in laminated carbon/glass fiber reinforced polymer matrix composite materials: A review of problem formulation and computational modeling," *Compos. Part A Appl. Sci. Manuf.*, vol. 101, pp. 543–553, 2017.

[18] T. Ogasawara, Y. Hirano, and A. Yoshimura, "Coupled thermal-electrical analysis for carbon fiber/epoxy composites exposed to simulated lightning current," *Compos. Part A Appl. Sci. Manuf.*, vol. 41, no. 8, pp. 973–981, 2010.

[19] V. Kumar *et al.*, "Effect of through-thickness electrical conductivity of CFRPs on lightning strike damages," *Compos. Part A Appl. Sci. Manuf.*, vol. 114, pp. 429–438, 2018.

[20] P. Feraboli and H. Kawakami, "Damage of Carbon/Epoxy Composite Plates Subjected to Mechanical Impact and Simulated Lightning," *J. Aircr.*, vol. 47, no. 3, pp. 999–1012, 2010.

[21] H. Kawakami and P. Feraboli, "Lightning strike damage resistance and tolerance of scarf-repaired mesh-protected carbon fiber composites," *Compos. Part A Appl. Sci. Manuf.*, vol. 42, no. 9, pp. 1247–1262, 2011.

[22] F. Rachidi *et al.*, "A review of current issues in lightning protection of new-generation wind-turbine blades," *IEEE Trans. Ind. Electron.*, vol. 55, no. 6, pp. 2489–2496, 2008.

[23] A. Candela Garolera, S. F. Madsen, M. Nissim, J. D. Myers, and J. Holboell, "Lightning Damage to Wind TurbineBlades From Wind Farms in the U.S," *IEEE Trans. Power Deliv.*, vol. 31, no. 3, pp. 1043–1049, 2016.

[24] J. Montanyà, O. van der Velde, and E. R. Williams, "Lightning discharges produced by wind turbines," *J. Geophys. Res. Atmos.*, vol. 119, no. 3, pp. 1455–1462, Feb. 2014.

[25] IEC, "61400 :Wind energy generation systems," *Part 24: Lightning protection*. 2010.

[26] S. F. Madsen, K. Bertelsen, T. H. Krogh, H. V Erichsen, A. N. Hansen, and K. B. Lønbæk,

"Proposal of New Zoning Concept Considering Lightning Protection of Wind Turbine Blades," pp. 108–117, 2012.

[27] L. Mishnaevsky, K. Branner, H. Petersen, J. Beauson, M. McGugan, and B. Sørensen, "Materials for Wind Turbine Blades: An Overview," *Materials (Basel).*, vol. 10, no. 11, p. 1285, 2017.

[28] Y. Wang and W. Hu, "Investigation of the effects of receptors on the lightning strike protection of wind turbine blades," *IEEE Trans. Electromagn. Compat.*, vol. 59, no. 4, pp. 1180–1187, 2017.

[29] V. Kumar *et al.*, "Effect of through-thickness electrical conductivity of CFRPs on lightning strike damages," *Compos. Part A Appl. Sci. Manuf.*, vol. 114, pp. 429–438, 2018.

[30] P.-C. Ma, N. A. Siddiqui, G. Marom, and J.-K. Kim, "Dispersion and functionalization of carbon nanotubes for polymer-based nanocomposites: A review," *Compos. Part A Appl. Sci. Manuf.*, vol. 41, no. 10, pp. 1345–1367, 2010.

[31] D. D. L. Chung, *Carbon Fiber Composites*. Butterworth-Heinemann, 1994.

[32] E. Frank, L. M. Steudle, D. Ingildeev, J. M. Spörl, and M. R. Buchmeiser, "Carbon fibers: precursor systems, processing, structure, and properties," *Angew. Chemie Int. Ed.*, vol. 53, no. 21, pp. 5262–5298, 2014.

[33] G. Savage, *Carbon-Carbon Composites*. Chapman & Hall, 1993.

[34] J.-B. Donnet, *Carbon black: science and technology*. CRC Press, 1993.

[35] G. Xin *et al.*, "Highly thermally conductive and mechanically strong graphene fibers," *Science (80-.).*, vol. 349, no. 6252, pp. 1083–1087, 2015.

[36] D. J. Johnson, C. N. Tyson, C. N. Tysont, and C. N. Tyson, "Low-angle X-ray diffraction and physical properties of carbon fibres," vol. 3, no. 4, p. 526, 1970.

[37] B. A. Newcomb, "Processing, structure, and properties of carbon fibers," *Compos. Part A Appl. Sci. Manuf.*, vol. 91, pp. 262–282, 2016.

[38] D. J. Johnson, "Structure-property relationships in carbon fibres," *J. Phys. D. Appl. Phys.*, vol. 20, no. 3, p. 286, 1987.

[39] R. Rolfes and U. Hammerschmidt, "Transverse thermal conductivity of CFRP laminates: a numerical and experimental validation of approximation formulae," *Compos. Sci. Technol.*,

vol. 54, no. 1, pp. 45–54, 1995.

[40] V. Šafářová and J. Grégr, “Electrical conductivity measurement of fibers and yarns,” in *7th International Conference, TEXSCI, Liberec, Czech Republic*, 2010.

[41] M. S. Dresselhaus, G. Dresselhaus, K. Sugihara, I. L. Spain, and H. A. Goldberg, *Graphite fibers and filaments*, vol. 5. Springer Science & Business Media, 2013.

[42] J. R. Gaier, Y. YoderVandenberg, S. Berkebile, H. Stueben, and F. Balagadde, “The electrical and thermal conductivity of woven pristine and intercalated graphite fiber-polymer composites,” *Carbon N. Y.*, vol. 41, no. 12, pp. 2187–2193, 2003.

[43] J. B. Donnet and R. C. Bansal, *Carbon Fibers, Third Edition*. Taylor & Francis, 1998.

[44] R. Rolfes and U. Hammerschmidt, “Transverse thermal conductivity of CFRP laminates: A numerical and experimental validation of approximation formulae,” *Compos. Sci. Technol.*, vol. 54, no. 1, pp. 45–54, 1995.

[45] C. Pradere, J. C. Batsale, J. M. Goyh??n??che, R. Pailler, and S. Dilhaire, “Thermal properties of carbon fibers at very high temperature,” *Carbon N. Y.*, vol. 47, no. 3, pp. 737–743, 2009.

[46] J. Heremans and C. P. Beetz, “Thermal conductivity and thermopower of vapor-grown graphite fibers,” *Phys. Rev. B*, vol. 32, no. 4, pp. 1981–1986, 1985.

[47] D. P. H. Hasselman and L. F. Johnson, “Effective thermal conductivity of composites with interfacial thermal barrier resistance,” *J. Compos. Mater.*, vol. 21, no. 6, pp. 508–515, 1987.

[48] M. R. Null, W. W. Lozier, and A. W. Moore, “Thermal diffusivity and thermal conductivity of pyrolytic graphite from 300 to 2700° K,” *Carbon N. Y.*, vol. 11, no. 2, pp. 81–87, 1973.

[49] T. R. Pozegic *et al.*, “Multi-functional carbon fibre composites using carbon nanotubes as an alternative to polymer sizing,” *Sci. Rep.*, vol. 6, p. 37334, 2016.

[50] S. Han and D. D. L. Chung, “Increasing the through-thickness thermal conductivity of carbon fiber polymer–matrix composite by curing pressure increase and filler incorporation,” *Compos. Sci. Technol.*, vol. 71, no. 16, pp. 1944–1952, 2011.

[51] K. Dong, K. Liu, L. Pan, B. Gu, and B. Sun, “Experimental and numerical investigation on the thermal conduction properties of 2.5D angle-interlock woven composites,” *Compos. Struct.*, vol. 154, pp. 319–333, 2016.

[52] J. Koráb, P. Štefánik, Š. Kavecký, P. Šebo, and G. Korb, “Thermal conductivity of unidirectional copper matrix carbon fibre composites,” *Compos. Part A Appl. Sci. Manuf.*, vol. 33, no. 4, pp. 577–581, 2002.

[53] M. Villière, D. Lecointe, V. Sobotka, N. Boyard, and D. Delaunay, “Experimental determination and modeling of thermal conductivity tensor of carbon/epoxy composite,” *Compos. Part A Appl. Sci. Manuf.*, vol. 46, pp. 60–68, 2013.

[54] C. Kostagiannakopoulou, E. Fiamegkou, G. Sotiriadis, and V. Kostopoulos, “Thermal Conductivity of Carbon Nanoreinforced Epoxy Composites,” *J. Nanomater.*, vol. 2016, pp. 1–12, 2016.

[55] C. Pradere *et al.*, “Thermal properties of carbon fibers at very high temperature,” *Carbon N. Y.*, vol. 47, no. 3, pp. 737–743, 2009.

[56] R. Atif, I. Shyha, and F. Inam, “Mechanical, thermal, and electrical properties of graphene-epoxy nanocomposites—A review,” *Polymers (Basel).*, vol. 8, no. 8, p. 281, 2016.

[57] X.-Y. Zhao and H.-J. Liu, “Review of polymer materials with low dielectric constant,” *Polym. Int.*, vol. 59, no. 5, pp. 597–606, May 2010.

[58] G. P. Johari, “Electrical properties of epoxy resins,” in *Chemistry and Technology of Epoxy Resins*, Springer, 1993, pp. 175–205.

[59] S. N. Leung, “Thermally conductive polymer composites and nanocomposites: Processing-structure-property relationships,” *Compos. Part B Eng.*, vol. 150, pp. 78–92, Oct. 2018.

[60] H. Chen *et al.*, “Thermal conductivity of polymer-based composites: Fundamentals and applications,” *Prog. Polym. Sci.*, vol. 59, pp. 41–85, Aug. 2016.

[61] N. Burger, A. Laachachi, M. Ferriol, M. Lutz, V. Toniazzo, and D. Ruch, “Review of thermal conductivity in composites: Mechanisms, parameters and theory,” *Prog. Polym. Sci.*, vol. 61, pp. 1–28, 2016.

[62] M. Akatsuka and Y. Takezawa, “Study of high thermal conductive epoxy resins containing controlled high-order structures,” *J. Appl. Polym. Sci.*, vol. 89, no. 9, pp. 2464–2467, Aug. 2003.

[63] T. R. Pozegic *et al.*, “Multi-functional carbon fibre composites using carbon nanotubes as an alternative to polymer sizing,” *Sci. Rep.*, vol. 6, p. 37334, 2016.

[64] A. Todoroki, M. Tanaka, and Y. Shimamura, “Measurement of orthotropic electric

conductance of CFRP laminates and analysis of the effect on delamination monitoring with an electric resistance change method," *Compos. Sci. Technol.*, vol. 62, no. 5, pp. 619–628, 2002.

[65] M. Louis, S. P. Joshi, and W. Brockmann, "An experimental investigation of through-thickness electrical resistivity of CFRP laminates," *Compos. Sci. Technol.*, vol. 61, no. 6, pp. 911–919, 2001.

[66] M. Kupke, K. Schulte, and R. Schüler, "No Title," *Compos. Sci. Technol.*, vol. 61, no. 6, pp. 837–847, 2001.

[67] M. Kupke, K. Schulte, and R. Schüler, "Non-destructive testing of FRP by d.c. and a.c. electrical methods," *Compos. Sci. Technol.*, vol. 61, no. 6, pp. 837–847, May 2001.

[68] M. Kupke, K. Schulte, and R. Schüler, "Non-destructive testing of FRP by d.c. and a.c. electrical methods," *Compos. Sci. Technol.*, vol. 61, no. 6, pp. 837–847, 2001.

[69] F. Lux, "Models proposed to explain the electrical conductivity of mixtures made of conductive and insulating materials," *J. Mater. Sci.*, vol. 28, no. 2, pp. 285–301, 1993.

[70] Z. Rimska, V. Křuesálek, and J. Spacek, "AC conductivity of carbon fiber–polymer matrix composites at the percolation threshold," *Polym. Compos.*, vol. 23, no. 1, pp. 95–103, 2002.

[71] M. T. Connor, S. Roy, T. A. Ezquerra, F. J. B. Calleja, and F. Baltá Calleja, "Broadband ac conductivity of conductor-polymer composites," *Phys. Rev. B*, vol. 57, no. 4, p. 2286, 1998.

[72] G. C. Psarras, "Charge transport properties in carbon black/polymer composites," *J. Polym. Sci. Part B Polym. Phys.*, vol. 45, no. 18, pp. 2535–2545, 2007.

[73] J. B. Park, T. K. Hwang, H. G. Kim, and Y. D. Doh, "Experimental and numerical study of the electrical anisotropy in unidirectional carbon-fiber-reinforced polymer composites," *Smart Mater. Struct.*, vol. 16, no. 1, pp. 57–66, 2007.

[74] Y. Lin, M. Gigliotti, M. C. Lafarie-Frenot, and J. Bai, "Effect of carbon nanotubes on the thermoelectric properties of CFRP laminate for aircraft applications," *J. Reinf. Plast. Compos.*, vol. 34, no. 2, pp. 173–184, 2014.

[75] J. H. Han *et al.*, "The combination of carbon nanotube buckypaper and insulating adhesive for lightning strike protection of the carbon fiber/epoxy laminates," *Carbon N. Y.*, vol. 94, pp. 101–113, 2015.

[76] Q. Dong, Y. Guo, X. Sun, and Y. Jia, “Coupled electrical-thermal-pyrolytic analysis of carbon fiber/epoxy composites subjected to lightning strike,” *Polym. (United Kingdom)*, vol. 56, pp. 385–394, 2015.

[77] T. Ogasawara, Y. Hirano, and A. Yoshimura, “Coupled thermal–electrical analysis for carbon fiber/epoxy composites exposed to simulated lightning current,” *Compos. Part A Appl. Sci. Manuf.*, vol. 41, no. 8, pp. 973–981, 2010.

[78] P. Feraboli and H. Kawakami, “Damage of Carbon/Epoxy Composite Plates Subjected to Mechanical Impact and Simulated Lightning,” *J. Aircr.*, vol. 47, no. 3, pp. 999–1012, 2010.

[79] P. Feraboli and M. Miller, “Damage resistance and tolerance of carbon/epoxy composite coupons subjected to simulated lightning strike,” *Compos. Part A Appl. Sci. Manuf.*, vol. 40, no. 6–7, pp. 954–967, 2009.

[80] I. El Sawi, P. A. Olivier, P. Demont, and H. Bougherara, “Processing and electrical characterization of a unidirectional CFRP composite filled with double walled carbon nanotubes,” *Compos. Sci. Technol.*, vol. 73, no. 1, pp. 19–26, 2012.

[81] Y. Hirano, T. Yamane, and A. Todoroki, “Through-thickness electric conductivity of toughened carbon-fibre-reinforced polymer laminates with resin-rich layers,” *Compos. Sci. Technol.*, vol. 122, pp. 67–72, 2016.

[82] Y. Wang, “Multiphysics analysis of lightning strike damage in laminated carbon/glass fiber reinforced polymer matrix composite materials: A review of problem formulation and computational modeling,” *Compos. Part A Appl. Sci. Manuf.*, vol. 101, pp. 543–553, 2017.

[83] F. Uhlig, “Contribution to the study of the lightning direct effects on the aircraft structural materials,” Universite de Paris, 1998.

[84] F. Kremer and A. Schönhals, *Broadband dielectric spectroscopy*. Springer Science & Business Media, 2012.

[85] N. Angelidis, C. Y. Wei, and P. E. Irving, “The electrical resistance response of continuous carbon fibre composite laminates to mechanical strain,” *Compos. Part A Appl. Sci. Manuf.*, vol. 35, no. 10, pp. 1135–1147, 2004.

[86] S. Wang and D. D. L. Chung, “Negative piezoresistivity in continuous carbon fiber epoxy-matrix composite,” *J. Mater. Sci.*, vol. 42, no. 13, pp. 4987–4995, 2007.

[87] N. Angelidis, C. Y. Wei, and P. E. Irving, “The electrical resistance response of continuous

carbon fibre composite laminates to mechanical strain," *Compos. Part A Appl. Sci. Manuf.*, vol. 35, no. 10, pp. 1135–1147, 2004.

[88] K. Schulte and C. Baron, "Load and failure analyses of CFRP laminates by means of electrical resistivity measurements," *Compos. Sci. Technol.*, vol. 36, no. 1, pp. 63–76, 1989.

[89] A. Todoroki, K. Suzuki, Y. Mizutani, and R. Matsuzaki, "Electrical resistance change of CFRP under a compression load," *J. Solid Mech. Mater. Eng.*, vol. 4, no. 7, pp. 864–874, 2010.

[90] A. Todoroki, M. Tanaka, and Y. Shimamura, "High performance estimations of delamination of graphite/epoxy laminates with electric resistance change method," *Compos. Sci. Technol.*, 2003.

[91] A. Vavouliotis, A. Paipetis, and V. Kostopoulos, "On the fatigue life prediction of CFRP laminates using the Electrical Resistance Change method," *Compos. Sci. Technol.*, vol. 71, no. 5, pp. 630–642, 2011.

[92] I. Kharabet, I. Patsora, H. Heuer, D. Joneit, and D. Tatarchuk, "Study of Carbon-Fiber-Reinforced Polymers conductivity's dependence on a mechanical strain," 2015, vol. 2015-Septe, pp. 26–29.

[93] B. A. Newcomb, "Processing, structure, and properties of carbon fibers," *Compos. Part A Appl. Sci. Manuf.*, vol. 91, pp. 262–282, 2016.

[94] N. Angelidis, C. Y. Wei, and P. E. Irving, "Response to discussion of paper: The electrical resistance response of continuous carbon fibre composite laminates to mechanical strain," *Compos. Part A Appl. Sci. Manuf.*, vol. 37, no. 9, pp. 1495–1499, 2006.

[95] D. G. Pearce, "Understanding CFRP as a design material," *Fibre Sci. Technol.*, vol. 3, no. 2, pp. 129–146, 1970.

[96] M. W. Pilling, B. Yates, M. A. Black, and P. Tattersall, "The thermal conductivity of carbon fibre-reinforced composites," *J. Mater. Sci.*, vol. 14, no. 6, pp. 1326–1338, 1979.

[97] M. Villière, D. Lecointe, V. Sobotka, N. Boyard, and D. Delaunay, "Experimental determination and modeling of thermal conductivity tensor of carbon/epoxy composite," *Compos. Part A Appl. Sci. Manuf.*, vol. 46, no. 1, pp. 60–68, 2013.

[98] J. Schuster, D. Heider, K. Sharp, and M. Glowania, "Thermal conductivities of three-dimensionally woven fabric composites," *Compos. Sci. Technol.*, vol. 68, no. 9, pp. 2085–2091, Jul. 2008.

[99] W. Fan, J. Li, Y. Zheng, T. Liu, X. Tian, and R. Sun, “Influence of thermo-oxidative aging on the thermal conductivity of carbon fiber fabric reinforced epoxy composites,” *Polym. Degrad. Stab.*, vol. 123, pp. 162–169, 2016.

[100] C. Kostagiannakopoulou, E. Fiamegkou, G. Sotiriadis, and V. Kostopoulos, “Thermal Conductivity of Carbon Nanoreinforced Epoxy Composites,” *J. Nanomater.*, vol. 2016, 2016.

[101] S. Han, J. T. Lin, Y. Yamada, and D. D. L. Chung, “Enhancing the thermal conductivity and compressive modulus of carbon fiber polymer–matrix composites in the through-thickness direction by nanostructuring the interlaminar interface with carbon black,” *Carbon N. Y.*, vol. 46, no. 7, pp. 1060–1071, 2008.

[102] F. Wang and X. Cai, “Improvement of mechanical properties and thermal conductivity of carbon fiber laminated composites through depositing graphene nanoplatelets on fibers,” *J. Mater. Sci.*, vol. 54, no. 5, pp. 3847–3862, Mar. 2019.

[103] E. Kandare *et al.*, “Improving the through-thickness thermal and electrical conductivity of carbon fibre/epoxy laminates by exploiting synergy between graphene and silver nano-inclusions,” *Compos. Part A Appl. Sci. Manuf.*, vol. 69, pp. 72–82, 2015.

[104] R. D. Sweeting and X. L. Liu, “Measurement of thermal conductivity for fibre-reinforced composites,” *Compos. Part A Appl. Sci. Manuf.*, vol. 35, no. 7, pp. 933–938, 2004.

[105] M. S. Dresselhaus, G. Dresselhaus, K. Sugihara, I. L. Spain, and H. A. Goldberg, *Graphite Fibers and Filaments*, vol. 5. Springer Science & Business Media, 2011.

[106] X. Yao, B. G. Falzon, S. C. Hawkins, and S. Tsantzalis, “Aligned carbon nanotube webs embedded in a composite laminate: A route towards a highly tunable electro-thermal system,” *Carbon N. Y.*, vol. 129, pp. 486–494, 2018.

[107] X. Zhang *et al.*, “Interfacial microstructure and properties of carbon fiber composites modified with graphene oxide,” *ACS Appl. Mater. Interfaces*, vol. 4, no. 3, pp. 1543–1552, 2012.

[108] X. Yao, X. Gao, J. Jiang, C. Xu, C. Deng, and J. Wang, “Comparison of carbon nanotubes and graphene oxide coated carbon fiber for improving the interfacial properties of carbon fiber/epoxy composites,” *Compos. Part B Eng.*, vol. 132, pp. 170–177, 2018.

[109] E. Kandare *et al.*, “Improving the through-thickness thermal and electrical conductivity of carbon fibre/epoxy laminates by exploiting synergy between graphene and silver nano-

inclusions," *Compos. Part A Appl. Sci. Manuf.*, vol. 69, pp. 72–82, 2015.

[110] W. Qin, F. Vautard, L. T. Drzal, and J. Yu, "Mechanical and electrical properties of carbon fiber composites with incorporation of graphene nanoplatelets at the fiber–matrix interphase," *Compos. Part B Eng.*, vol. 69, pp. 335–341, 2015.

[111] T. R. Pozegic *et al.*, "Multi-functional carbon fibre composites using carbon nanotubes as an alternative to polymer sizing," *Sci. Rep.*, vol. 6, p. 37334, 2016.

[112] N. C. Adak, S. Chhetri, N. C. Murmu, P. Samanta, T. Kuila, and J. H. Lee, "Experimental and numerical investigation on the mechanical characteristics of polyethylenimine functionalized graphene oxide incorporated woven carbon fibre/epoxy composites," *Compos. Part B Eng.*, vol. 156, pp. 240–251, Jan. 2019.

[113] H. Mahmood, L. Vanzetti, M. Bersani, and A. Pegoretti, "Mechanical properties and strain monitoring of glass-epoxy composites with graphene-coated fibers," *Compos. Part A Appl. Sci. Manuf.*, vol. 107, pp. 112–123, 2018.

[114] F. Wang and X. Cai, "Improvement of mechanical properties and thermal conductivity of carbon fiber laminated composites through depositing graphene nanoplatelets on fibers," *J. Mater. Sci.*, Nov. 2018.

[115] J. Karger-Kocsis, H. Mahmood, and A. Pegoretti, "Recent advances in fiber/matrix interphase engineering for polymer composites," *Prog. Mater. Sci.*, vol. 73, pp. 1–43, 2015.

[116] J. Chu *et al.*, "Realizing the theoretical stiffness of graphene in composites through confinement between carbon fibers," *Compos. Part A Appl. Sci. Manuf.*, vol. 113, pp. 311–317, 2018.

[117] J. Karger-Kocsis, H. Mahmood, and A. Pegoretti, "Recent advances in fiber/matrix interphase engineering for polymer composites," *Prog. Mater. Sci.*, vol. 73, pp. 1–43, 2015.

[118] L. Chen *et al.*, "Role of a gradient interface layer in interfacial enhancement of carbon fiber/epoxy hierarchical composites," *J. Mater. Sci.*, vol. 50, no. 1, pp. 112–121, 2015.

[119] F. Yavari, M. A. Rafiee, J. Rafiee, Z. Z. Yu, and N. Koratkar, "Dramatic increase in fatigue life in hierarchical graphene composites," *ACS Appl. Mater. Interfaces*, vol. 2, no. 10, pp. 2738–2743, 2010.

[120] X. Yao, X. Gao, J. Jiang, C. Xu, C. Deng, and J. Wang, "Comparison of carbon nanotubes and graphene oxide coated carbon fiber for improving the interfacial properties of carbon

fiber/epoxy composites," *Compos. Part B Eng.*, vol. 132, pp. 170–177, Jan. 2018.

[121] N. Yamamoto, R. Guzman de Villoria, and B. L. Wardle, "Electrical and thermal property enhancement of fiber-reinforced polymer laminate composites through controlled implementation of multi-walled carbon nanotubes," *Compos. Sci. Technol.*, vol. 72, no. 16, pp. 2009–2015, 2012.

[122] Q. Wu, R. Zhao, Q. Ma, and J. Zhu, "Effects of degree of chemical interaction between carbon fibers and surface sizing on interfacial properties of epoxy composites," *Compos. Sci. Technol.*, 2018.

[123] L. T. Drzal, M. J. Rich, M. F. Koenig, and P. F. Lloyd, "Adhesion of graphite fibers to epoxy matrices: II. The effect of fiber finish," *J. Adhes.*, vol. 16, no. 2, pp. 133–152, 1983.

[124] S. Tamrakar, Q. An, E. T. Thostenson, A. N. Rider, B. Z. Haque, and J. W. Gillespie Jr, "Tailoring interfacial properties by controlling carbon nanotube coating thickness on glass fibers using electrophoretic deposition," *ACS Appl. Mater. Interfaces*, vol. 8, no. 2, pp. 1501–1510, 2016.

[125] E. Bekyarova *et al.*, "Multiscale carbon nanotube− carbon fiber reinforcement for advanced epoxy composites," *Langmuir*, vol. 23, no. 7, pp. 3970–3974, 2007.

[126] H. Mahmood, L. Vanzetti, M. Bersani, and A. Pegoretti, "Mechanical properties and strain monitoring of glass-epoxy composites with graphene-coated fibers," *Compos. Part A Appl. Sci. Manuf.*, vol. 107, pp. 112–123, 2018.

[127] N. Yamamoto, R. Guzman de Villoria, and B. L. Wardle, "Electrical and thermal property enhancement of fiber-reinforced polymer laminate composites through controlled implementation of multi-walled carbon nanotubes," *Compos. Sci. Technol.*, vol. 72, no. 16, pp. 2009–2015, 2012.

[128] T. R. Pozegic *et al.*, "Low temperature growth of carbon nanotubes on carbon fibre to create a highly networked fuzzy fibre reinforced composite with superior electrical conductivity," *Carbon N. Y.*, vol. 74, pp. 319–328, 2014.

[129] H. Qian, A. Bismarck, E. S. Greenhalgh, G. Kalinka, and M. S. P. Shaffer, "Hierarchical Composites Reinforced with Carbon Nanotube Grafted Fibers: The Potential Assessed at the Single Fiber Level," *Chem. Mater.*, vol. 20, no. 5, pp. 1862–1869, Mar. 2008.

[130] N. C. Adak, S. Chhetri, N. C. Murmu, P. Samanta, T. Kuila, and J. H. Lee, "Experimental and numerical investigation on the mechanical characteristics of polyethylenimine

functionalized graphene oxide incorporated woven carbon fibre/epoxy composites," *Compos. Part B Eng.*, vol. 156, pp. 240–251, 2019.

[131] I. Gaztelumendi, M. Chapartegui, R. Seddon, S. Flórez, F. Pons, and J. Cinquin, "Enhancement of electrical conductivity of composite structures by integration of carbon nanotubes via bulk resin and/or buckypaper films," *Compos. Part B Eng.*, vol. 122, pp. 31–40, 2017.

[132] A. K. Pathak, M. Borah, A. Gupta, T. Yokozeki, and S. R. Dhakate, "Improved mechanical properties of carbon fiber/graphene oxide-epoxy hybrid composites," *Compos. Sci. Technol.*, vol. 135, pp. 28–38, 2016.

[133] I. El Sawi, P. A. Olivier, P. Demont, and H. Bougherara, "Processing and electrical characterization of a unidirectional CFRP composite filled with double walled carbon nanotubes," *Compos. Sci. Technol.*, vol. 73, pp. 19–26, 2012.

[134] R. Umer, Y. Li, Y. Dong, H. J. Haroosh, and K. Liao, "The effect of graphene oxide (GO) nanoparticles on the processing of epoxy/glass fiber composites using resin infusion," *Int. J. Adv. Manuf. Technol.*, vol. 81, no. 9–12, pp. 2183–2192, 2015.

[135] U. Szeluga, S. Pusz, B. Kumanek, K. Olszowska, A. Kobyliukh, and B. Trzebicka, "Effect of graphene filler structure on electrical, thermal, mechanical, and fire retardant properties of epoxy-graphene nanocomposites-a review," *Crit. Rev. Solid State Mater. Sci.*, pp. 1–36, 2019.

[136] T. M. H. O. Vryonis T. Andritsch A. S. Vaughan and P. L. Lewin, "Solvent Mixing and Its Effect on Epoxy Resin Filled with Graphene Oxide," in *2nd IEEE INTERNATIONAL CONFERENCE ON DIELECTRICS (ICD)*, 2018.

[137] H. Ismail and R. Ramli, "Organoclay Filled Natural Rubber Nanocomposites: The Effects of Filler Loading and Mixing Method," *J. Reinf. Plast. Compos.*, vol. 27, no. 16–17, pp. 1909–1924, Nov. 2008.

[138] O. Vryonis, T. M. Harrell, T. Andritsch, A. S. Vaughan, and P. L. Lewin, "Solvent Mixing and Its Effect on Epoxy Resin Filled with Graphene Oxide," in *2018 IEEE 2nd International Conference on Dielectrics (ICD)*, 2018, pp. 1–4.

[139] O. Vryonis, T. Andritsch, A. S. Vaughan, and P. L. Lewin, "Effect of surfactant molecular structure on the electrical and thermal performance of epoxy/functionalized-graphene nanocomposites," *Polym. Compos.*, vol. n/a, no. n/a, Mar. 2020.

[140] S. Wu *et al.*, "Aligning multilayer graphene flakes with an external electric field to improve multifunctional properties of epoxy nanocomposites," *Carbon N. Y.*, vol. 94, pp. 607–618, 2015.

[141] A. S. Krieg, J. A. King, D. C. Jaszczak, I. Miskoglu, O. P. Mills, and G. M. Odegard, "Tensile and conductivity properties of epoxy composites containing carbon black and graphene nanoplatelets," *J. Compos. Mater.*, vol. 52, no. 28, pp. 3909–3918, 2018.

[142] T. Andritsch, D. Fabiani, and I. R. Vazquez, "Nanodielectrics-examples of preparation and microstructure," *IEEE Electr. Insul. Mag.*, vol. 29, no. 6, pp. 21–28, 2013.

[143] V. Kumar *et al.*, "Effect of through-thickness electrical conductivity of CFRPs on lightning strike damages," *Compos. Part A Appl. Sci. Manuf.*, Sep. 2018.

[144] Y. Lin, M. Gigliotti, M. C. Lafarie-Frenot, and J. Bai, "Effect of carbon nanotubes on the thermoelectric properties of CFRP laminate for aircraft applications," *J. Reinf. Plast. Compos.*, vol. 34, no. 2, pp. 173–184, 2014.

[145] J. Chen, J. Wu, H. Ge, D. Zhao, C. Liu, and X. Hong, "Reduced graphene oxide deposited carbon fiber reinforced polymer composites for electromagnetic interference shielding," *Compos. Part A Appl. Sci. Manuf.*, vol. 82, pp. 141–150, 2016.

[146] D. Domingues, E. Logakis, and A. A. A. Skordos, "The use of an electric field in the preparation of glass fibre/epoxy composites containing carbon nanotubes," *Carbon N. Y.*, vol. 50, no. 7, pp. 2493–2503, Jun. 2012.

[147] C. Kostagiannakopoulou, E. Fiamegkou, G. Sotiriadis, and V. Kostopoulos, "Thermal Conductivity of Carbon Nanoreinforced Epoxy Composites," *J. Nanomater.*, vol. 2016, pp. 1–12, 2016.

[148] S. Wu *et al.*, "Aligning carbon nanofibres in glass-fibre/epoxy composites to improve interlaminar toughness and crack-detection capability," *Compos. Sci. Technol.*, vol. 152, no. Supplement C, pp. 46–56, 2017.

[149] Z. Li, L. Wang, Y. Li, Y. Feng, and W. Feng, "Carbon-based functional nanomaterials: Preparation, properties and applications," *Compos. Sci. Technol.*, vol. 179, pp. 10–40, 2019.

[150] As.-Y. Lee, M.-H. Chong, M. Park, H.-Y. Kim, and S.-J. Park, "Effect of chemically reduced graphene oxide on epoxy nanocomposites for flexural behaviors," *Carbon Lett.*, vol. 15, no. 1, pp. 67–70, 2014.

[151] S. Stankovich *et al.*, “Graphene-based composite materials,” *Nature*, vol. 442, no. 7100, p. 282, 2006.

[152] D. G. Papageorgiou, I. A. Kinloch, and R. J. Young, “Mechanical properties of graphene and graphene-based nanocomposites,” *Prog. Mater. Sci.*, vol. 90, pp. 75–127, Oct. 2017.

[153] M. A. Rafiee, J. Rafiee, Z. Wang, H. Song, Z.-Z. Yu, and N. Koratkar, “Enhanced mechanical properties of nanocomposites at low graphene content,” *ACS Nano*, vol. 3, no. 12, pp. 3884–3890, 2009.

[154] M. A. Rafiee, J. Rafiee, Z. Wang, H. Song, Z.-Z. Yu, and N. Koratkar, “Enhanced mechanical properties of nanocomposites at low graphene content,” *ACS Nano*, vol. 3, no. 12, pp. 3884–3890, 2009.

[155] S.-C. Shiu and J.-L. Tsai, “Characterizing thermal and mechanical properties of graphene/epoxy nanocomposites,” *Compos. Part B Eng.*, vol. 56, pp. 691–697, 2014.

[156] J. D. Renteria *et al.*, “Strongly anisotropic thermal conductivity of free-standing reduced graphene oxide films annealed at high temperature,” *Adv. Funct. Mater.*, vol. 25, no. 29, pp. 4664–4672, 2015.

[157] X. Mu, X. Wu, T. Zhang, D. B. Go, and T. Luo, “Thermal transport in graphene oxide–from ballistic extreme to amorphous limit,” *Sci. Rep.*, vol. 4, p. 3909, 2014.

[158] P. Feraboli and H. Kawakami, “Damage of Carbon/Epoxy Composite Plates Subjected to Mechanical Impact and Simulated Lightning,” *J. Aircr.*, vol. 47, no. 3, pp. 999–1012, 2010.

[159] M. Gagné and D. Therriault, “Lightning strike protection of composites,” *Prog. Aerosp. Sci.*, vol. 64, pp. 1–16, 2014.

[160] J. Han *et al.*, “The combination of carbon nanotube buckypaper and insulating adhesive for lightning strike protection of the carbon fiber/epoxy laminates,” *Carbon N. Y.*, vol. 94, pp. 101–113, 2015.

[161] E. C. Senis, I. O. Golosnoy, J. Dulieu-Barton, O. T. Thomsen, and S. F. Madsen, “Characterization of through-thickness thermal conductivity of wind turbine blade CFRP materials using a steady-state technique,” in *ICCM International Conferences on Composite Materials*, 2017, vol. 2017-Augus.

[162] IEC and I. E. C, “61400 :Wind energy generation systems,” *Part 24: Lightning protection*. 2010.

[163] A. A. M. Laudani, I. O. Golosnoy, and O. T. Thomsen, “Numerical Computation of Lightning Time-Domain Voltages Using the Fourier Analysis and the Finite Element Method,” in *Tenth International Conference on Computational Electromagnetics (CEM 2019)*, 2019, p. 6.

[164] X. Yao, S. C. Hawkins, and B. G. Falzon, “An advanced anti-icing/de-icing system utilizing highly aligned carbon nanotube webs,” *Carbon N. Y.*, vol. 136, pp. 130–138, 2018.

[165] L. Gao, R. Veerakumar, Y. Liu, and H. Hu, “Quantification of the 3D shapes of the ice structures accreted on a wind turbine airfoil model,” *J. Vis.*, vol. 22, no. 4, pp. 661–667, 2019.

[166] L. Battisti, *Wind Turbines in Cold Climates*. Cham: Springer International Publishing, 2015.

[167] N. Dalili, A. Edrisy, and R. Carriveau, “A review of surface engineering issues critical to wind turbine performance,” *Renew. Sustain. Energy Rev.*, vol. 13, no. 2, pp. 428–438, 2009.

[168] X. Yao, B. G. Falzon, S. C. Hawkins, and S. Tsantzalis, “Aligned carbon nanotube webs embedded in a composite laminate: A route towards a highly tunable electro-thermal system,” *Carbon N. Y.*, vol. 129, pp. 486–494, 2018.

[169] R. HART and O. ZHUPANSKA, “Four Probe Electrical Resistance Characterization of Carbon Fiber and Carbon Nanotube Buckypaper Composites,” in *Proceedings of the American Society for Composites: Thirty-First Technical Conference*, 2016.

[170] D. D. L. Chung, *Functional Materials: Electrical, Dielectric, Electromagnetic, Optical and Magnetic Applications : (with Companion Solution Manual)*. World Scientific, 2010.

[171] M. Louis, S. P. Joshi, and W. Brockmann, “An experimental investigation of through-thickness electrical resistivity of CFRP laminates,” *Compos. Sci. Technol.*, vol. 61, no. 6, pp. 911–919, 2001.

[172] E. B. Jeon, T. Fujimura, K. Takahashi, and H. S. Kim, “An investigation of contact resistance between carbon fiber/epoxy composite laminate and printed silver electrode for damage monitoring,” *Compos. Part A Appl. Sci. Manuf.*, vol. 66, pp. 193–200, 2014.

[173] J. C. Tan, S. A. Tsipas, I. O. Golosnoy, J. A. Curran, S. Paul, and T. W. Clyne, “A steady-state Bi-substrate technique for measurement of the thermal conductivity of ceramic coatings,” *Surf. Coatings Technol.*, vol. 201, no. 3, pp. 1414–1420, 2006.

[174] O. Vryonis, T. Andritsch, A. S. Vaughan, and P. L. Lewin, “Structural and chemical

comparison between moderately oxygenated and edge oxygenated graphene: mechanical, electrical and thermal performance of the epoxy nanocomposites," *SN Appl. Sci.*, vol. 1, no. 10, p. 1275, 2019.

[175] L. Mishnaevsky, K. Branner, H. Petersen, J. Beauson, M. McGugan, and B. Sørensen, "Materials for Wind Turbine Blades: An Overview," *Materials (Basel).*, vol. 10, no. 11, p. 1285, 2017.

[176] A. E. Zantout and O. I. Zhupanska, "On the electrical resistance of carbon fiber polymer matrix composites," *Compos. Part A Appl. Sci. Manuf.*, vol. 41, no. 11, pp. 1719–1727, 2010.

[177] E.-B. B. Jeon, T. Fujimura, K. Takahashi, and H.-S. S. Kim, "An investigation of contact resistance between carbon fiber/epoxy composite laminate and printed silver electrode for damage monitoring," *Compos. Part A Appl. Sci. Manuf.*, vol. 66, pp. 193–200, 2014.

[178] L. Shen, J. Li, B. M. Liaw, F. Delale, and J. H. Chung, "Modeling and analysis of the electrical resistance measurement of carbon fiber polymer–matrix composites," *Compos. Sci. Technol.*, vol. 67, no. 11–12, pp. 2513–2520, Sep. 2007.

[179] R. Holm, *Electric contacts: theory and application*. Springer Science & Business Media, 2013.

[180] Y. J. Chen, X. J. Ren, P. Zhang, T. Zhang, and A. B. Wu, "Measurement of Thermal Conductivity of CFRPs and Thermal Conductance of the Cold-to-Warm Joint at Low Temperatures," *IEEE Trans. Appl. Supercond.*, vol. 22, no. 3, 2012.

[181] D. M. Price and M. Jarratt, "Thermal conductivity of PTFE and PTFE composites," *Thermochim. Acta*, vol. 392–393, pp. 231–236, Sep. 2002.

[182] X. Huang, P. Jiang, and T. Tanaka, "A review of dielectric polymer composites with high thermal conductivity," *IEEE Electr. Insul. Mag.*, vol. 27, no. 4, pp. 8–16, 2011.

[183] O. A. Sergeev, A. G. Shashkov, and A. S. Umanskii, "Thermophysical properties of quartz glass," *J. Eng. Phys.*, vol. 43, no. 6, pp. 1375–1383, 1982.

[184] J.-K. Kim and Y.-W. Mai, *Engineered interfaces in fiber reinforced composites*. Elsevier, 1998.

[185] S. U. Khan and J.-K. Kim, "Improved interlaminar shear properties of multiscale carbon fiber composites with bucky paper interleaves made from carbon nanofibers," *Carbon N.*

Y., vol. 50, no. 14, pp. 5265–5277, Nov. 2012.

[186] K. J. Bowles and S. Frimpong, “Void Effects on the Interlaminar Shear Strength of Unidirectional Graphite-Fiber-Reinforced Composites,” *J. Compos. Mater.*, vol. 26, no. 10, pp. 1487–1509, Oct. 1992.

[187] S. T. M. for S.-B. S. of P. M. C. M. and T. L. ASTM D2344/D2344M-16 ASTM International West Conshohocken PA 2016 www.astm.org, “ASTM D2344 / D2344M-16, Standard Test Method for Short-Beam Strength of Polymer Matrix Composite Materials and Their Laminates, ASTM International, West Conshohocken, PA, 2016, www.astm.org.” .

[188] M. J. Baker, C. S. Hughes, and K. A. Hollywood, *Biophotonics: Vibrational Spectroscopic Diagnostics*. Morgan & Claypool Publishers, 2016.

[189] A. Kaniyoor and S. Ramaprabhu, “A Raman spectroscopic investigation of graphite oxide derived graphene,” *Aip Adv.*, vol. 2, no. 3, p. 32183, 2012.

[190] “ASTM D257-14, Standard Test Methods for DC Resistance or Conductance of Insulating Materials, ASTM International, West Conshohocken, PA, 2014, www.astm.org.” .

[191] Y. Bai, N. L. Post, J. J. Lesko, and T. Keller, “Experimental investigations on temperature-dependent thermo-physical and mechanical properties of pultruded GFRP composites,” *Thermochim. Acta*, vol. 469, no. 1, pp. 28–35, 2008.

[192] T. M. H. O. Vryonis T. Andritsch, A. S. Vaughan and P. L. Lewin *et al.*, “Solvent Mixing and Its Effect on Epoxy Resin Filled with Graphene Oxide,” in *2018 IEEE 2nd International Conference on Dielectrics (ICD)*, 2018, pp. 1–4.

[193] H. Chen, O. Jacobs, W. Wu, G. Rüdiger, and B. Schädel, “Effect of dispersion method on tribological properties of carbon nanotube reinforced epoxy resin composites,” *Polym. Test.*, vol. 26, no. 3, pp. 351–360, 2007.

[194] M. T. H. Sultan *et al.*, “On impact damage detection and quantification for CFRP laminates using structural response data only,” *Mech. Syst. Signal Process.*, vol. 25, no. 8, pp. 3135–3152, 2011.

[195] K. K. Schulte and C. Baron, “Load and failure analyses of CFRP laminates by means of electrical resistivity measurements,” *Compos. Sci. Technol.*, vol. 36, no. 1, pp. 63–76, 1989.

[196] J. Gu *et al.*, “Highly thermally conductive flame-retardant epoxy nanocomposites with reduced ignitability and excellent electrical conductivities,” *Compos. Sci. Technol.*, vol. 139,

pp. 83–89, Feb. 2017.

[197] Y. Lin, M. Gigliotti, M. C. Lafarie-Frenot, J. Bai, D. Marchand, and D. Mellier, “Experimental study to assess the effect of carbon nanotube addition on the through-thickness electrical conductivity of CFRP laminates for aircraft applications,” *Compos. Part B Eng.*, vol. 76, pp. 31–37, Jul. 2015.

[198] W. Qin, F. Vautard, L. T. Drzal, and J. Yu, “Mechanical and electrical properties of carbon fiber composites with incorporation of graphene nanoplatelets at the fiber–matrix interphase,” *Compos. Part B Eng.*, vol. 69, pp. 335–341, 2015.

[199] R. Umer, Y. Li, Y. Dong, H. J. Haroosh, and K. Liao, “The effect of graphene oxide (GO) nanoparticles on the processing of epoxy/glass fiber composites using resin infusion,” *Int. J. Adv. Manuf. Technol.*, vol. 81, no. 9–12, pp. 2183–2192, 2015.

[200] H. Chen, O. Jacobs, W. Wu, G. Rüdiger, and B. Schädel, “Effect of dispersion method on tribological properties of carbon nanotube reinforced epoxy resin composites,” *Polym. Test.*, vol. 26, no. 3, pp. 351–360, 2007.

[201] S. Wu *et al.*, “Aligning multilayer graphene flakes with an external electric field to improve multifunctional properties of epoxy nanocomposites,” *Carbon N. Y.*, vol. 94, pp. 607–618, Nov. 2015.

[202] H. Hiroshi and T. Minoru, “Equivalent inclusion method for steady state heat conduction in composites,” *Int. J. Eng. Sci.*, vol. 24, no. 7, pp. 1159–1172, 1986.

[203] A. Surnova, D. Balkaev, D. Musin, R. Amirov, and A. M. Dimiev, “Fully exfoliated graphene oxide accelerates epoxy resin curing, and results in dramatic improvement of the polymer mechanical properties,” *Compos. Part B Eng.*, vol. 162, pp. 685–691, Apr. 2019.

[204] J. Karger-Kocsis, H. Mahmood, and A. Pegoretti, “Recent advances in fiber/matrix interphase engineering for polymer composites,” *Prog. Mater. Sci.*, vol. 73, pp. 1–43, 2015.

[205] Z. Z. Liu *et al.*, “Electric-field-induced out-of-plane alignment of clay in poly (dimethylsiloxane) with enhanced anisotropic thermal conductivity and mechanical properties,” *Compos. Sci. Technol.*, vol. 165, pp. 39–47, 2018.

[206] M. Monti, M. Natali, L. Torre, and J. M. Kenny, “The alignment of single walled carbon nanotubes in an epoxy resin by applying a DC electric field,” *Carbon N. Y.*, vol. 50, no. 7, pp. 2453–2464, Jun. 2012.

[207] C. Ma *et al.*, "Alignment and dispersion of functionalized carbon nanotubes in polymer composites induced by an electric field," *Carbon N. Y.*, vol. 46, no. 4, pp. 706–710, Apr. 2008.

[208] T. Prasse, J.-Y. Cavaillé, and W. Bauhofer, "Electric anisotropy of carbon nanofibre/epoxy resin composites due to electric field induced alignment," *Compos. Sci. Technol.*, vol. 63, no. 13, pp. 1835–1841, Oct. 2003.

[209] C.-S. Lim, A. J. Rodriguez, M. E. Guzman, J. D. Schaefer, and B. Minaie, "Processing and properties of polymer composites containing aligned functionalized carbon nanofibers," *Carbon N. Y.*, vol. 49, no. 6, pp. 1873–1883, May 2011.

[210] M.-K. Schwarz, W. Bauhofer, and K. Schulte, "Alternating electric field induced agglomeration of carbon black filled resins," *Polymer (Guildf).*, vol. 43, no. 10, pp. 3079–3082, May 2002.

[211] G. H. Kim, D. K. Moeller, and Y. M. Shkel, "Orthotropic Polymeric Composites with Microstructure Tailored by Electric Field," *J. Compos. Mater.*, vol. 38, no. 21, pp. 1895–1909, Nov. 2004.

[212] G. Kim and Y. M. Shkel, "Polymeric composites tailored by electric field," *J. Mater. Res.*, vol. 19, no. 4, pp. 1164–1174, 2004.

[213] L. D. Landau and E. M. Lifshitz, "Electrodynamics of Continuous Media, Vol. 8 (Course of Theoretical Physics) Pergamon Press," *New York*, 1984.

[214] R. Casalini, S. Corezzi, A. Livi, G. Levita, and P. A. Rolla, "Dielectric parameters to monitor the crosslink of epoxy resins," *J. Appl. Polym. Sci.*, vol. 65, no. 1, pp. 17–25, 1997.

[215] O. Osazuwa, A. A. Vasileiou, M. Kontopoulou, and A. Docoslis, "Electric-field induced filler association dynamics and resulting improvements in the electrical conductivity of polyester/multiwall carbon nanotube composites," *Polym. Compos.*, vol. 38, no. 8, pp. 1571–1578, Aug. 2017.

[216] E. C. Sengezer, G. D. Seidel, and R. J. Bodnar, "Phenomenological characterization of fabrication of aligned pristine-SWNT and COOH-SWNT nanocomposites via dielectrophoresis under AC electric field," *Polym. Compos.*, vol. 36, no. 7, pp. 1266–1279, Jul. 2015.

[217] F. Tuinstra and J. L. Koenig, "Raman Spectrum of Graphite," *J. Chem. Phys.*, vol. 53, no. 3, pp. 1126–1130, Aug. 1970.

[218] M. A. Pimenta, G. Dresselhaus, M. S. Dresselhaus, L. G. Cançado, A. Jorio, and R. Saito, "Studying disorder in graphite-based systems by Raman spectroscopy," *Phys. Chem. Chem. Phys.*, vol. 9, no. 11, pp. 1276–1290, 2007.

[219] G. Venugopal, M.-H. Jung, M. Suemitsu, and S.-J. Kim, "Fabrication of nanoscale three-dimensional graphite stacked-junctions by focused-ion-beam and observation of anomalous transport characteristics," *Carbon N. Y.*, vol. 49, no. 8, pp. 2766–2772, Jul. 2011.

[220] N. Melanitis, P. L. Tetlow, and C. Galiotis, "Characterization of PAN-based carbon fibres with laser Raman spectroscopy," *J. Mater. Sci.*, vol. 31, no. 4, pp. 851–860, 1996.

[221] I. Balberg, "A comprehensive picture of the electrical phenomena in carbon black–polymer composites," *Carbon N. Y.*, vol. 40, no. 2, pp. 139–143, 2002.

[222] E. C. Senis, I. O. Golosnoy, J. M. Dulieu-Barton, and O. T. Thomsen, "Enhancement of the electrical and thermal properties of unidirectional carbon fibre/epoxy laminates through the addition of graphene oxide," *J. Mater. Sci.*, pp. 1–16, 2019.

[223] R. F. Hill and P. H. Supancic, "Thermal Conductivity of Platelet-Filled Polymer Composites," *J. Am. Ceram. Soc.*, vol. 85, no. 4, pp. 851–857, Apr. 2002.

[224] Z. Liu *et al.*, "Electric-field-induced out-of-plane alignment of clay in poly(dimethylsiloxane) with enhanced anisotropic thermal conductivity and mechanical properties," *Compos. Sci. Technol.*, vol. 165, pp. 39–47, Sep. 2018.

[225] Y. Su, J. J. Li, and G. J. Weng, "Theory of thermal conductivity of graphene-polymer nanocomposites with interfacial Kapitza resistance and graphene-graphene contact resistance," *Carbon N. Y.*, vol. 137, pp. 222–233, 2018.

[226] R. J. Young, I. A. Kinloch, L. Gong, and K. S. Novoselov, "The mechanics of graphene nanocomposites: A review," *Compos. Sci. Technol.*, vol. 72, no. 12, pp. 1459–1476, Jul. 2012.

[227] J. S. Jayan, A. Saritha, and K. Joseph, "Innovative materials of this era for toughening the epoxy matrix: A review," *Polym. Compos.*, vol. 39, no. S4, pp. E1959–E1986, Dec. 2018.

[228] G. Ramos-Fernandez, M. Muñoz, J. C. García-Quesada, I. Rodriguez-Pastor, and I. Martin-Gullon, "Role of graphene oxide surface chemistry on the improvement of the interlaminar mechanical properties of resin infusion processed epoxy-carbon fiber composites," *Polym. Compos.*, vol. 39, no. S4, pp. E2116–E2124, Dec. 2018.

[229] A. P. Mouritz, “Review of z-pinned composite laminates,” *Compos. Part A Appl. Sci. Manuf.*, vol. 38, no. 12, pp. 2383–2397, Dec. 2007.

[230] C. Yu *et al.*, “Enhanced through-plane thermal conductivity of boron nitride/epoxy composites,” *Compos. Part A Appl. Sci. Manuf.*, vol. 98, pp. 25–31, 2017.